


**ADVANCED VOLTAGE REGULATOR TECHNIQUES
AS APPLIED TO
MAXIMUM POWER POINT TRACKING SYSTEMS
FOR THE
NIMBUS METEOROLOGICAL SATELLITE**

**FINAL REPORT
16 JUNE 1965 THROUGH 10 OCTOBER 1967
CONTRACT NO. NAS5-3248**

Prepared for

**NATIONAL AERONAUTICS AND
SPACE ADMINISTRATION
WASHINGTON, D.C.**

Prepared by

**ASTRO-ELECTRONICS DIVISION
DEFENSE ELECTRONIC PRODUCTS
RADIO CORPORATION OF AMERICA 
PRINCETON, NEW JERSEY**

PRECEDING PAGE BLANK NOT FILMED.

PREFACE

This is the Final Report on the research and development of advanced power control techniques and their adaptation to Pulse Width Modulation (PWM) regulation technology in the manner necessary to form a maximum-power-point-tracking (MPPT) spacecraft power system. The MPPT (or Maximum-power-tracker - MPT) system is oriented towards application to the Nimbus meteorological satellite power supply subsystem, however, the concepts and techniques developed are extendable to most spacecraft. This program was performed by the Astro-Electronics Division of RCA, for the National Aeronautics and Space Administration under Contract No. NAS5-3248. The period covered by the report extends from 16 June, 1965 to 10 October, 1967.

TABLE OF CONTENTS

Section	Page
	xvii
1.0	1-1
1.1	1-1
1.2	1-3
1.3	1-7
2.0	2-1
2.1	2-1
2.1.1	2-1
2.1.2	2-4
a.	2-4
b.	2-6
c.	2-7
2.1.3	2-8
a.	2-12
Series vs. Parallel	2-12
b.	2-13
Parallel Tracker	2-13
2.1.4	2-15
a.	2-15
Current Sharing	2-15
b.	2-16
2.2	2-18

TABLE OF CONTENTS (Continued)

Section	Page
2.2.1 Energy Balance Comparisons	2-18
a. Nimbus A Power System	2-20
b. Modified Nimbus A Power System	2-24
c. Series MPT Power System	2-28
d. Parallel MPT Power System	2-35
e. System Comparison	2-36
2.2.2 Scan Frequency and Tracking	
Accuracy	2-37
2.3 System Operational Description	2-40
2.3.1 System Function	2-40
2.3.2 Modes of Operation	2-40
a. Discharge Mode	2-40
b. Charge Mode	2-42
(1) Excess Array Capability	2-42
(a) Control Unit	2-43
(b) Battery Module	2-43
(2) Sufficient Array	
Capability	2-46
(a) Control Unit	2-46
(b) Battery Module	2-49
(c) Summary	2-51
(3) Insufficient Array	
Capability	2-52

TABLE OF CONTENTS (Continued)

Section	Page
	(a) Control Unit 2-52
	(b) Battery Module 2-53
	(c) Summary 2-53
2.3.3	Protection Functions 2-54
a.	Battery Voltage Limit 2-54
b.	Battery Current Limit 2-55
c.	Battery Temperature Cut-off 2-56
2.4	Selected Circuit Descriptions 2-56
2.4.1	Power Switch Drive Circuitry 2-59
2.4.2	Output Current Peak Detector 2-62
2.4.3	Pulse Width Modulator 2-64
2.4.4	Scanner Circuits 2-66
2.4.5	Other Circuits 2-69
3.0	EXPERIMENTAL MODEL 3-1
3.1	Description of Equipment 3-2
3.1.1	Basic Equipment Layout 3-2
3.1.2	Construction Techniques 3-5
3.1.3	Filtering and Noise 3-7
a.	Array Filter 3-7
b.	Input Filters 3-7
c.	Output Filters 3-7
d.	Power Supply Decoupling 3-8
e.	Shielding 3-8
f.	Synchronization 3-8

TABLE OF CONTENTS (Continued)

Section	Page
3.1.4 Harnessing and Cabling	3-8
3.1.5 System Losses	3-9
a. Transfer Losses	3-10
b. Shunt Losses	3-11
3.2 Laboratory Testing and Results	3-13
3.2.1 Test Objectives	3-13
3.2.2 Test Conditions	3-14
3.2.3 Performance Test Results	3-14
a. Power Transfer Efficiency	3-14
b. Charge Current Sharing	3-18
c. Maximum Charge Rate	3-21
d. Trickle Charge Rate	3-22
e. Shunt Loss	3-23
f. Tracking Error	3-25
g. Interaction of Variables	3-27
h. MPT Calibration	3-27
3.2.4 System Test Results	3-28
a. Auxiliary Power Supply	3-29
b. System Configuration A	3-29
c. System Configuration B	3-32
d. Availability of Solutions	3-38

TABLE OF CONTENTS (Continued)

Section	Page
3.2.5 Conclusions	3-38
a. Design and Performance Goals	3-38
(1) Power Transfer Efficiency	3-38
(2) Charge Current Sharing	3-40
(3) Maximum	3-40
(4) Trickle Charge Rate	3-40
(5) Shunt Loss	3-41
(6) Tracking Error	3-41
(7) Summary	3-41
b. System Interface and Application	3-41
3.3 Summary	3-42
4.0 SECOND GENERATION MPT SYSTEM	4-1
4.1 Reasons for a New Concept	4-1
4.2 Second Generation System Concept	4-3
4.2.1 Basic System Operation	4-4
a. Source Characteristics	4-3
b. Multiplier	4-5
c. Peak Detector	4-5
d. Pulse Absence Detector (PAD)	4-6
e. Toggle	4-6
f. Load	4-6
4.2.2 System Protective Mode Operation	4-9
4.3 High Speed MPT Circuits	4-12
4.3.1 Power Sensor Circuit	4-12
4.3.2 Peak Power Detector Circuit	4-22

TABLE OF CONTENTS (Continued)

Section		Page
4.4	Working Model	4-26
4.4.1	Basic Equipment Layout	4-26
4.4.2	Grounding and Noise Suppression	4-27
4.5	Laboratory Evaluation	4-28
4.5.1	Power Transfer Efficiency	4-30
4.5.2	Charge Current Sharing	4-31
4.5.3	Maximum Charge Rate Control	4-31
4.5.4	Trickle Charge Rate Control	4-31
4.5.5	Shunt Loss	4-32
4.5.6	Tracking Error	4-33
4.5.7	Load Transient Susceptability Problem	4-34
4.5.8	Off-Bias Operation Problem	4-35
4.5.9	Rapidly Varying Solar Array	4-36
4.6	Summary of Results	4-37
5.0	PROGRAM RECOMMENDATIONS	5-1
5.1	Battery Current Controls	5-1
5.2	Power Sensor Circuits	5-1
5.3	Multiple Battery Channel Operation	5-2
5.4	System Operating Frequency	5-2
6.0	REFERENCES	6-1

TABLE OF CONTENTS (Continued)

APPENDIX		Page
I	POWER TRACKER PERFORMANCE ANALYSIS	I-1
	A. INTRODUCTION	I-1
	B. ANALYTICAL CALCULATIONS	I-2
	1. Input Parameters	I-2
	2. Output Power	I-2
	3. Charge Current	I-3
	4. Battery Charge Voltage	I-3
	5. Output Current	I-3
	6. Load-Bus Regulator Input Current	I-3
	7. Load-Bus Regulator Input Voltage	I-3
	8. Load-Bus Regulator Output Power	I-4
	9. Battery Discharge Current	I-4
	10. Battery Discharge Voltage	I-4
	11. Output Current	I-4
	12. Load-Bus Regulator Input Current	I-5
	13. Load-Bus Regulator Input Voltage	I-5
	14. Output Power	I-5
II	GRAPHICAL ANALYSIS OF MPT SYSTEM OPERATION	II-1
	A. GENERAL	II-1
	B. ANALYSIS BY OPERATING MODES	II-6
	1. Discharge (Night) Mode	II-6
	2. Normal Tracking (Day) Mode	II-7
	3. Full-Time System Mode	II-14

TABLE OF CONTENTS (Continued)

APPENDIX		Page
III	DERIVATION OF AN EXPRESSION FOR SCAN FREQUENCY . .	III-1
	1. Analytical Solution	III-6
	2. Graphical Solution	III-7

LIST OF ILLUSTRATIONS

Figure		Page
1-1	A Typical, State-of-the-Art Solar Power System . .	1-2
1-1	Maximum Available Array Power and Power Utilized by a Conventional Solar Power System vs. Sun-Time	1-3
1-3	Variation of Operating Point with Load	1-5
1-4	Basic PWM, Simplified Schematic	1-6
1-5	PWM Control of Load Line	1-7
1-6	Source P-V and I-V Curves	1-8
1-7	PWM Device with Battery Load	1-9
1-8	Short-Term Battery I-V Curve	1-10
1-9	PWM Control of Battery Type Load Line	1-10
2-1	Power-Flow Diagram for a Power System	2-1
2-2	Some Basic Power System Configurations	2-3
2-3	Series Power Tracker	2-5
2-4	Full-Time Parallel Power Tracker	2-7
2-5	Part-Time Parallel Power Tracker	2-8
2-6	Performance Comparison of Tracker Systems	2-9
2-7	Hysteresis of Operating Points, Part-Time System	2-12
2-8	Load Power Profile No. 22, Nimbus A	2-19
2-9	Nimbus A, F-1, Average Array Temperature vs. Daytime (Orbit 15 Data)	2-20
2-10	Rudimentary Form of Nimbus A Power Supply Subsystem	2-21
2-11	Load Current Profile, Including Shunt Losses	2-22

LIST OF ILLUSTRATIONS (Continued)

Figure		Page
2-12	Nimbus A Solar Array: Available Current at 34 Volts vs. Time and Temperature.	2-24
2-13	Effective Load Current Profile, Including Shunt Losses	2-26
2-14	Basic Form of Series MPT Power System	2-28
2-15	Load Power Profile in Watts at Regulated Bus . . .	2-29
2-16	Maximum Available Power vs. Array Temperature . .	2-32
2-17	Average Available Array Power vs. Life in Orbit	2-33
2-18	Graphical Solution for V_{SL} and V_{su}	2-39
2-19	Maximum Power Tracker, Functional Diagram	2-41
2-20	MPT Control Unit, Schematic Diagram	2-57
2-21	MPT Battery Module Electronics, Schematic Diagram	2-58
2-22	Power Switch Drive, Schematic Diagram	2-60
2-23	Output Current Peak Detector, Schematic Diagram	2-63
2-24	Pulse Width Modulator, Schematic Diagram	2-65
2-25	Scanner Circuit, Schematic Diagram	2-67
3-1	MPT Breadboard Set-up	3-1
3-2	MPT Control Unit	3-3
3-3	MPT Battery Module, Exterior View	3-4
3-4	MPT Control Unit, Interior View	3-5
3-5	MPT Battery Module, Interior View	3-6
3-6	MPT Performance Test Configuration	3-15
3-7	Four Channel MPT System, Power Transfer vs. Array Power	3-16

LIST OF ILLUSTRATIONS (Continued)

Figure		Page
3-8	MPT System, Power Transfer vs. Array Power	3-16
3-9	MPT System, Charge Current Sharing vs. Array Power	3-19
3-10	MPT System, Maximum Charge Rage vs. Array Power	3-21
3-11	MPT System, Trickle Charge Rate vs. Array Power	3-22
3-12	MPT System, Shunt Loss vs. Array Power	3-24
3-13	MPT System Test Configuration A	3-30
3-14	MPT System Test Configuration B	3-33
3-15	PWM Regulator Input Characteristics	3-35
3-16	Solar Array I-V Characteristic and Load Lines for Battery	3-36
3-17A	Solar Array/Battery System	3-36
3-17B	Solar Array/MPT/Battery System	3-37
3-18	Composite I-V Characteristic, I_O vs. V_{SA}	3-39
4-1	Basic System Diagram	4-4
4-2	Source Characteristics	4-5
4-4	High Speed MPT System, Functional Diagram	4-10
4-5	High Speed MPT Control Unit, Schematic Diagram	4-13
4-6	High Speed MPT Battery Module, Schematic Diagram	4-14

LIST OF ILLUSTRATIONS (Continued)

Figure		Page
4-7	DC Power Sensor, Functional Diagram	4-16
4-8	Output Voltage Waveform	4-18
4-9	Magnetic Core Characteristics and State for $I_d = 0$ and I_G Present	4-19
4-10	I_d Characteristics	4-19
4-11	Core Field Intensity vs. Time	4-20
4-12	Practical I_d Generator Characteristics	4-22
4-13	Peak Power Detector Circuit, Schematic Diagram	4-23
4-14	High Speed MPT, Working Model Layout	4-26
4-15	High Speed MPT, Ground Plan	4-28
4-16	Simulated Solar Array Characteristics	4-29
4-17	High Speed MPT Power Transfer Efficiency	4-30
4-18	Shunt Loss Current vs. Array Power	4-32
4-19	MPT System Test Configuration	4-34
II-1	Graph of Equation, $p_s = p_l + p_b$	II-2
II-2	Typical Solar-Array $p_s - v_s$ Characteristic	II-3
II-3	Load Power - Regulator Input Characteristic	II-4
II-4	Battery $p_b - v_b$ Characteristics	II-5
II-5	Operating Point for Battery Discharge ($p_s = 0$)	II-7
II-6	Graph of $p = p_l + p_e$ versus v_s	II-9
II-7	Graph of $p_s = p_l + p_b$ versus v_s	II-10
II-8	Simplified Graph of $p_s = p_l + p_b$ versus v_s	II-11
II-9	Location of Operation Point for Small Values of α	II-13

LIST OF ILLUSTRATIONS (Continued)

Figure		Page
II-10	Multiple Operating Points for Large Values of α	II-14
II-11	Location of Operating Point for Normal MPT Operation	II-15
II-12	Peak Load Handling for Full-Time Tracker Systems	II-16
II-13	Peak Load Handling for Part-Time Parallel Tracker Systems	II-17
II-14	Available Power vs. Source Voltage for Part-Time Tracker	II-18
III-1	Incremental Source Characteristics	III-2
III-2	Graphical Solution to Power Equation	III-8

FOREWORD

The contract work was formulated around typical parameters applicable to the early design of the Nimbus B spacecraft. However, the techniques and their adaptation are suitable for any earth-orbiting space vehicles. It should be noted that wherever references appear herein to the Nimbus B spacecraft, the parameters are typical of those specified early in the design and should not be construed to be actual specified values of the present Nimbus B configuration.

The technical guidance was provided, since the inception of work, by Mr. Charles M. MacKenzie, NASA Technical Officer; the technical direction at AED was provided by Mr. R. C. Greene, Project Manager for this contract. The following personnel of the RCA Astro-Electronics Division contributed significantly to the successful completion of the contract.

Mr. C. A. Berard
Mr. A. S. Cherdak
Mr. F. E. Colucci
Mr. J. L. Douglas

Mr. A. O. Johnson
Mr. L. T. McCloskey
Mr. P. S. Nekrasov

1.0 INTRODUCTION

1.1 Summary

During the past few years, considerable effort has been spent by both industry and government to improve the performance of space power systems. One of the significant advances has been the development of practical Maximum Power Point Tracking (MPPT) systems which offer greatly increased operational capability over conventional systems. This report presents the background and evolution of practical MPPT space power systems from the basic technology of pulse-width-modulated switching voltage regulators.

First generation (low-speed) MPPT systems operated on the principle of slowly varying the operating point of the source to locate the maximum power point. A sensing mechanism measures MPPT output current and utilizes the impedance multiplication transformation properties of a constant frequency pulse-width-modulated regulator to locate and track the maximum power point. However, this system has several severely limiting properties (e.g., susceptibility to load transients, and inability to locate the maximum power point under certain load conditions) which preclude its use on many spacecraft.

Therefore, the requirements for the second generation (high-speed) MPPT system are as follows:

- Must be capable of tracking the maximum power point regardless of the load input characteristics;
- Must be capable of maintaining proper MPPT operation for a fluctuating source (e.g., spin-stabilized spacecraft with fixed solar arrays);

- Must provide performance characteristics comparable to the low-speed system (i.e., power transfer efficiency, multiple-battery-channel operation, and load protection features);
- Must be capable of responding to load transients as rapidly as does the source (solar array); and
- Must be capable of operation with source voltages up to 100 volts d-c, source powers in excess of 1000 watts, and output currents up to 15 amperes per channel.

The basic concept for the high-speed MPPT system employs the techniques of a variable-frequency, pulse-width-modulated (transistor) switch. Opening and closing the switch shifts the operating point either towards the open-circuit-voltage or short-circuit-current condition of the source, respectively. Instantaneous source power is sensed and allows the source maximum power point to be detected; this, in turn, causes the state of the switch to change and reverses the direction of the operating point shift. Repetition of this process causes the system operating point to oscillate about the maximum power point of the source at the operating frequency of the transistor switch. Thus, the speed of response to load changes is approximately that of the source. The control circuitry associated with the sensing and logic functions operates at rates up to 100 kHz to allow adequate source power sampling during each state of the switch. Integrated circuits are used for logic and analog functions in the control circuitry and reduce control-circuit bias power.

Experimental models of both low and high-speed MPPT systems were constructed, tested, and delivered. Results of the tests are presented herein.

The second-generation MPPT system provides a means of efficient power conditioning which can result in significant increases in space power system capability. Of additional importance is the applicability of the basic technology to all types of spacecraft, and the wide variety of power system configurations with which the high-speed MPPT system concept may be used.

1.2 General

A typical power system for an earth-orbiting satellite is shown on Figure 1-1. The system consists of a solar-cell-array primary energy source, a nickel-cadmium energy storage system, and appropriate power control circuits. Orbit periods of 90 to 120 minutes with sun-time/occultation ratios of 2-to-1 are common for systems of this type.

Ideally, during the sunlit portion of an orbit, all available energy from the array would be delivered, either to spacecraft loads through an efficient non-dissipative load bus regulator, or to charge the battery through appropriate battery charge control and protection circuits. During the dark portion of the orbit, energy stored in the battery during the charge cycle is delivered to the load. Proper design assures energy balance during the life-time of the spacecraft.

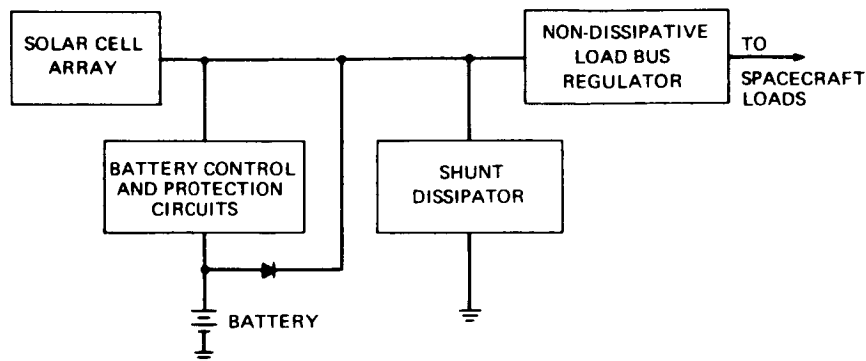


Figure 1-1. A Typical, State-of-the-Art Solar Power System

There are potential problems associated with the commonly used power system configuration. As the array emerges from the Earth's shadow, the low solar cell temperature drives the array maximum power point to a voltage far in excess of the operating voltage range (determined by the maximum battery charge voltage) for which the system shown on Figure 1-1 is customarily designed. The array output voltage is clamped to a relatively low initial battery recharge voltage level, plus a small charge regulator drop. The resulting quiescent power point is at a level far below the potential power capability of a cold-cell array. The advantage of having nearly the same current flow at the array output, but at a much larger voltage is not realized. Figure 1-2, based on actual data for an earth-orbiting spacecraft, typifies the situation. The solid line on the graph indicates maximum available power during satellite day. The associated energy could be stored in the battery or delivered to loads. The dotted line optimistically indicates the maximum power extracted from the array

by the conventional system. In this case, utilization of maximum available power would allow roughly a 100 watt, or 20 percent reduction, in solar array power requirements. Based on nominal solar array costs of \$250/watt, this would result in a new savings of \$25,000 per spacecraft.

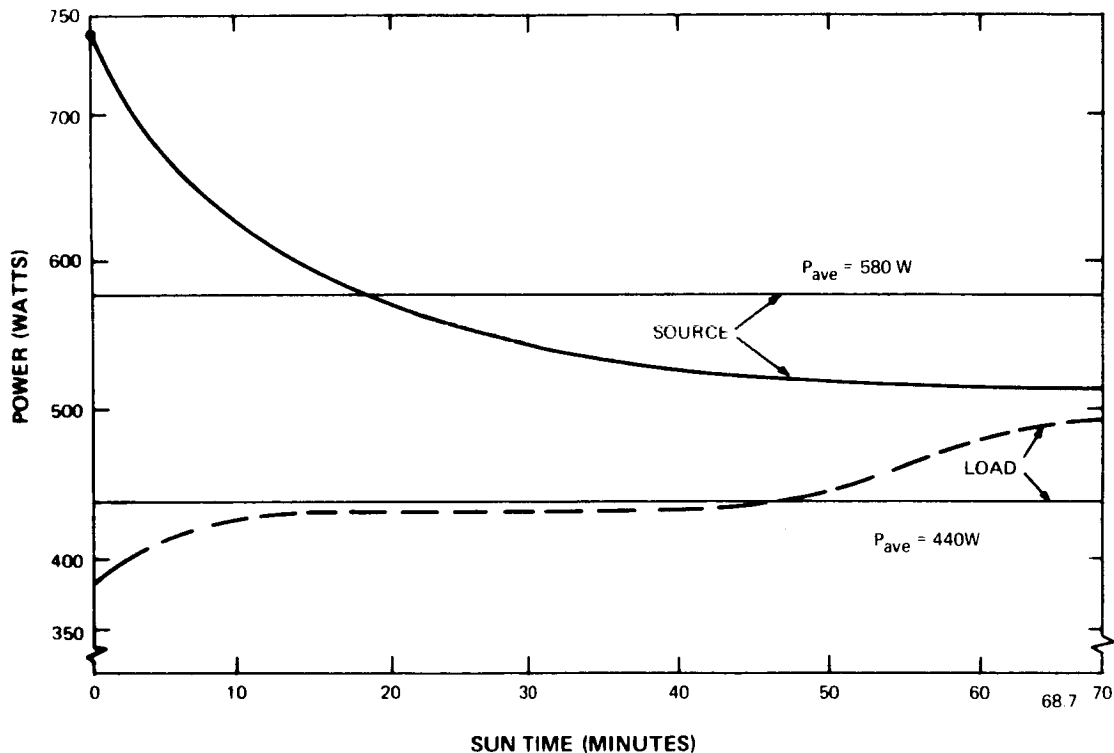


Figure 1-2. Maximum Available Array Power and Power Utilized By a Conventional Power System Vs. Sun-Time.

As the spacecraft goes further into the sun-illuminated portion of flight, the solar cell temperature rises, thus reducing the maximum power point voltage of the array to more nearly match the battery charge voltage. When battery recharge is accomplished, the charge mechanism reduces the charge current, thereby creating a condition of excess

energy, and as a result, excess voltage at the array output. Generally, the excess energy is absorbed either in the charge controller or in a specially designed excess-power dissipator. In either case, intolerably large amounts of power may have to be dissipated. The resulting spacecraft thermal balance problem becomes particularly severe where there is a large design difference between the beginning-of-life and end-of-life array output.

The application of recent advances in power-conditioning technology will substantially increase spacecraft life, or load capability, by assuring an optimum source-to-load energy transfer. This concept, referred to as "Maximum Power Tracking" (MPT), involves the delivery of maximum available source power (in this case, solar-array power) to the spacecraft, regardless of source variations caused by environment or time. Optimum energy transfer results from the adaptive control of pulse width modulation (PWM) power-conditioning circuits. These effectively match the input impedance of the spacecraft to the output impedance of the solar array at its maximum power point. The spacecraft storage system plays an important role, in that any instantaneously available array energy not immediately required for spacecraft loads is delivered to storage. Storage overcharge control, which is fully automatic, is achieved by overriding the maximum power tracking control and intentionally mismatching the system and array impedances to produce a less-than-optimum transfer of power. Load demand is always accomplished on a preferential basis. Use of this mismatching technique completely obviates the need for a power sink, such as a shunt limiter, and eliminates a severe thermal problem.

1.3 Impedance Matching Through PWM Techniques and Attaining Maximum Power Transfer

The solar array operating point can be changed by changing the load impedance to which it is applied. This is illustrated by Figure 1-3.

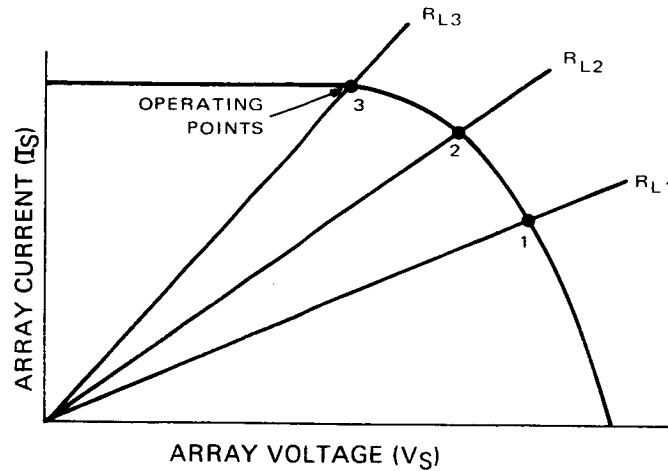


Figure 1-3. Variation of Operating Point With Load

A PWM regulator is, in effect, a d-c impedance transformer capable of making a single load-resistance appear as an infinitely variable load to the array.

The impedance transformation properties of a PWM device are shown on Figure 1-4. Here, the switch opens and closes at a constant repetition rate of frequency, f . The ratio of closure time t_{ON} , to the period, T , is the duty-cycle α , which is controllable.

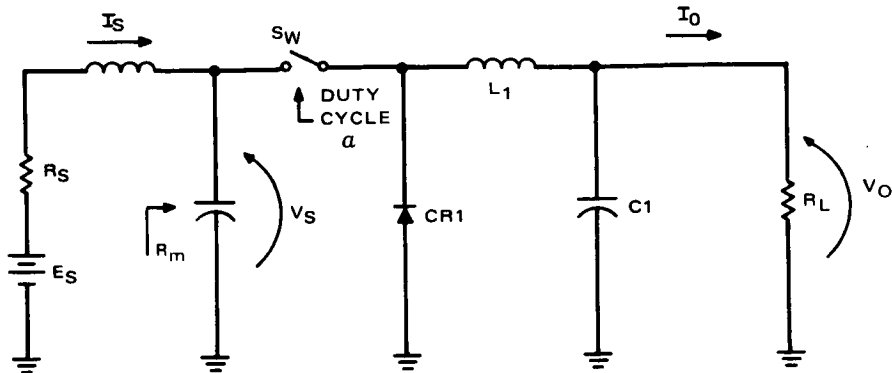


Figure 1-4. Basic PWM Circuit, Simplified Schematic

If the average power delivered to R_L is the dc power, and losses in the switch and the filters are negligible, then

$$R_m = \frac{(V_S)^2}{P_S} \quad (1.1)$$

where:

P_S = power delivered by source

but, if the switching network is essentially non-dissipative,

$$P_S = P_O = \frac{(V_O)^2}{R_L} \quad (1.2)$$

and,

$$R_m = \frac{(V_S)^2}{(V_O)^2} R_L \quad (1.3)$$

However, if the filter, $L_1 - C_1 - CR_1$, is an averaging filter, then

$$V_o = \alpha V_s \quad (1.4)$$

or

$$V_s = \frac{V_o}{\alpha}$$

Therefore,

$$R_m = \frac{V_o^2 R_L}{V_o^2 \alpha^2} = \frac{R_L}{\alpha^2} \quad (1.5)$$

Therefore, controlling the duty-cycle of a PWM device will control its input impedance.

This is shown graphically on Figure 1-5

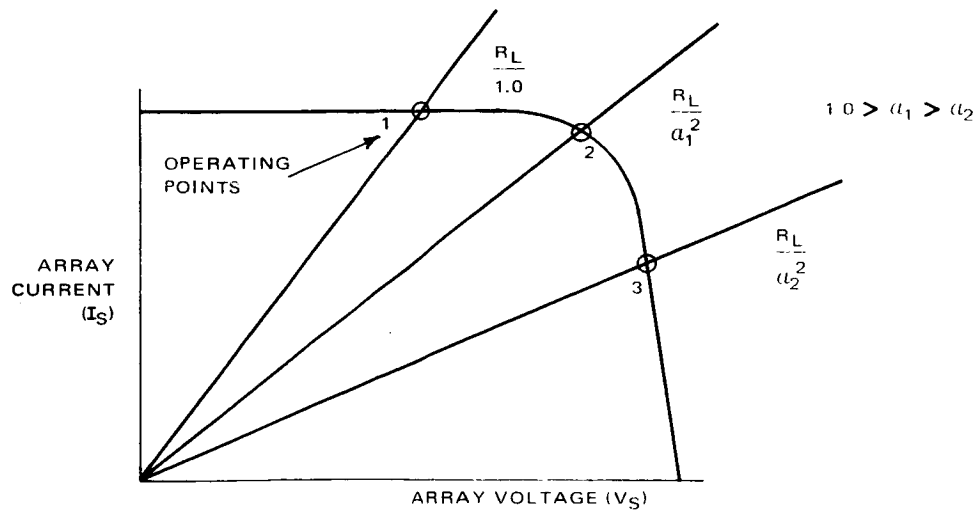


Figure 1-5. PWM Control of Load Line

Thus indicating operating point control by controlling α .

Assuming the PWM to be non-dissipative as before,

$$P_O = P_S \quad (1.6)$$

and the array power is then delivered to the load resistor.

As shown on Figure 1-6, by selecting R_L to intersect the $I_s - V_s$ characteristic at a voltage lower than the maximum power voltage, an α can be found which will result in maximum array power being delivered to R_L .

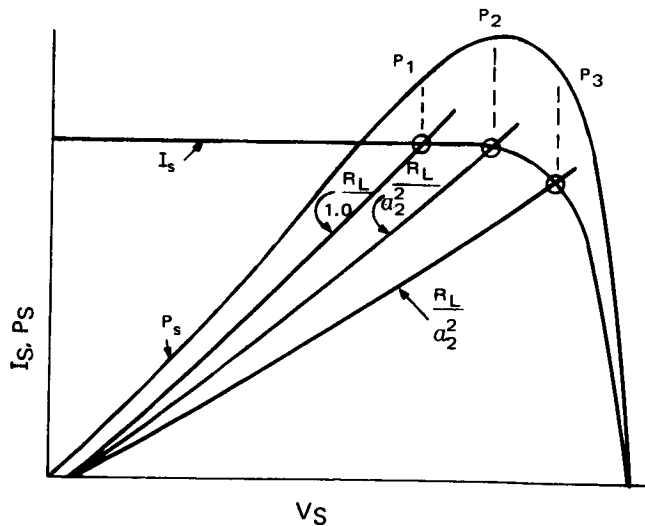


Figure 1-6. Source P-V and I-V Curves

Substitution of a low impedance load, such as a battery, does not change control capability. This is shown on Figure 1-7.

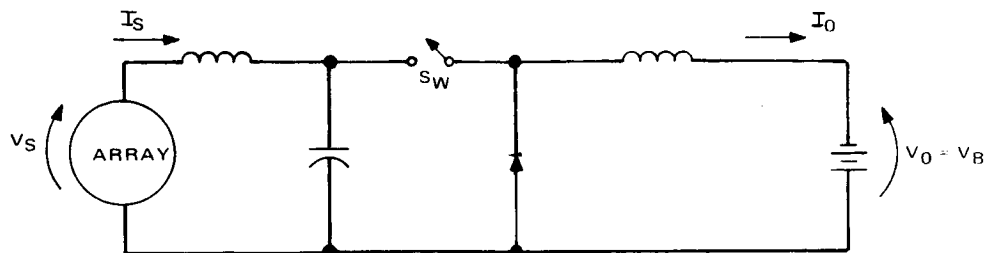


Figure 1-7. PWM Device with Battery Load

The average output voltage is now determined by the battery terminal voltage.

$$V_o = V_B = \alpha V_S$$

The voltage presented to the source side of the switch becomes

$$V_S = \frac{V_B}{\alpha} \quad (1.7)$$

Graphically, (Figure 1-8) the short term I-V characteristic of a battery is almost a vertical line.

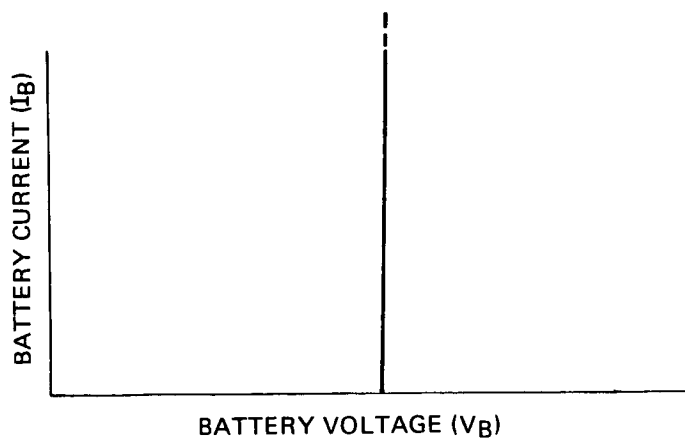


Figure 1-8. Short Term Battery I-V Curve

The battery voltage, when reflected to the PWM input terminals as modified by the duty-cycle, α , is shown on Figure 1-9 for values of α less than 1.0.

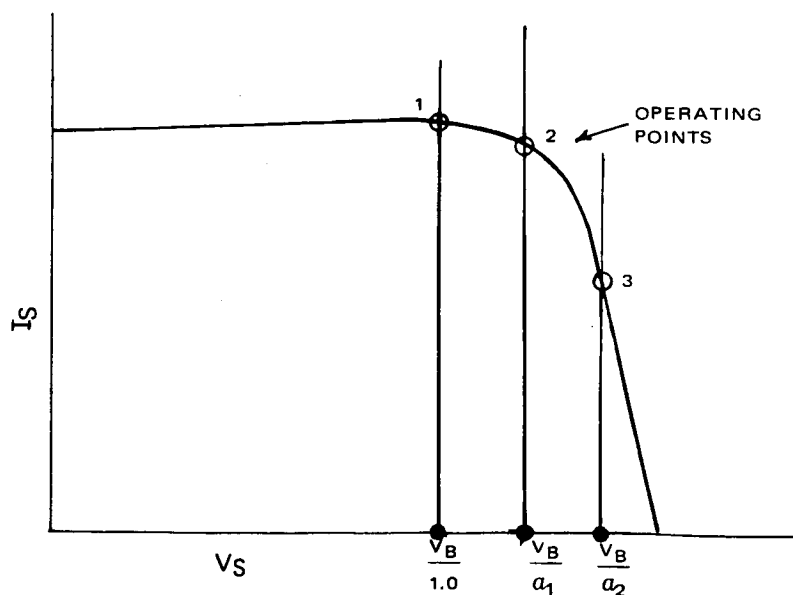


Figure 1-9. PWM Control of Battery Type Load Line

By selecting V_B to be lower than the maximum power voltage of the array, an α can be found such that maximum source power will be delivered to the battery.

2.0 SYSTEM CONSIDERATIONS

2.1 System Design

The successful adaptation of the maximum power tracking technique to spacecraft power systems requires careful consideration of various possible source-to-load power flow configurations. The following section considers general system configurations and presents an in-depth study of a specific "part-time parallel tracking system" selected for implementation.

2.1.1 General Configuration

Topologically, the power flow in a spacecraft power system would appear as in Figure 2-1. The arrows indicate the direction of power flow.

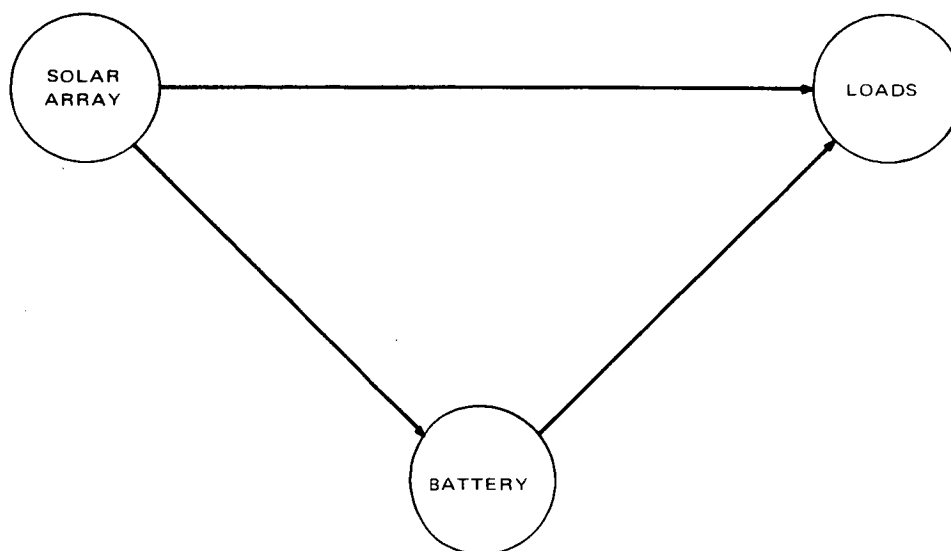


Figure 2-1. Power-Flow Diagram For A Power System

The extension of the power flow diagram to a rudimentary power system diagram becomes obvious when one considers the differences in the nature of available and acceptable power. That is, the loads require power in a form different from that available directly from array and battery, and the battery in general, requires power in a form not directly available from the array. Insertion of the appropriate power conditioning functions into the power flow diagram results in the basic power system of Figure 2-2(a).

Since this arrangement is highly suggestive of a delta-connected system, it immediately implies the possibility of transformation to other configurations. Figure 2-2(b) and (c) represent two possibilities, the Wye and the open delta configurations respectively. Note that in all three cases, the fundamental power flow topology shown in Figure 2-1, and indicated by the arrows, is preserved.

Selection of a specific configuration, which might be termed the optimum, necessarily involves a detailed study of the implications of each. (The nature of each of the undesignated boxes in Figure 2-2 and related parameters.)

The system configuration of Figure 2-2(b) was employed to develop the MPT concept. However, the principles of MPT System design evolved in this program are also applicable to the other configurations.

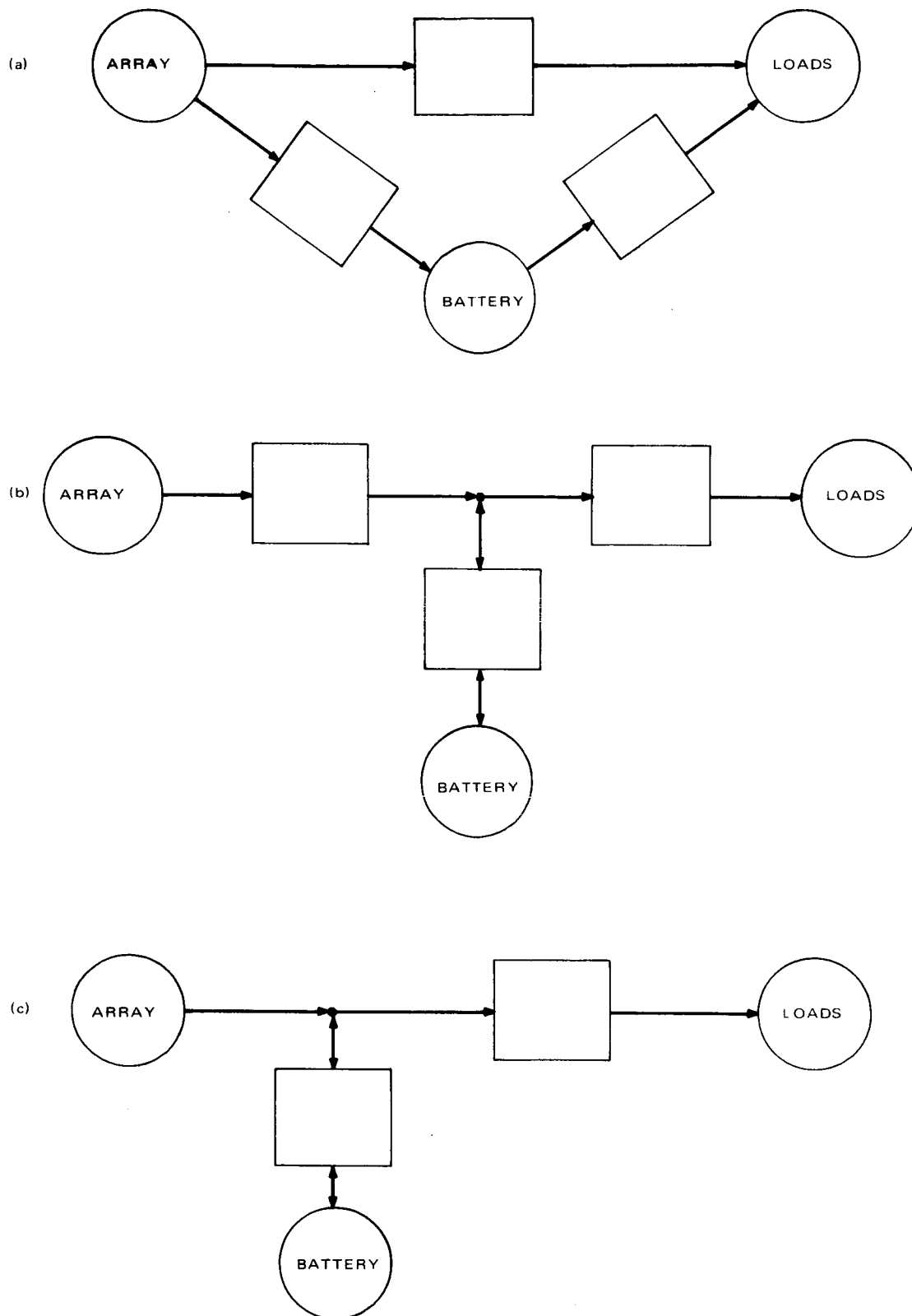


Figure 2-2. Some Basic Power System Configurations

2.1.2 Power Tracker Configurations

Following the selection of a system configuration, analyses and tradeoffs of the various power trackers were made to determine their relative ability to maintain the spacecraft in a state of energy balance. Results of the analyses were indicative of the efficiency of each system compared and served to recommend the most suitable approach for use in a particular mission. The Nimbus meteorological satellite is a typical mission which was used as a basis of comparison in this program.

Three tracking systems were investigated and compared to a non-tracking Nimbus ⁽¹⁾ power subsystem using a PWM load bus regulator. A brief description of each of the three tracking systems is given below.

a. Series Tracker

The block diagram of Figure 2-3 shows a two-module series tracker, but it is understood that many more modules can be involved.

The tracker is placed in series with the array. V_{\max} , I_{\max} of the array appears at the tracker input at all times (less allowance for losses), regardless of the load magnitude at the regulated bus voltage V_R . The

¹ The Nimbus B Power Subsystem is described in "Nimbus Power Systems 1960-1969", C.M. MacKenzie, NASA, Goddard Space Flight Center, R.C. Greenblatt and A.S. Cherdak, RCA, presented at 1966 Aerospace and Electronic Systems Convention, Wash. D. C., October, 1966.

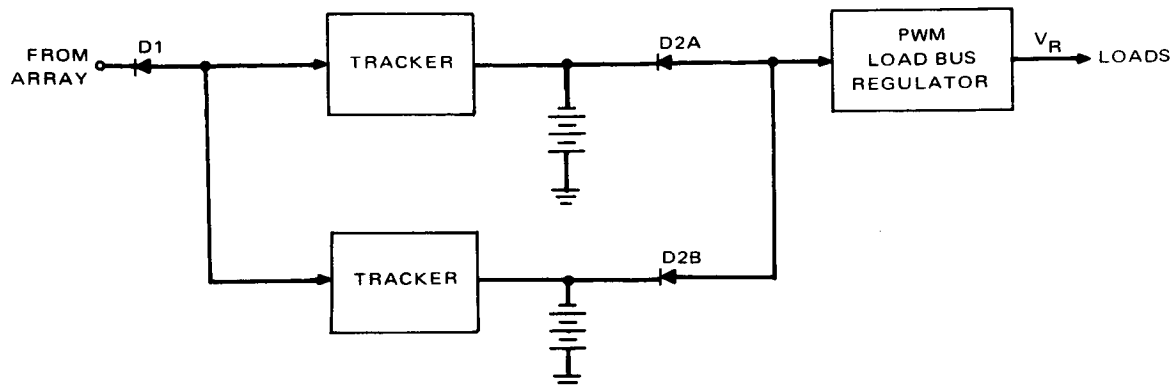


Figure 2-3. Series Power Tracker

series tracker output voltage is determined by the battery as shown; but the product of the tracker output power is equal to $V_{\max} \times I_{\max}$ of the array, times a more or less fixed efficiency factor of the tracker (neglecting minor losses peculiar to the method of P_{\max} acquisition to be explained later). The series tracker output is thus equal to the P_{\max} of the solar array at any time, less unavoidable losses; the tracker system of this type is full-time, since P_{\max} is tracked at all times regardless of the load magnitude.

The series tracker output is shared by the battery, and by the PWM regulator input requirement determined by the instantaneous load.

The battery protection mechanism is not shown on the block diagram. It consists of circuits designed to monitor various battery quantities such as voltage, current, and temperature, and to cause a decrease of the battery charge current by decreasing the tracker output, whenever a safe combination of the three measured quantities are exceeded.

b. Full-time Parallel Tracker

In a parallel tracker, the tracking device is placed in series with the battery; the series combination is electrically in parallel with the array and the load as shown in Figure 2-4. The parallel tracker maximizes the power difference between the array output and the load requirement during charge. The array V_{\max} thus appears at the tracker input, as in the series tracker. During daytime discharge, V_{\max} is maintained causing maximum array power (less circuit losses) to be delivered to the load through the PWM Load Bus Regulator. The required power difference (as during a peak load) is taken from the battery through the PWM discharge regulator (DR).

The full-time parallel tracker system is designed so that the battery discharge during a daytime peak load is minimized. Even though the tracker unit is no longer active during discharge, the PWM load bus regulator will then set the operating point at approximately the array maximum voltage, if there is sufficient load demand. Maximum array output is thus drawn first, before the battery is allowed to discharge. Lowest possible battery discharge is therefore assured.

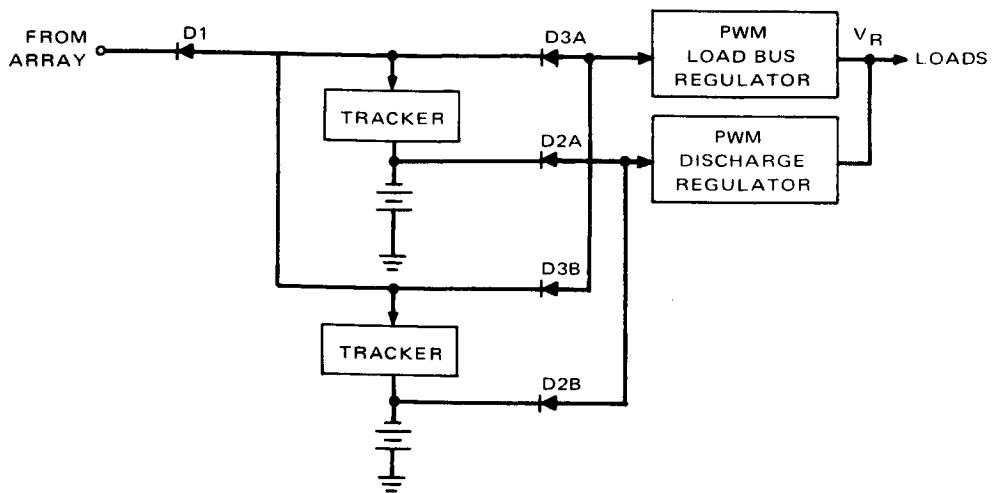


Figure 2-4. Full-Time Parallel Power Tracker

The battery protection implementation is very similar to that described for the series tracker in Paragraph 2.1.2a.

c. Part-Time Parallel Tracker

The part-time parallel tracker operation is, in every way, identical to that of the full-time parallel tracker, so long as the power system remains in the battery charge mode. During battery discharge, however, the array V_{max} voltage can no longer be maintained, at which time the system is operated in the non-tracking mode as is the Nimbus B System.

It can be seen (Figure 2-5) that in the part-time tracker the battery discharge path (thru D2 diodes) is connected to the PWM regulator input. Isolation between the PWM regulator input and the battery discharge voltages can thus no longer

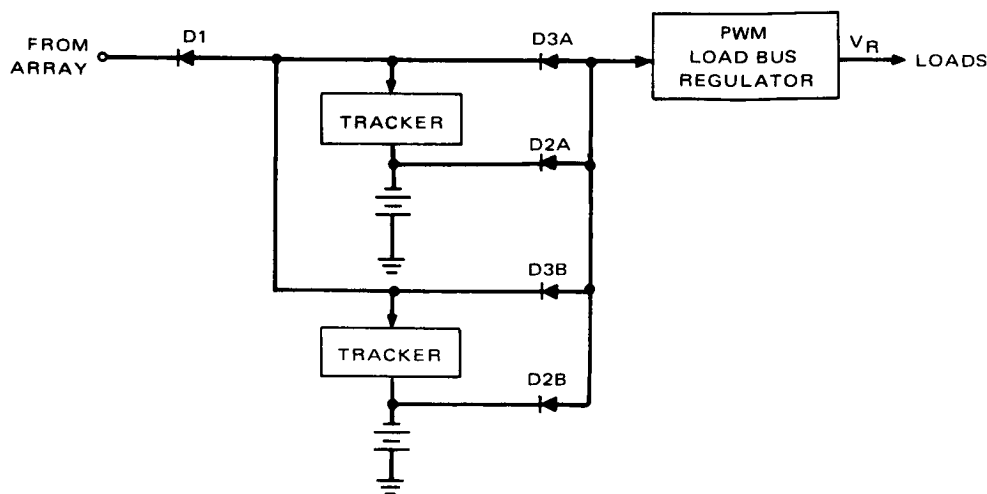


Figure 2-5. Part-Time Parallel Power Tracker

be maintained in the manner in which it was in the full-time parallel tracker which was discussed in the preceding section. Consequently, in the part-time tracker, the PWM regulator input voltage is roughly equal to the battery voltage when in discharge; usually several volts removed from the array V_{max} .

2.1.3 Comparison of Power Trackers

As a method of comparison of the three configurations it will be assumed that the most desirable performance is achieved when the battery charge is maximized (or, when battery discharge is minimized) for any given set of fixed conditions of load and array temperature. With this approach adopted as a standard of quality, the method of comparison consisted of plots of available battery charge and discharge currents vs. load, for different array outputs, for each of the systems compared. The basis for the analysis and a sample calculation are shown in Appendix I.

An alternate approach would be to compute the energy transfer efficiencies for each system and to compare the efficiency factors. In order to pursue that approach, however, a particular set of power requirements would have to be assumed which would result in a loss of generality. This type of analysis is presented in Paragraph 2.2.

Both extremes of the end-of-life array temperature were considered, i.e., the coldest array as when emerging from the earth's shadow (-80°C , and corresponding roughly to the steady-state, or thermal equilibrium temperature ($+40^{\circ}\text{C}$). Two states of the array output result in two families of battery current vs. load plots as shown in Figure 2-6.

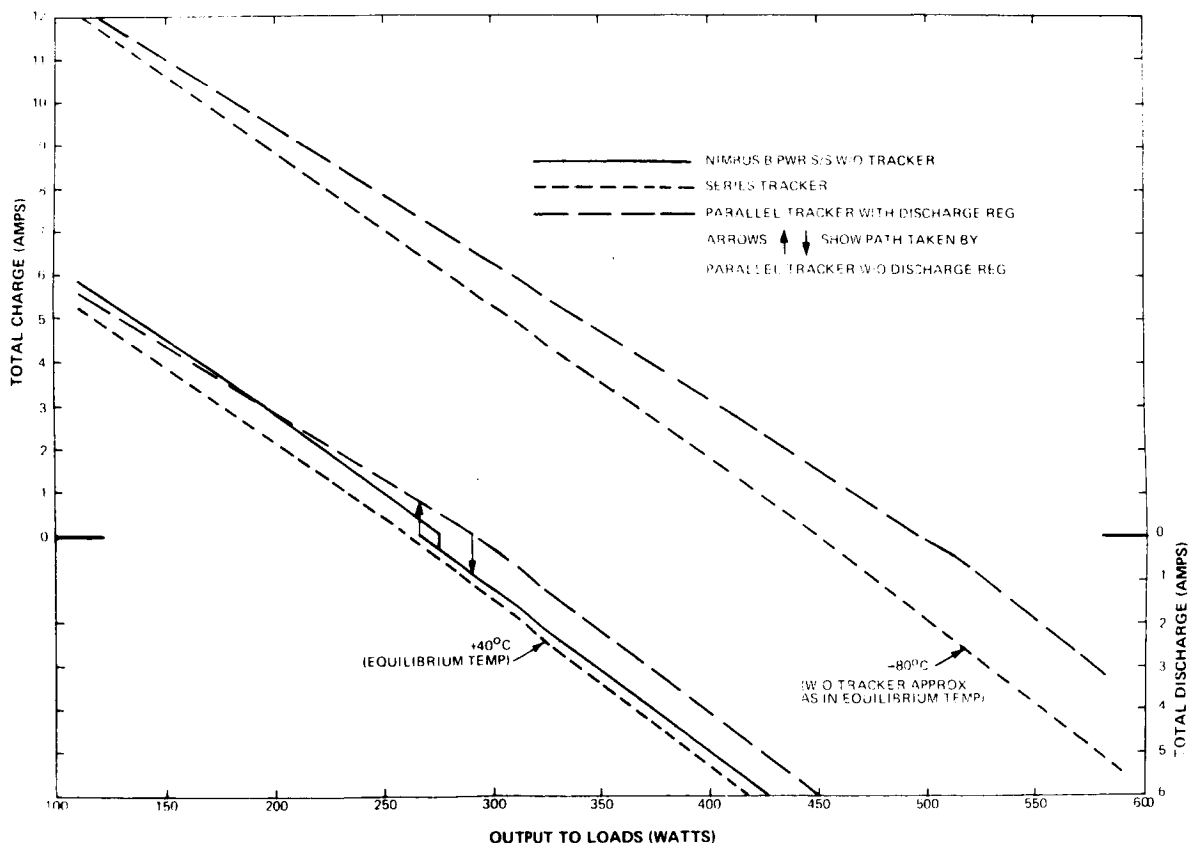


Figure 2-6. Performance Comparison of Tracker Systems

The non-tracking system performance shown on the graph has been obtained from Nimbus B data. Even though the plot shown applies to $+40^{\circ}\text{C}$ array temperature, it can be stated that colder array temperatures would have little effect on the solid-line plot shown for the non-tracking system.

The tracking system performance, on the other hand, is greatly influenced by the array temperatures as shown. The plot clearly shows the superiority of a tracking system because it is able to take advantage of the increased array power during the temperature transient, by being able to supply a much larger total charge current for a time (given a fixed load requirement).

During steady-state array temperature, a tracking system should show little, if any, advantage over a well-designed conventional non-tracking approach. Therefore, the plots corresponding to the steady-state temperature are located relatively close to one another, as expected.

Another significant conclusion drawn from the graph is that a full-time parallel tracker is always more efficient (i.e., it supplies more charge, draws less discharge) than the series tracker, regardless of the load magnitude or the array temperature. Confirmation of this conclusion may be established, if it is considered that in the series approach all of the array power is subject to the tracker inefficiency, whereas in the parallel tracker only the battery charge is subjected to that loss.

It has been stated that the part-time parallel tracker operates the same as its full-time counterpart when in "charge". The graph shows, at equilibrium temperature, both types of parallel trackers continuing together up to a load of about 291 watts; for a slightly higher load, the part-time tracker drops out of the tracking mode as shown by the arrow pointing downwards to the plot of the non-tracking system, and continues along the latter plot for all higher loads.

As the load is decreased, the part-time tracker follows the non-tracking plot until zero discharge condition is reached. The graph shows this to correspond to about 268 watts load. Further slight load decrease causes the system to resume tracking; added power suddenly released by the array is delivered as a step charge to the battery, as shown by the upward-pointing arrow.

The apparent hysteresis effect occurring over the 268-291-watt range can be illustrated further, using the familiar P-V plot (Figure 2-7).

Based on the foregoing analysis, the various power-tracker configurations and their relative advantages are considered below:

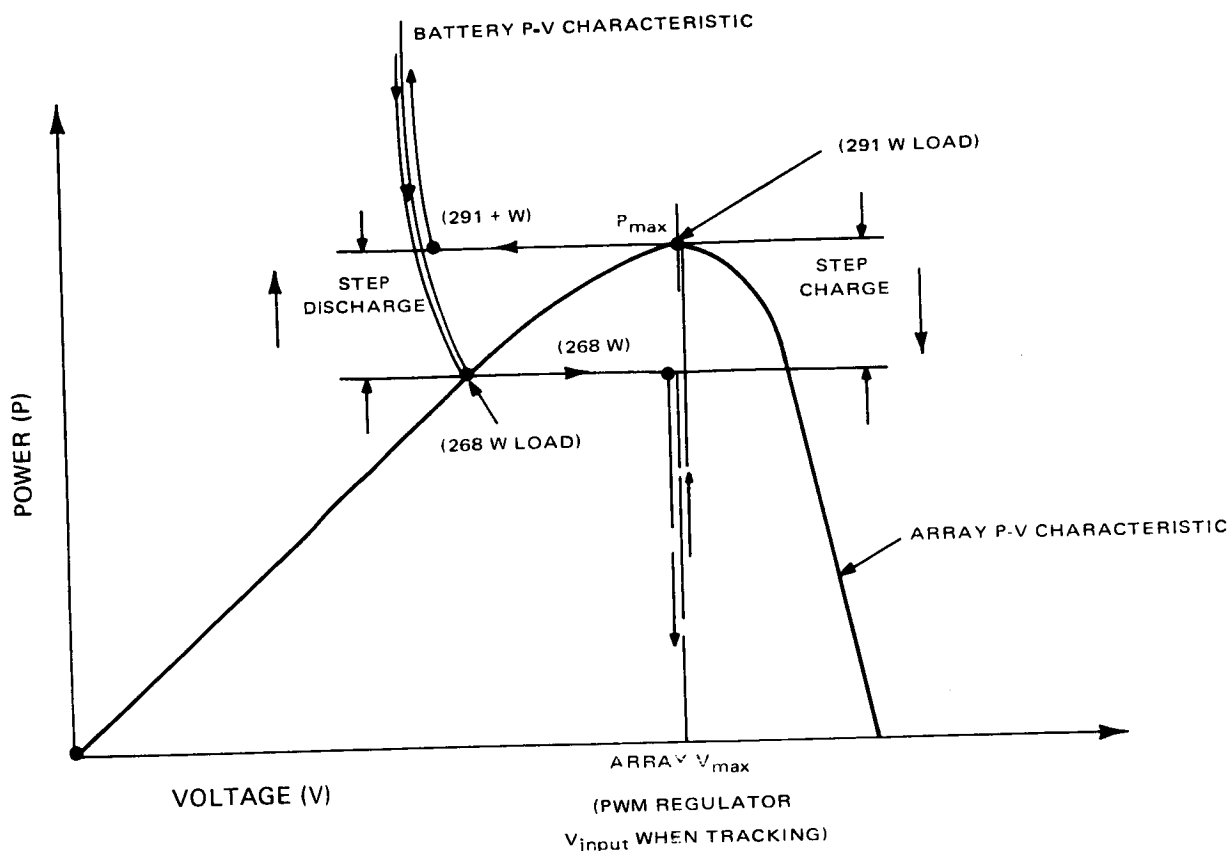


Figure 2-7. Hysteresis of Operating Points, Part-Time System

a. Full-Time Trackers; Series vs. Parallel

The most significant advantage of the series tracker approach is that it is the simplest system with a full-time tracking capability. The two salient disadvantages of this configuration are: First, the series tracker reduces the effective P_{max} output of the solar array by an amount greater than the equivalent parallel tracker; and second, load sharing problems can occur in a series tracker due, primarily, to differences in battery voltage.

Compared to a series tracker, the full-time parallel tracker in the Nimbus system (see Figure 2-6) will produce as much as one ampere more charge current, depending on load: the greater the load, the more advantageous the parallel tracker, since less array power is subject to the tracker loss.

In discharge, the series tracker demands a greater total discharge current by slightly more than one ampere.

The foregoing applies to the steady-state array temperature condition. Colder array temperatures point up the efficiency advantages of a full-time parallel tracker even more, thus, the charge is greater by up to about 1.5 amperes, and the discharge is lower by two amperes when the array temperature is minimum.

For the end-of-life Nimbus system, the full-time parallel tracker would provide nearly one ampere-hour more recharge per orbit, compared to a series tracker. This is a considerable advantage, in view of the fact that the total recharge per orbit at end-of-life is on the order of five ampere-hours.

b. Parallel Tracker, Full-Time vs. Part-Time

The full-time version of this type of tracker requires the complexity of a discharge regulator to maintain isolation between the PWM regulator input and the battery bus, and

sensing and logic circuitry to turn it on at the proper time as well as to keep it off during the charge cycle. The part-time tracker is, therefore, a much simpler approach, and the final tradeoff should be based on the duration of the discharge anticipated during daytime and on the timing of the peak load causing the discharge.

Since the part-time parallel tracker cannot track during discharge, it will draw more battery discharge current during a peak load. In fact, the discharge will equal the amount drawn in the non-tracking Nimbus B system. In equilibrium temperature, the difference is approximately one ampere. Thus, the part-time tracker will cause an added total discharge of one ampere-minute, per minute of peak load duration, under conditions of steady-state array temperature. For a ten-minute peak, and assuming eight four-ampere-hour batteries, the added discharge would amount to 0.5 percent of the total stored capacity.

Under conditions of colder array temperature, the difference would be greater, if a large enough peak load is applied.

It can be concluded that, although the full-time parallel tracker will perform better, given a perfectly general application, the performance improvement over the part-time tracker will be slight (if any) under certain selected conditions. If there

are no peak loads during daytime, the two will perform equally well; if the peak loads are short-duration, and particularly, if they occur during the latter part of the satellite daytime, the difference will be small.

In view of the typical requirements considered above, and based on the discussion of the relative merits of the three tracker systems, it was concluded that the part-time parallel tracker was most suitable in a Nimbus type mission and was therefore adopted for development in this program.

2.1.4 Other System Considerations

The following are areas considered fundamental to any one of the MPT system configurations, to the extent that a practical system could not be implemented without solutions for these requirements.

a. Multiple Batteries and Current Sharing

A basic requirement placed upon an MPT system has been that of operating with one or more batteries (with eight as a practical limit). There are several reasons for this: one being the fact that the MPT was developed with the Nimbus application in mind (up to eight parallel batteries) and another being increasing load demands, particularly in long term manned missions. The latter has dictated electrochemical-energy-storage capacity far beyond the state-of-the-art for

a single battery. It must be concluded, after examination of many spacecraft power systems, that direct parallel charging of the commonly used batteries (Ni-Cd, Ag-Cd) is not desirable and, in fact, is to be avoided.

This requirement has dictated separate charging mechanisms for each battery. It is conceivable, that through some judicious set of procedures, the electronic circuits comprising each separate charging mechanism might be made identical in performance. Despite any such matching, the inherent differences between batteries which preclude direct parallel charging would certainly negate the matching efforts. In addition, the costs involved in producing electronic assemblies, in matched sets of eight, plus spares become prohibitive.

In order to overcome the inherent differences in both batteries and in similar electronic assemblies, the multiple battery system must have provision for actively and equally sharing available charge current. This provision has been made in the MPT system and is described in Paragraph 2.3.

b. Battery Considerations

In the MPT System, the battery must be capable of accepting recharge at high rates. Without this capability, instantaneously available array power, not required by the load, might not be completely useable. This would result in an effective decrease

in the average available array power and consequently, either a loss in programming capability for a given array, or a larger array for a given load than would otherwise be required.

High rate charging of conventional nickel-cadmium batteries does not appear to present any significant problems until the state-of-charge of the battery approaches 80 percent. At this point, generation of high, internal cell pressures and the possibility of hydrogen evolution render the high charge rate unattractive.

Application of the auxiliary or third electrode, Ni-Cd, battery cell would appear a promising solution to this problem. This type of cell is reported to have the capability for accepting recharge in a cyclical routine at rates through the "C" rate.

Another possible solution is the use of a conventional Ni-Cd battery with an ampere-hour meter. The meter would recognize the onset of the fully charged condition and would cause the power system to act, based on the state-of-charge, in such a manner as to eliminate the possibility of damage to the battery.

Any of the above alternatives require that protective functions be introduced into the power system to prevent irreversible damage to batteries as a result of excessive overcharge. A detailed description of the battery protection functions is included in Paragraph 2.3.

2.2 Systems Analysis

There are obviously many approaches to be taken in evaluating the performance and/or relative worth of a power system. An energy-balance analysis comparing the full-time tracking systems with a conventional power system (Nimbus A power system), is discussed in the following paragraph. A second analysis, utilizing a graphical approach for ascertaining instantaneous behavior of a tracker system is presented in Appendix II.

In order to design a power tracking system, it is necessary to predict the scanning frequency and tracking accuracy which will be obtained. Analytical expressions for these parameters are presented.

2.2.1 Energy Balance Comparisons

A basis for comparison of the effectiveness of spacecraft power systems in transferring source power is the obtainable additional operating load which can be supported in orbit for consistent source and required-load profile characteristics for the period of a fixed mission.

The existing Nimbus power systems are compared here with a Maximum Power Tracker (MPT) system in terms of operating load with a typical Nimbus A load power profile, as shown in Figure 2-8, as required load. Solar array performance is predicted upon degradations and tolerances formulated by RCA for the Nimbus A configuration as of March 25, 1964. The array temperature profile

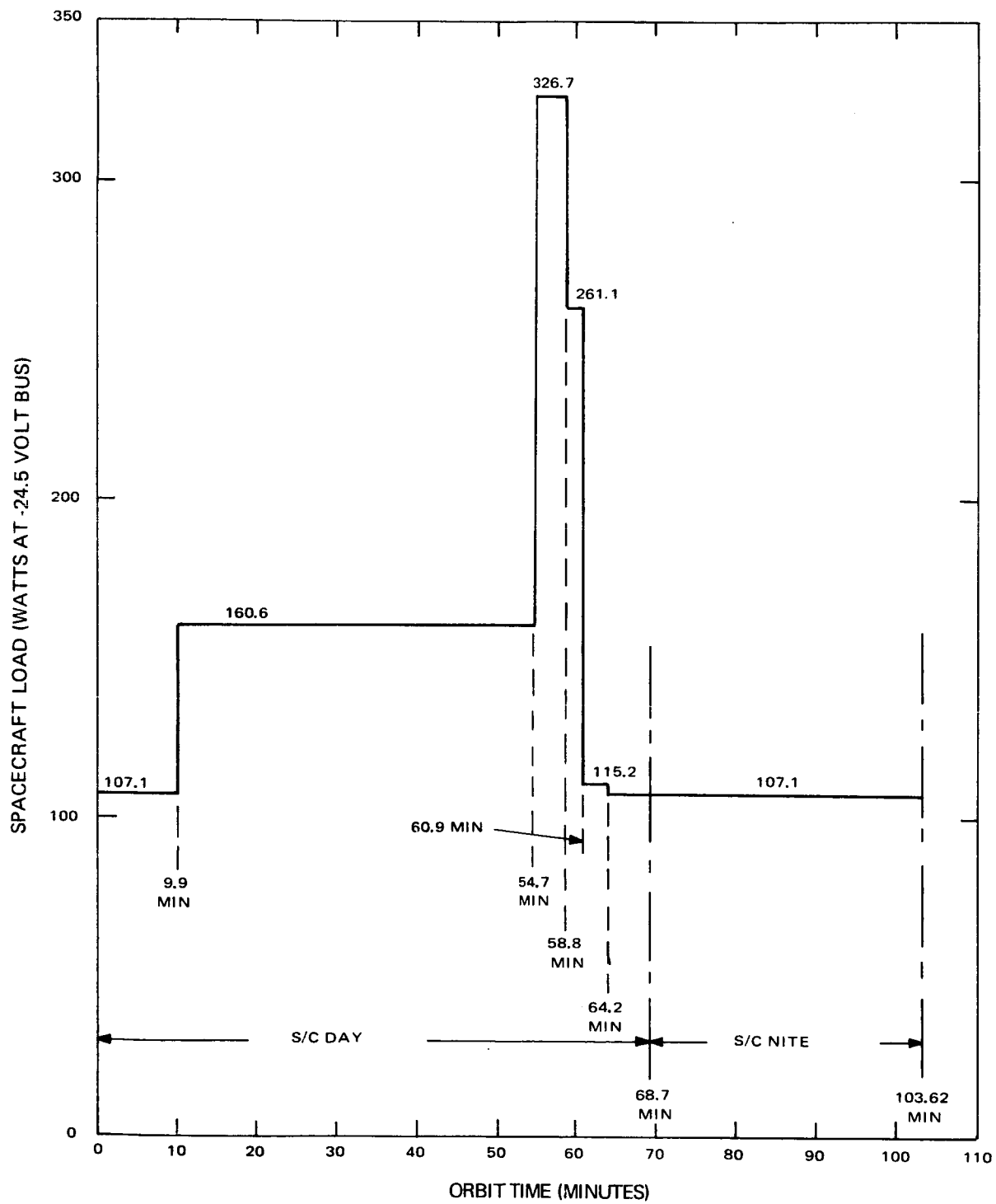


Figure 2 8. Load Power Profile No. 22, Nimbus A

employed, Figure 2-9, was constructed primarily from telemetry data from Orbit 15 of the Nimbus A Flight One vehicle.

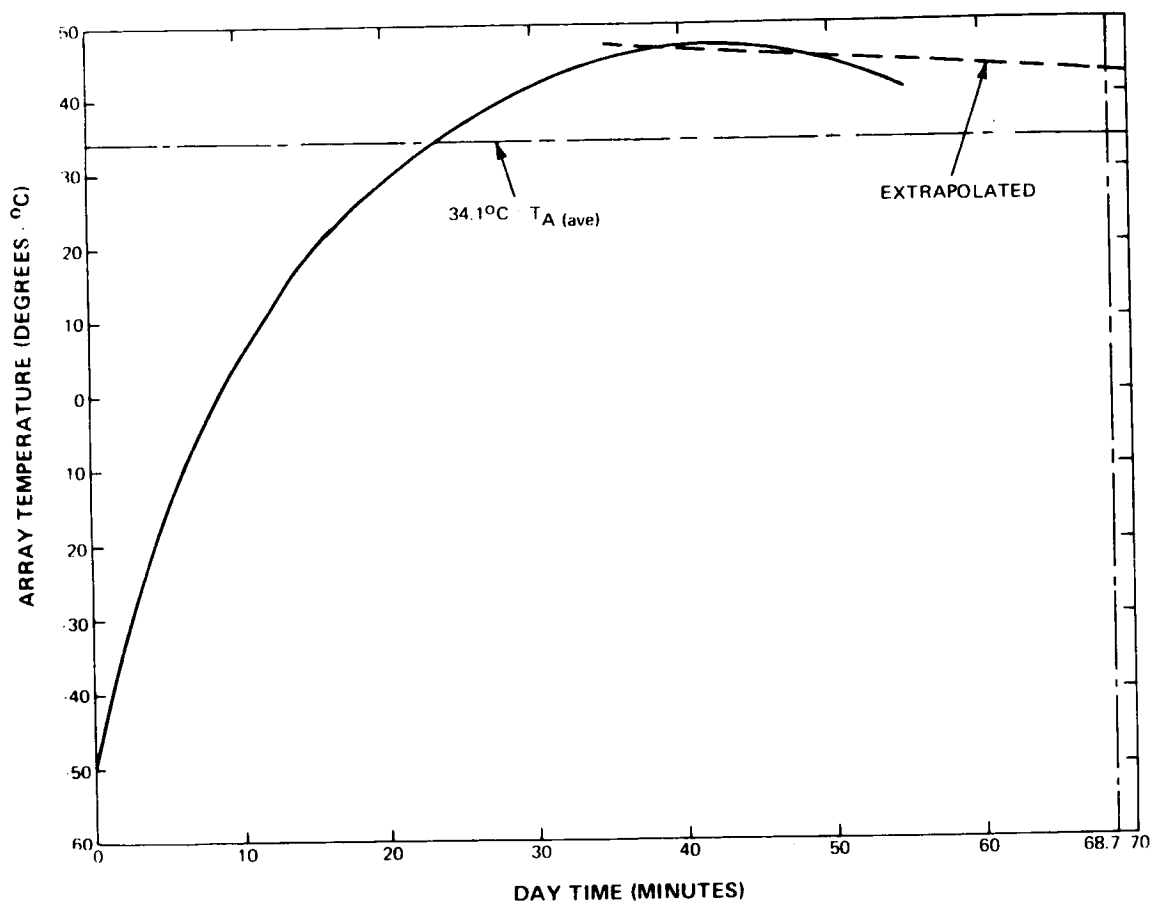


Figure 2.9. Nimbus A, F-1 Average Array Temperature vs. Day Time (Orbit 15 Data)

a. Nimbus A Power System

This system, in its rudimentary form as shown in Figure 2-10, will be the base-line system for the following analysis.

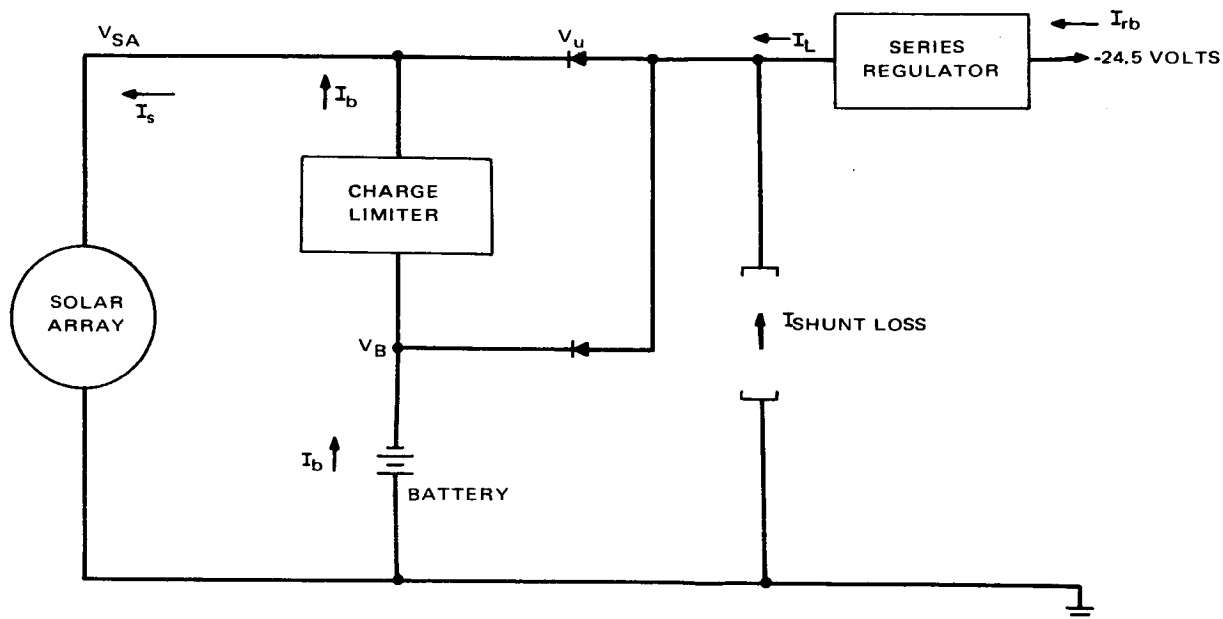


Figure 2-10. Rudimentary Form of Nimbus A Power Supply Subsystem

Here, there is a direct correspondence between load and battery, and array current. As such, the average daytime array current required to support the load power profile may be determined and used to estimate orbital life. Figure 2-11 shows the load power profile converted to load current at the -24.5 volt bus with shunt losses of 1.2 amperes (day) and 0.8 ampere (night) added. The regulated bus current, I_{rb} , is equal to the load current, I_L , using the passive series voltage regulator.

An energy balance equation in terms of ampere-minutes determines the average array current (I_s) required per orbit.

$$\int_{T_D} i_s dt = \int_{T_D} i_{load} dt + K_B \int_{T_D + T_N} i_{Battery Discharge} dt \quad (2.1)$$

where K_B = charge-to-discharge ratio of battery, a function of temperature. Assume $K_B = 1.2$

and, from Figure 2-11

$$\begin{aligned} 68.7 I_s = & \left[(5.57 \times 9.9) + (7.75 \times 44.8) + (6.2 I_s) \right. \\ & \left. + (5.9 \times 3.3) + (5.57 \times 4.5) \right] \\ & + 1.2 \left[(14.55 - I_s) (4.1) + (11.85 - I_s) (2.1) \right. \\ & \left. + (5.17 \times 34.9) \right] \end{aligned} \quad (2.2)$$

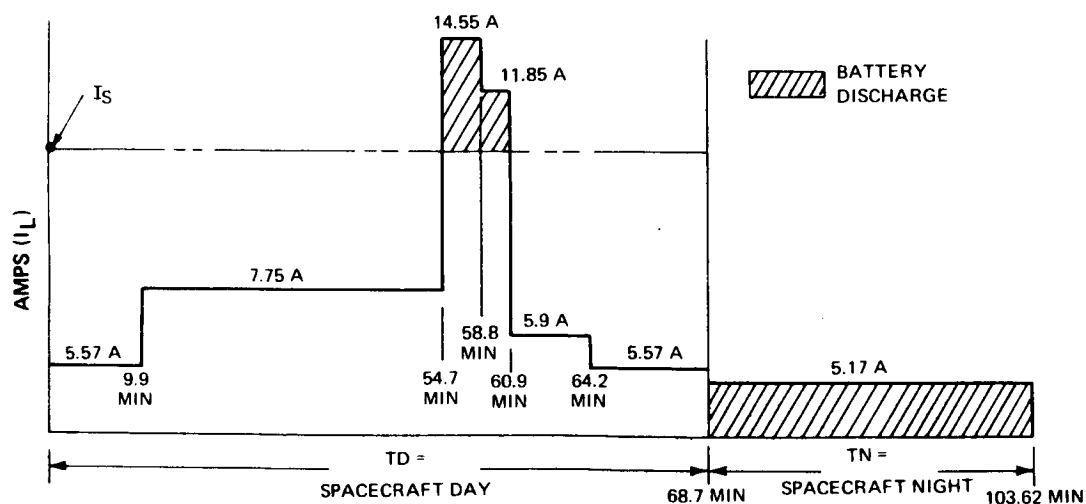


Figure 2-11. Load Current Profile Including Shunt Losses

solving for I_s ,

$$I_s = 10.9 \text{ amperes}$$

This is the minimum average array current required per orbit to maintain positive energy balance with the Nimbus A power system.

This current must be delivered to the power system at an unregulated voltage level V_u which is compatible with the series regulator, battery, and charge limiter.

Assume (for nominal operating temperatures):

$$\text{Average } V_B \text{ charge} = 1.42\text{V/cell} \times 23 \text{ cells} = 32.16 \text{ V}$$

$$\text{Charge limiter} + \text{diodes} + \text{other insertion loss} = 2.0\text{V}$$

$$\text{Total} = 34.16\text{V}$$

$$\text{Allow } V_{SA} = 34 \text{ V}$$

Therefore, the array must deliver 10.9 amperes (average) at 34 volts (average). Figure 2-12 is a plot of array current available at 34 volts for the Nimbus A solar array as a function of time in orbit and with temperature as a parameter. The average daytime array temperature is obtained from Figure 2.9 as 34.1°C . The array current characteristic for this temperature will fall between those for 28°C and 55°C in Figure 2-12.

On this basis, the estimated operational life for the above power system is approximately 100 days in orbit.

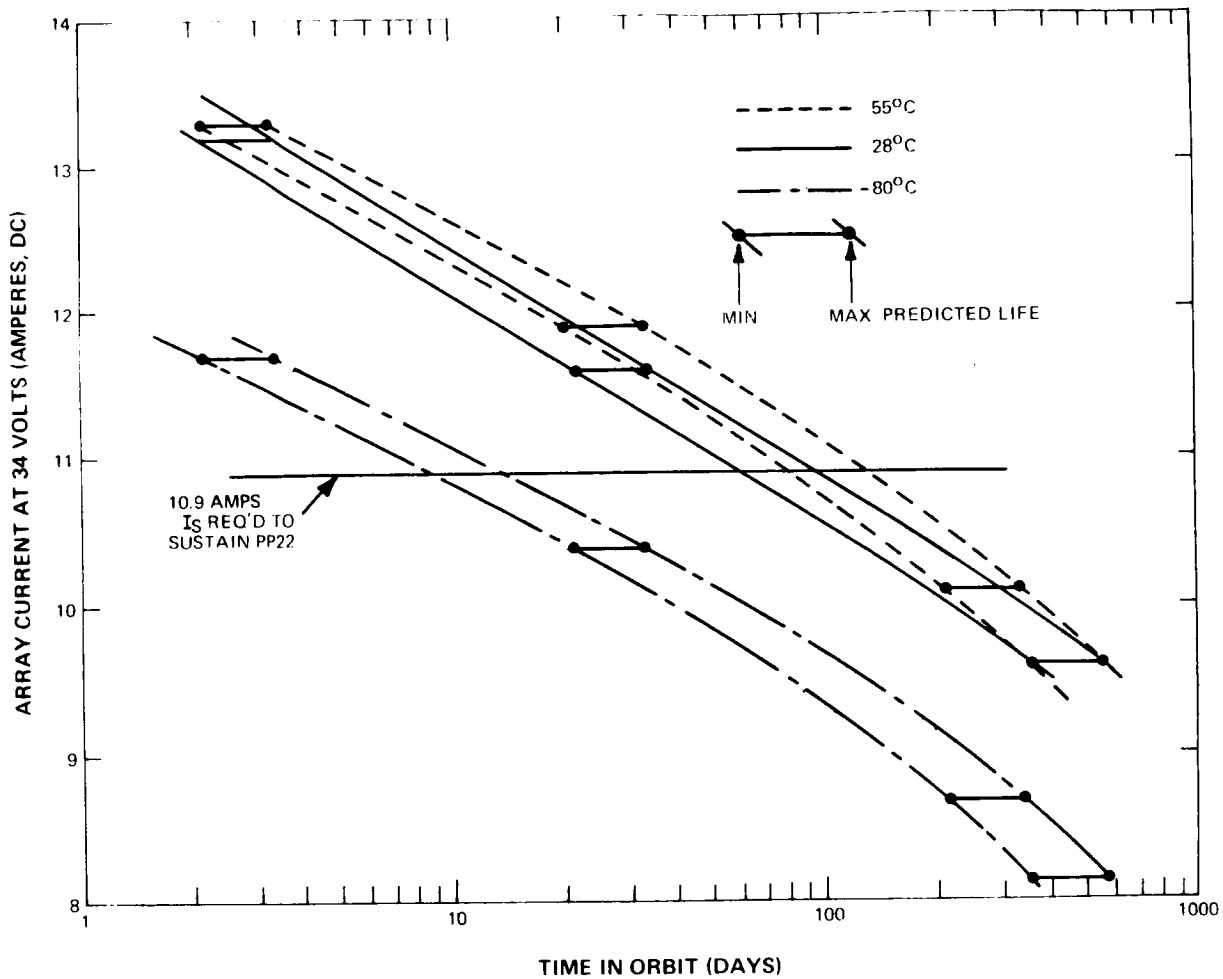


Figure 2-12. Nimbus A Solar Array Available Current at 34 Volts vs. Time and Temperature

b. Modified Nimbus A Power System

The power system shown on Figure 2-10 was modified by substituting a PWM voltage regulator for the passive series regulator.

Analysis of this system requires that the load power profile be expressed in terms of current at the regulator input. This is accomplished by applying the assumed regulator efficiency factor $\eta_t = 0.9$ to the load power and converting to current for

an average unregulated bus voltage as follows:

Average unregulated bus voltage when battery is charging is:

$$V_{uch} = V_{SA} - V_D = 34.0 - .45 \approx 33.5 \text{ volts}$$

Average unregulated bus voltage when battery is discharging is:

$$\begin{aligned} V_{ud} &= V_{bd} - V_D \\ &= (1.2 \text{ V/cell} \times 23 \text{ cells}) - .45 = 27.6 - .45 = 27.15 \end{aligned}$$

Allow $V_{ud} = 27V.$

In addition, a daytime shunt loss of 0.4 amperes is included for the charge controller and other losses. The effective load current profile is shown in Figure 2-13.

Solving by means of Equations (2.1) and (2.2)

$$I_s = 8.73 \text{ amperes}$$

is the minimum average array current required to maintain the system in positive energy balance. This is 80.1 percent of the current required by the Nimbus A system.

This creates an average current of

$$\Delta I_s = I_s - I_{s \text{ required}} = 10.9 - 8.73 = 2.17 \text{ amperes}$$

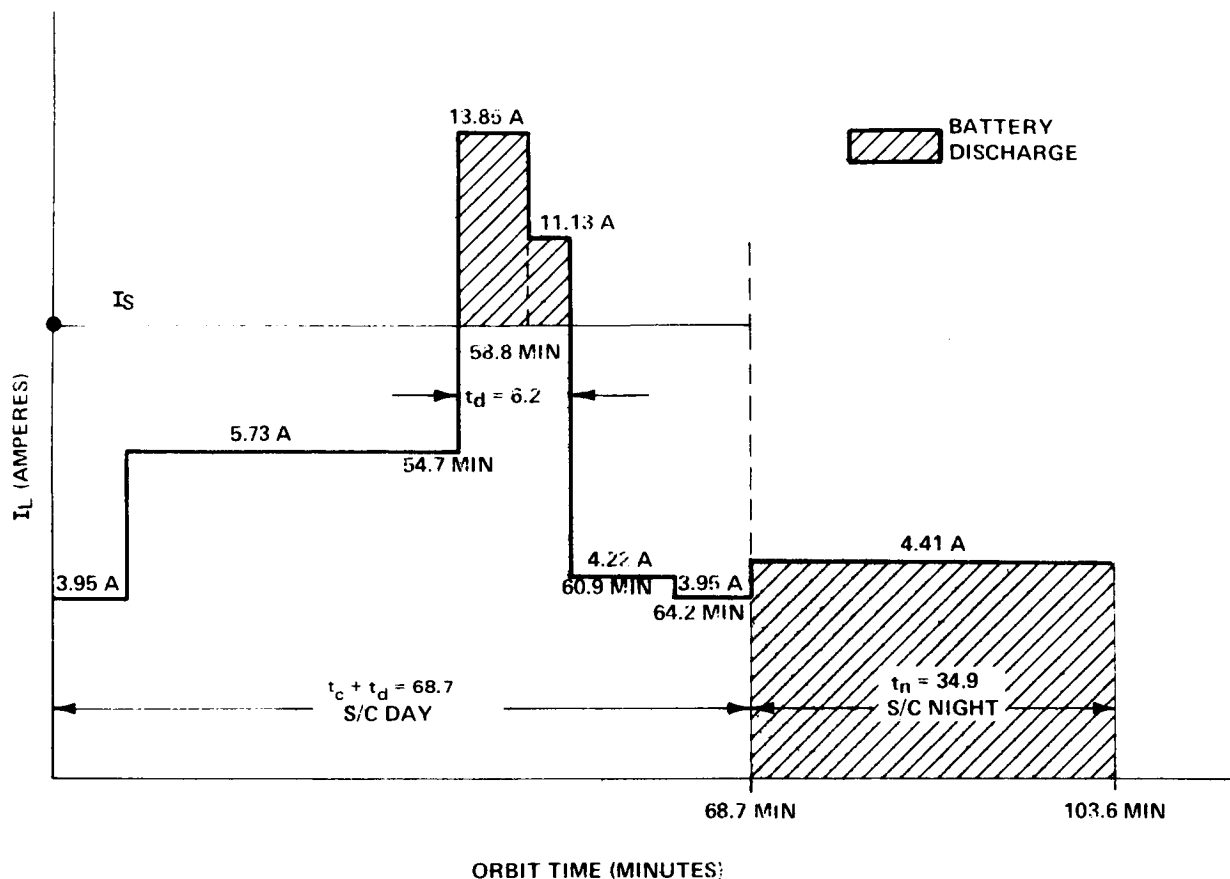


Figure 2-13. Effective Load Current Profile (Including Shunt Losses)

which is available for programming additional loads for the 100 day orbital lifetime. Assume the added load is constant throughout the orbit and is given by:

$$\Delta P_L = \frac{\eta_T \Delta I_s (t_c + t_d)}{\left[\frac{t_c}{V_{uch}} + \frac{t_d}{V_{ud}} + K_B \frac{t_n}{V_{ud}} \right]} \quad (2.3)$$

where:

$\eta_t = 0.9$ is regulator average efficiency

$\Delta I_s = 2.17$ amperes is the excess array current

$t_c = 62.5$ minutes is duration of daytime battery charge

$t_d = 6.2$ minutes is duration of daytime battery discharge

$t_n = 34.9$ minutes is duration of nighttime battery discharge

$K_B = 1.2$ is battery charge-to-discharge ratio

and

$$\Delta P_L = 36.7 \text{ watts}$$

The average day and night load power is given by:

$$P_{oave} = \frac{1}{t_c + t_d + t_n} \int_{t_c + t_d + t_n} p \, dt \quad (2.4)$$

and may be calculated to give

$$P_{oave} = 142.5 \text{ watts for the load profile of Figure 2-8.}$$

The increased load capability is then given as

$$P_L \times 100 = \frac{36.7 \text{ watts}}{142.5 \text{ watts}} \times 100 = 25.8\% \quad (2.5)$$

c. Series MPT Power System

This system, in its basic form, is shown in Figure 2-14.

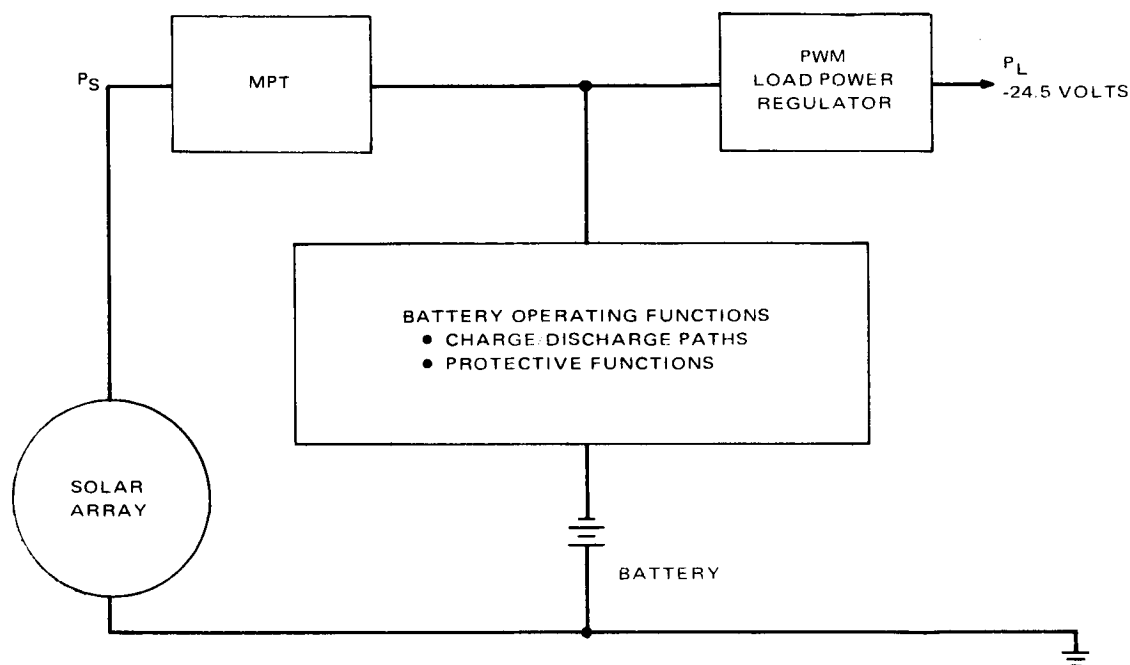


Figure 2-14. Basic Form of Series MPT Power System

The analysis of this system is not as definitive as that for the previously considered Nimbus A systems in view of the impedance transformation properties of the MPT and the load regulator, both being pulse-width modulation devices. A more fundamental form of energy balance equation must be employed to determine the minimum average array power (P_S) which will support the load profile.

Figure 2-15 shows spacecraft power requirements in terms of load power at the regulated bus.

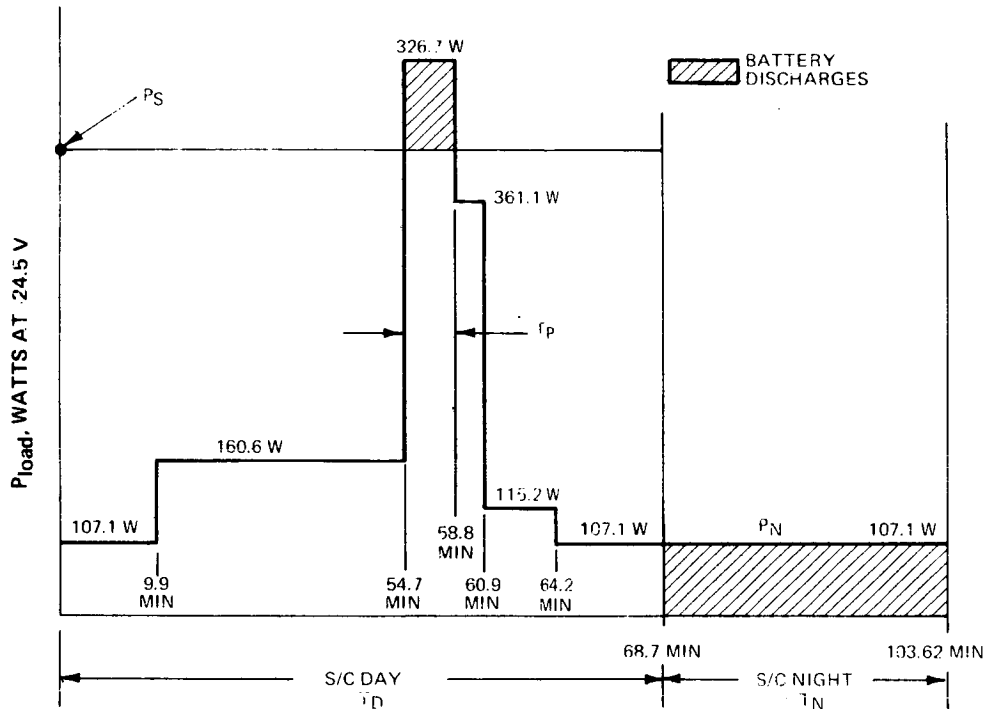


Figure 2-15. Load Power Profile in Watts at Regulated Bus

The energy balance equation relates average array energy, W_s (in watt-minutes), to load and battery energy.

$$W_s = \frac{W_{LA}}{\eta_a} + \frac{\eta_d}{\eta_b \eta_c} \left(\frac{V_{BC}}{V_{BD}} \right) (W_{LB} + W_N) \quad (2.6)$$

where

- W_{LA} = load energy directly from array
- W_{LB} = load energy from battery during T_D
- W_N = load energy from battery during T_N
- η_a = array to load power transfer efficiency
- η_b = battery to load power transfer efficiency
- η_c = array to battery power transfer efficiency
- η_d = battery charge/discharge ratio
- V_{BC} = average cell charge voltage
- V_{BD} = average cell discharge voltage
- P_L = load power
- P_S = average source power

By definition,

$$W = \int p \, dt \quad (2.7)$$

where: p = instantaneous power

and

$$\begin{aligned} \int_{T_D} p_s \, dt &= \frac{\eta_d}{\eta_b \eta_c} \frac{V_{BC}}{V_{BD}} \left[\int_{T_D} p_L \, dt \Big|_{p_L < p_s} + \int_{T_N} p_n \, dt \right] \\ &+ \frac{1}{\eta_a} \int_{T_D} p_L \, dt \Big|_{p_L < p_s} \end{aligned} \quad (2.8)$$

this expression may be evaluated directly from Figure 2-15 and the following values for the constants involved.

$$\begin{aligned}\eta_a &= 0.81 \text{ average} \\ \eta_b &= 0.9 \text{ average} \\ \eta_c &= 0.9 \text{ average} \\ \eta_d &= 1.2 \\ V_{BC} &= 1.42 \text{ volts/cell} \\ V_{BD} &= 1.2 \text{ volts/cell}\end{aligned}$$

and,

$$\begin{aligned}68.7 P_s &= \left(\frac{1.2}{.9 \times .9} \right) \left(\frac{1.42}{1.2} \right) \left[4.1 (326.7 - P_s) + 34.92 (107.1) \right] \\ &+ \frac{1}{.81} \left[9.9 (107.1) + 44.8 (160.6) + 4.1 P_s \right. \\ &\left. + 2.1 (261.1) + 3.3 (115.2) + 4.5 (107.1) \right] \quad (2.9)\end{aligned}$$

solving equation (2.9) for P_s

$$P_s = 313 \text{ watts}$$

is the minimum average array power which will support the load with the series MPT power system. This is 73.6 percent of the available average array power of 425 watts.

Figure 2-16 is a plot of available array power (i.e. at the maximum power point) versus array temperature with orbital life time as a parameter.

Figure 2-16, used in conjunction with the array temperature profile of 2.9, yields the array power as a function of sun time. Performing time integration over an orbit then provides the average available array power which is shown versus time-in-orbit in Figure 2-17.

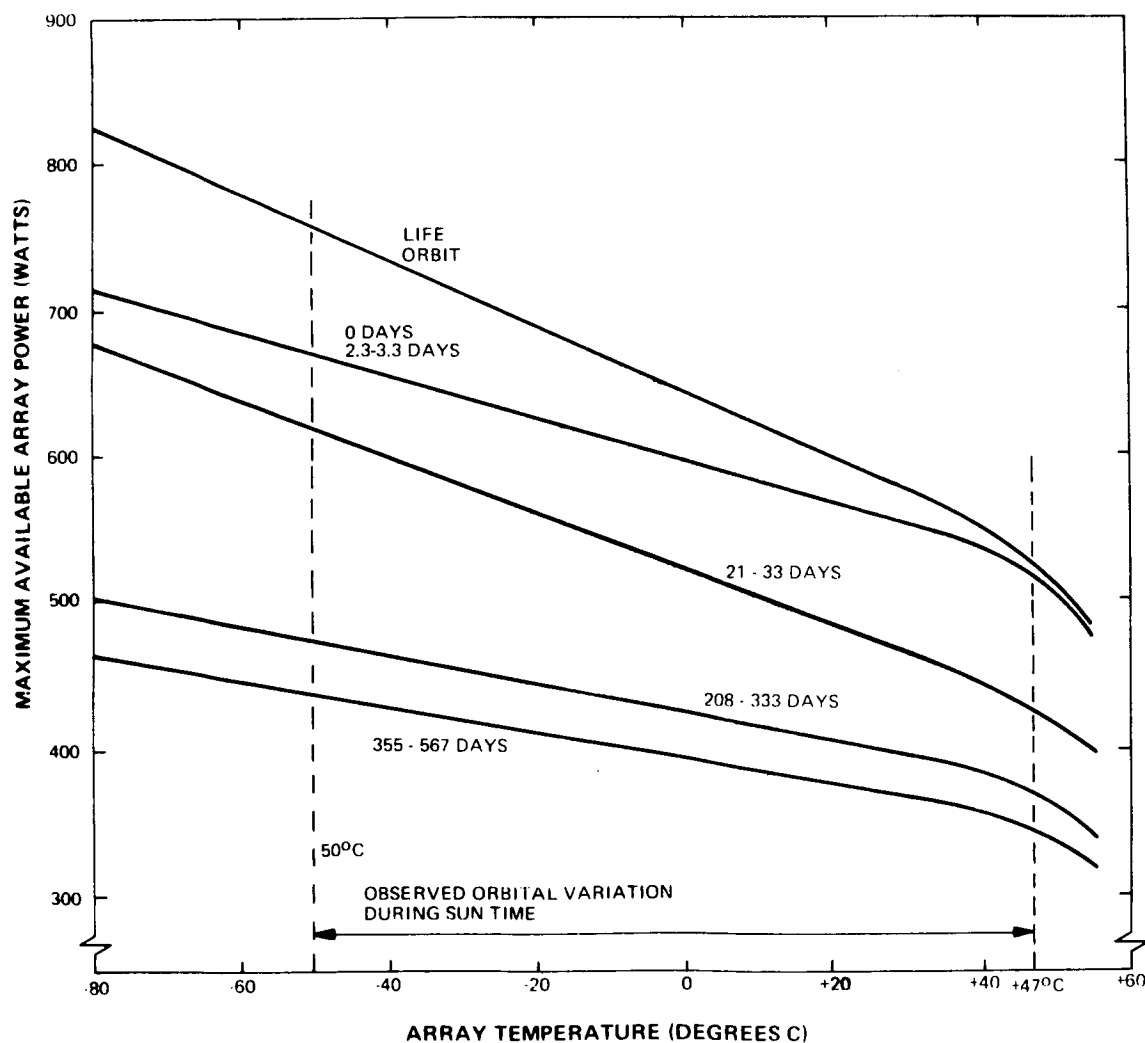


Figure 2-16. Maximum Available Power vs. Array Temperature (RCA Predictions for Nimbus A Solar Array with Life in Orbit as a Parameter.)

Note that the MPT system could permit operation in excess of 600 days in orbit based on Figure 2-17.

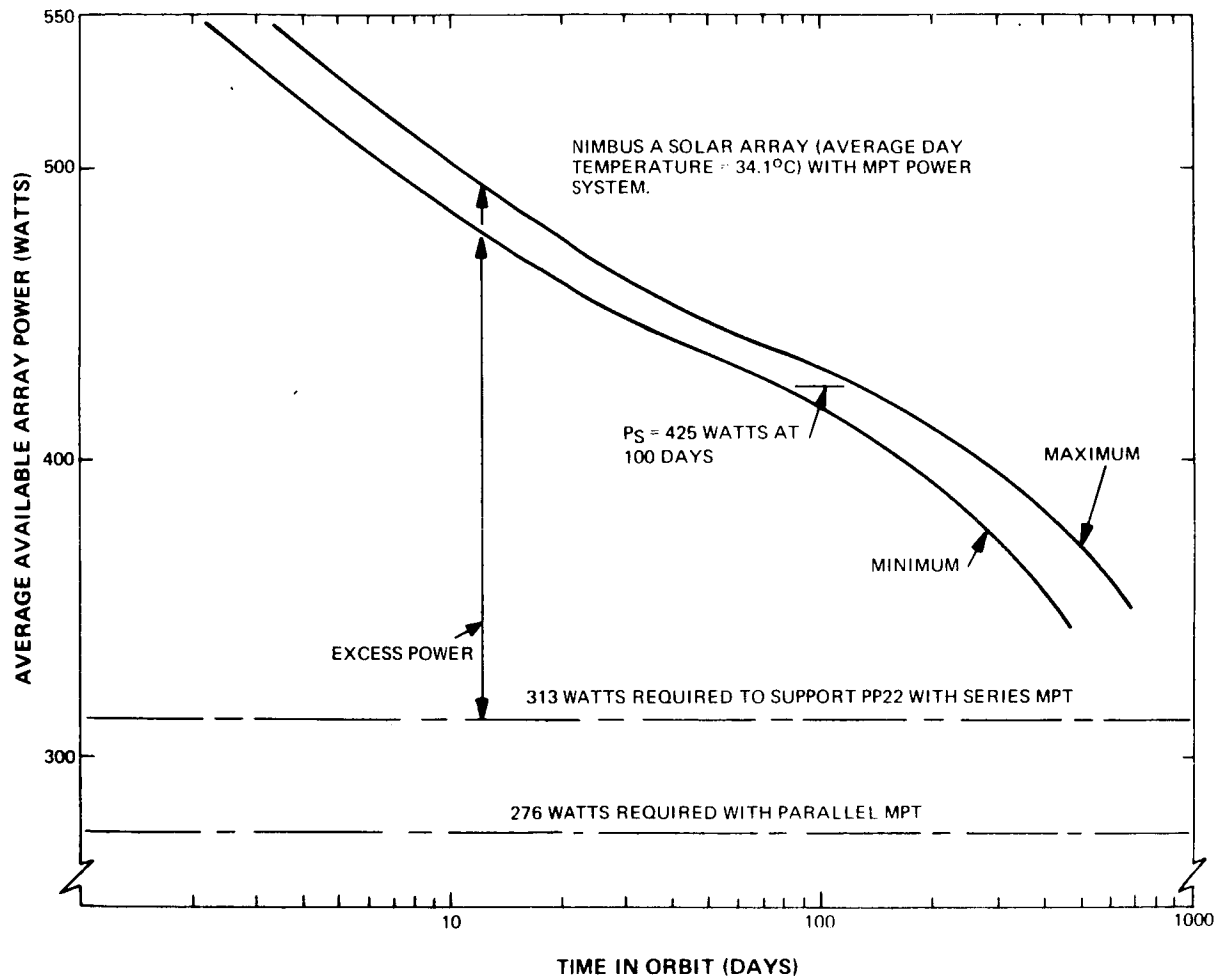


Figure 2.17. Average Available Array Power vs. Life in Orbit

After 100 days in orbit, a system using a series MPT will have an excess power of

$$\begin{aligned}\Delta P_S &= P_{s \text{ available}} - P_{s \text{ required}} \\ &= 425 \text{ watts} - 313 \text{ watts} = 112 \text{ watts}\end{aligned}\tag{2.10}$$

which is available for additional load programming, thus increasing the usefulness and versatility of the spacecraft.

If this excess power were used to charge batteries, it would result in an increase in nighttime load power as follows:

The additional nighttime load,

$$\Delta P_N = \frac{\Delta P_S T_D}{T_N} \frac{\eta_b \eta_c}{\eta_d} \frac{V_{BD}}{V_{BC}} \quad (2.11)$$

$$\Delta P_N = \frac{112 \times 68.7}{34.92} \frac{0.9 \times 0.9}{1.2} \frac{1.2}{1.42}$$

$$\Delta P_N = 125.8 \text{ watts}$$

or, the total average nighttime load capability would be

$$P_N = P_{NO} + \Delta P_N = 107.1 + 125.8 = 232.9 \text{ watts} \quad (2.12)$$

As the basis for comparison with the other system, assume the extra load power is evenly distributed over the entire orbit as:

$$\Delta P_L = \frac{\Delta P_S T_D}{\left[\frac{T_D}{\eta_a} + \eta_d \frac{T_N}{\eta_b \eta_c} \left(\frac{V_{bc}}{V_{bd}} \right) \right]} \quad (2.13)$$

$$\Delta P_L = \frac{112 \times 68.7}{\left[\left(\frac{68.7}{.81} + 1.2 \right) \times \left(\frac{34.92}{0.9 \times 0.9} \right) \left(\frac{1.42}{1.2} \right) \right]}$$

$$\Delta P_L = 52.7 \text{ watts of additional loads}$$

The increase in load capability is then given as

$$\frac{\Delta P_L}{P_o} 100 = \frac{52.7}{142.5} \frac{\text{watts}}{\text{watts}} 100 = 37.0\% \quad (2.14)$$

for the series MPT system.

d. Parallel MPT Power System

The basic configuration of the parallel MPT is as shown in Figure 2-4.

The analysis follows that of the series MPT exactly except for different efficiency factors. The following values for the constants are use,

$$\begin{aligned}\eta_a &= 0.9 \text{ average} \\ \eta_b &= 0.9 \text{ average} \\ \eta_c &= 0.9 \text{ average} \\ \eta_d &= 1.2\end{aligned}$$

Re-evaluating Equation 2.8, it is found that the minimum average array power which will support the assumed load profile is

$$P_s = 276 \text{ watts}$$

Again from Figures 2-16 and 2-17, it is shown that the expected operational life will be greater than 600 days in orbit.

The excess source power after 100 days in orbit is

$$P_s = 149 \text{ watts}$$

Assuming the excess source power is evenly distributed over the entire orbit, the additional load is calculated using Equation (2.13) as:

$$\Delta P_L = 71.0 \text{ watts}$$

The increase in load capability is given as:

$$\frac{\Delta P_L}{P_o} 100 = \frac{71.0 \text{ watts}}{142.5 \text{ watts}} 100 = 49.8\%$$

e. System Comparison

From the foregoing analyses, it can be seen that the parallel maximum power tracking system is the most efficient one, based on either load capability or useful operational life. The following list shows the relative additional load capability of each system based on 100 days in orbit with a Nimbus A solar array:

Nimbus A (passive regulator) relative load power	= 100% (baseline)
Modified Nimbus A (PWM regulator)	= 126%
Series MPT w/PWM regulator	= 137%
Parallel MPT w/PWM regulator	= 150%

By applying the advantage gained from the use of a power tracking system, the size of the solar array can be reduced. The following list shows the relative solar array requirements based on 100 days in orbit with the Nimbus A solar array and the load profile of Figure 2-8:

Nimbus A (passive regulator) relative array output	= 100% (baseline)
Modified Nimbus A (PWM regulator)	= 80%
Series MPT w/PWM regulator	= 74%
Parallel MPT w/PWM regulator	= 65%

2.2.2 Scan Frequency and Tracking Accuracy

The frequency at which the system oscillates about the maximum power point in steady-state operation and the accuracy of the tracking controls may be evaluated from the system parameters.

The scan frequency is given by

$$f_s = \frac{R}{2^{V_b} \left(\frac{1}{V_{sL}} - \frac{1}{V_{su}} \right)} \quad (2.15)$$

where:

f_s = the scan frequency in cycles per second.

R = the rate at which the power switch duty-cycle is changed by the scanner in %/100 per second.

V_B = the power tracker output (battery) terminal voltage.

V_{sL} = the lower scan limit of the source voltage.

V_{su} = the upper scan limit of the source voltage.

In order to evaluate the equation, it is necessary to determine the limits of the source voltage, V_{sL} and V_{su} . These limits are a function of the sensitivity of the output-current peak detection circuitry, the power-transfer efficiency of the tracker system, and the I-V characteristic of the source (solar array). A solution using an analytical expression for the solar array I-V Characteristic results in a transcendental equation which may be solved by computer.

A more practical method for evaluating the source voltage limits is by means of graphical analysis. The maximum error in input power is given as

$$\Delta P_s = \frac{\Delta I_b V_B}{\eta_T} \quad (2.16)$$

where:

ΔP_s = is the maximum difference between the maximum source power and the source power used.

ΔI_b = is the maximum change in output current before scan reversal i.e., the sensitivity of the output-current-peak-detector.

η_T = is the power transfer efficiency of the tracker system.

The power equation is given as:

$$P_s = P_{s \max} - \Delta P_s \quad (2.17)$$

where:

P_s is the source power actually used.

$P_{s \max}$ is the maximum source power,

which may be solved graphically as shown in Figure 2-18, permitting evaluation of the scan frequency.

Continuation of the analysis permits an expression for the tracking accuracy to be found.

From Equation (2.17),

$$P_s = P_{s \max} (1 - E_T) = P_{s \max} \left(1 - \frac{\Delta I_b V_B}{\eta_T P_{s \max}} \right) \quad (2.18)$$

where:

$$E_T = \frac{\Delta I_b V_B}{\eta_T P_{s \max}} \text{ is the tracking error, and}$$

$(1-E_T)$ = the tracking accuracy.

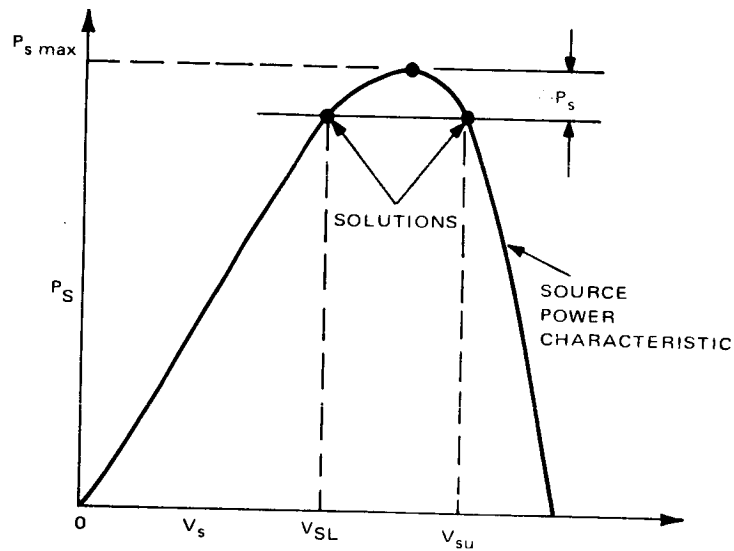


Figure 2-18. Graphical Solution for V_{SL} and V_{SU}

Thus, the effectiveness of the power tracking system in maintaining the operating point of the source at its maximum power point may be evaluated. Design control of the tracking error is obtained by varying the peak detector sensitivity (ΔI_b).

Control of the scan frequency may be obtained by varying the scan rate (R) and the peak detector sensitivity (ΔI_p). The details of the derivation of the above equations are presented in Appendix III.

2.3 System Operational Description

2.3.1 System Function

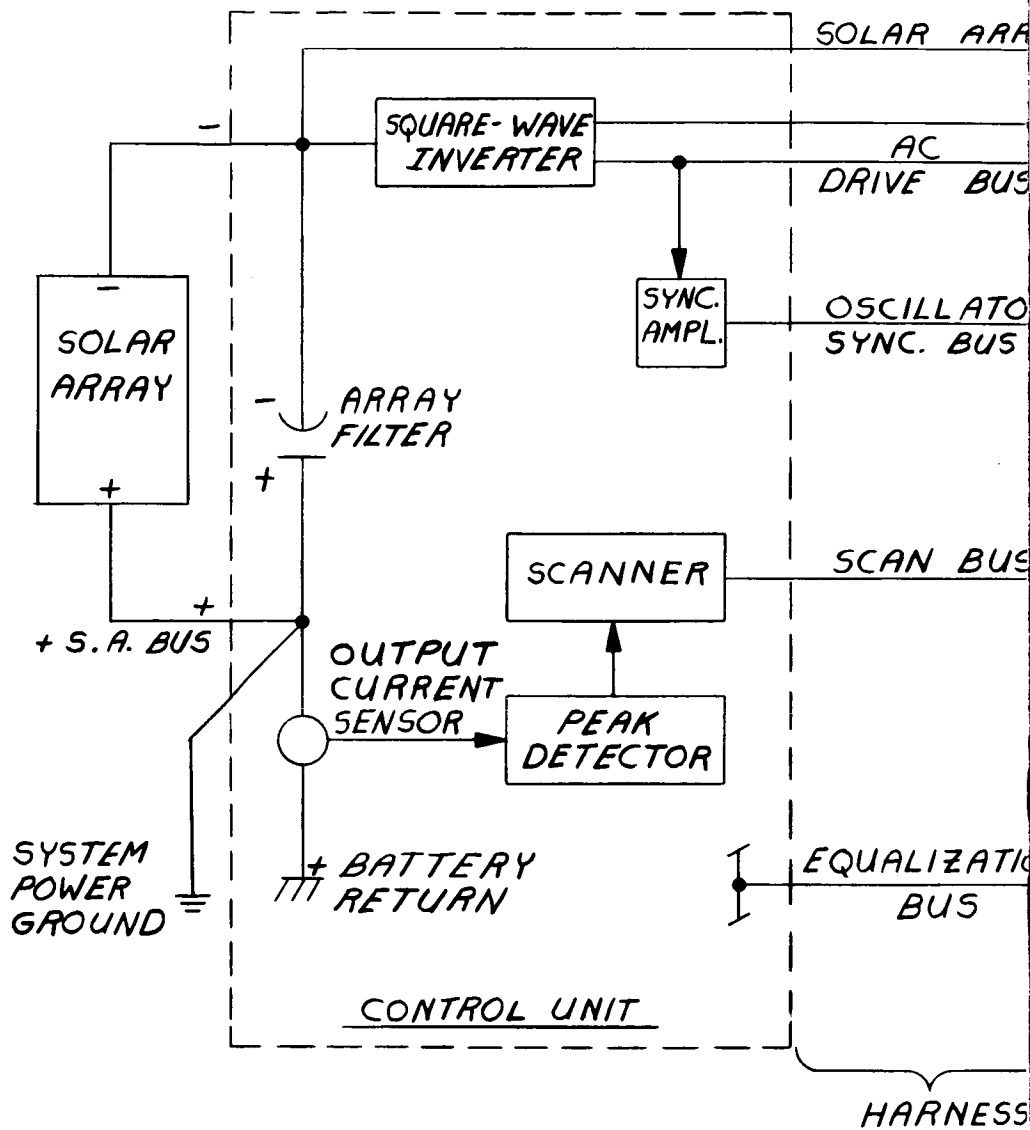
The function of the Maximum Power Tracker is to provide for the maximum transfer of energy from the source (solar array) to the energy storage devices (batteries). This takes into account the voltage and current limitations of the batteries and the present capability of the source. The various operating modes are described below. A system functional diagram is shown on Figure 2-19.

2.3.2 Modes of Operation

The Maximum Power Tracker has two basic modes of operation, corresponding to orbital day and night.

a. Discharge Mode

The discharge mode occurs during the dark or night portion of the orbit. Operation of the Maximum Power Tracker during this mode is as follows:



2

FOLDOUT FRAME 1

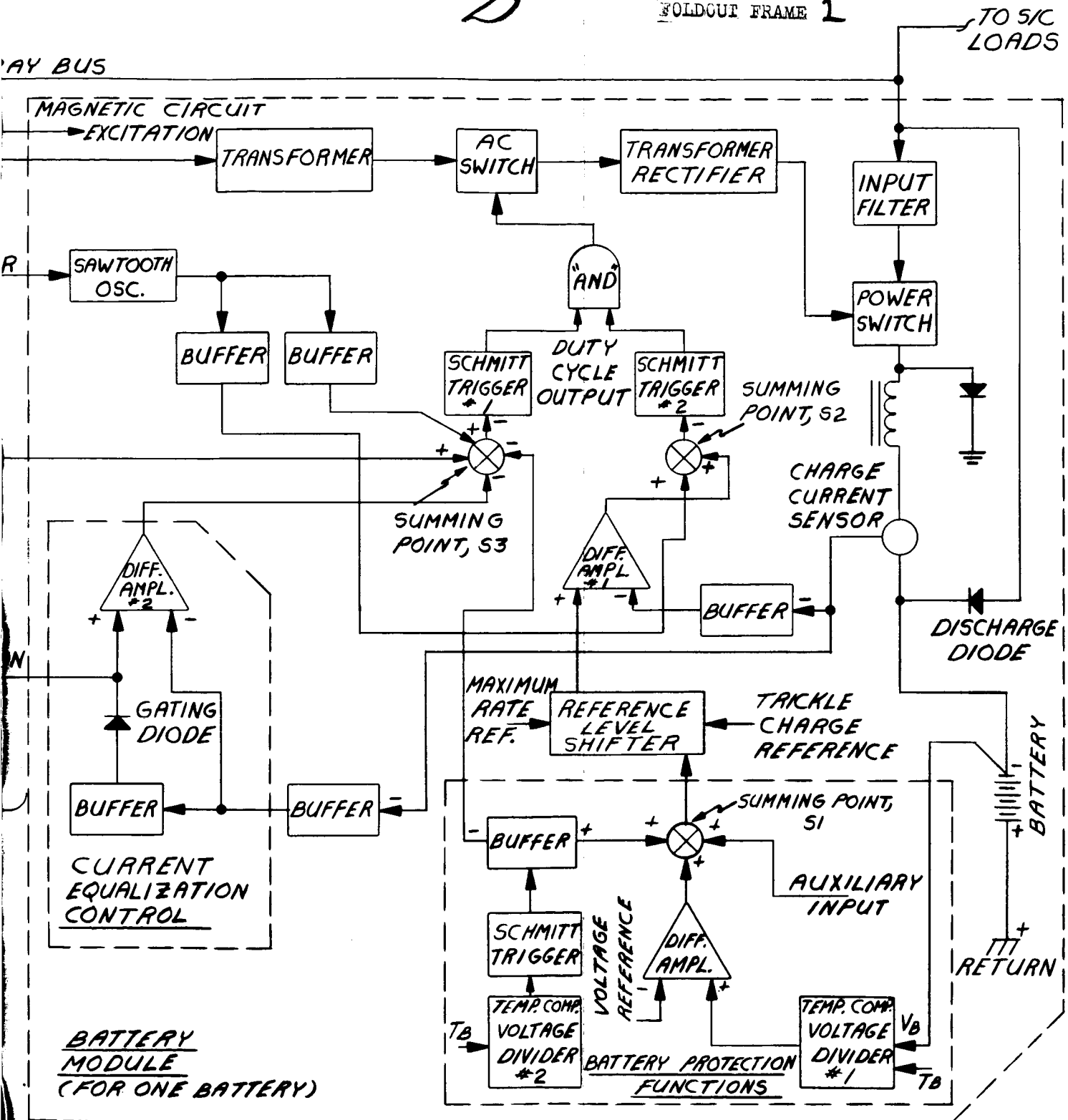


Figure 2-19. Maximum Power Tracker, Functional Diagram
(RCA Dwg. SK 1968309)

The beginning of spacecraft night is characterized by the source (array) output becoming essentially zero. The solar array bus voltage falls until it is slightly lower than the battery voltage, at which time the discharge diodes become forward biased. The batteries now supply the load power requirements through the discharge diodes. Note that with the discharge diodes conducting, the battery charge electronics cannot function.

b. Charge Mode

The normal charge mode occurs during the daylight portion of the orbit and can be considered for three conditions of source capability. The first is the capability of the array to supply more power than the batteries and spacecraft loads require; the second occurs when the array can supply both the battery and load requirements only if active control of the operating point is used; and the third is that in which the array can no longer satisfy the requirements of both loads and batteries.

(1) Excess Array Capability

In this condition, the source has more power available than the loads and the batteries require and the array is operated (off the maximum power point) on its I-V characteristic at a point as determined by the actual system load requirements. This is essentially a fixed operating point operation.

a. Control Unit

The current sensor, peak detector, and scanner functions are not required in this case and are not permitted to control the operation by the battery modules. They do however, continually attempt to sense the maximum power point of the source. The square-wave inverter is used to provide drive and synchronization for all the battery modules.

b. Battery Module

The operation of a battery module is as follows: In this mode, the battery voltage and temperature are assumed to be within the acceptable limits and no signal is applied to the reference level shifter from the battery protective function(s). The array is activated as the spacecraft enters the daylight portion of the orbit and the batteries begin to charge. The reference-level-shifter output senses that the maximum charge current is allowable. This current level is preset and is designed into the equipment, however, manual adjustment over the range from 12 to 15 amperes is provided.

Since there is excess array power available, the batteries will charge at the maximum allowable rate. The charge-current sensor provides an analog output

which is applied to difference amplifier No. 1 where it is compared with the signal from the reference level shifter. If the current sensed is greater than maximum allowable current, then the output to summing point S_2 increases. Also at point S_2 , the synchronized sawtooth signal which determines operating frequency is added to the charge-current-error signal. This combined signal is threshold-detected by Schmitt trigger No. 2. The Schmitt trigger output controls the a-c switch which applies and removes the drive from the power switch. An increasing output from difference amplifier No. 1 results in an increasing duty cycle (off time) of Schmitt trigger No.2, thereby increasing the on time of the power switch, which in turn, tends to decrease the charge current.

The charge current sensor output is also applied to the charge-current-equalization comparator where it is compared with the current levels in other battery modules. An error signal is generated and is applied to summing point S_3 , to adjust the power switch duty cycle and compensate for the unequal currents. In addition, the scanner and the sawtooth signals are added to the summing point, S_3 . The total signal at point S_3 determines the duty cycle of the power switch when the protection functions are inactive. Since the array power is greater than

the load demand, the deliverable current (if the array were operated at the maximum power point) is greater than the limiting current, as determined by the protection function. The AND function input to the a-c switch allows the Schmitt trigger (modulator), to be activated for a shorter period of time to control the power switch duty cycle. Therefore, the current limiting protective function (which requires a shorter duty cycle) controls the power switch, causing the maximum power tracking function (Schmitt trigger No.1) to be inhibited.

An automatic adjustment is made to the charge rate when the protection functions detect overvoltage, high temperature conditions, or when an auxiliary input signal is sensed. At this time a signal is generated at summing point S1, which causes the reference level shifter output to provide the trickle charge rate reference to difference amplifier No. 1. When this decrease in maximum allowable charge current occurs, the action of all functions is as described above, except that the system is operated at a lower quiescent point.

- c. The operation under conditions of excess array capability can be summarized as follows: The charge current is limited to preset values which

have been established for safe battery charging. The source is biased to a point which satisfies the demands of both the loads and the batteries. This condition would normally occur during the beginning of a mission (before the array has degraded) or later in the mission if load power requirements are unusually low. Note that transition between this operating condition and those to be discussed below is automatic.

(2) Sufficient Array Capability

In this state, the solar array (source) has enough power capability to satisfy the requirements of the loads and charge the batteries, if active control is exercised over its operating point. If a fixed operating point were to be used, the batteries might not be fully recharged each orbit and the spacecraft would not be in positive energy balance.

a. Control Unit

The control unit is designed to detect the maximum power point of the source and to exercise control over the battery charge modules such that the source is operated at or near that point.

The output current sensor provides a signal which is proportional to instantaneous power at the operating point. This signal is then fed to the peak detector which monitors the instantaneous power.

Noting that the battery module contains a constant frequency, pulse-width modulated, regulator, the output (battery) voltage is proportional to the input (array) voltage by a factor equal to the power switch duty cycle. The output voltage is essentially fixed by the battery so that by controlling the duty cycle the battery input voltage is controlled. If these variations in duty cycle are controlled, then the operating point of the source is being controlled. In this system, control of the duty cycle is derived from detection of the source maximum power point as indicated by the output current.

The scanner generates a signal which is capable of varying the duty cycle from 0 to 100 percent corresponding to all possible source operating points. The scanner is free-running and automatically reverses if it reaches 0 or 100 percent duty cycle before maximum power is detected.

To understand the acquisition and tracking of the maximum power point, assume that the scanner is indicating zero percent duty cycle and its output is changing towards an indication of 100 percent duty cycle. As the scanner output changes, the duty cycles of the battery module power switches are increasing and the source voltage decreases as determined by battery voltage and duty cycle.

For the system configuration shown on Figure 2-19, it is necessary to assume that the source has a point of maximum power and that this point is at some voltage greater than the battery voltage.

It should be noted that other systems can be devised using the same basic concept and similar techniques for different sources (e.g. voltage at maximum power is less than battery voltage). The discussion applies to this configuration only. If this were not assumed, then duty cycles in excess of 100 percent would be required to operate at the maximum power point. The only necessary assumption for the power tracking system is that the source has a point of maximum power. As the source voltage decreases, the source power output increases.

The instantaneous output current is sensed and fed to the peak detector which compares this level to the previous level which was sensed. If the most recent sensed level is of an increase

in source power output over the previous level, the the new level replaces the previous one in a memory device and the process repeats. If the most recent sensed level is of a decrease in source output power, then a signal is transmitted which causes the scanner to reverse direction (towards zero percent duty cycle) and the most recent sensed level replaces that previously applied to the memory device. Note that it is necessary to pass the maximum power point in order to detect the peak power and that as the duty cycle now decreases, the source output power is again increasing and the entire process repeats. In this manner the source operating point continually makes small excursions to either side of the maximum power point and tracks that point, performing system adjustments automatically. Operation does not depend on the initial conditions of the scanner.

b. Battery Module

The battery module circuits act in response to sensed battery conditions, and duty-cycle control information received from the power-tracker control unit.

In this mode, it is assume that the battery voltage and temperature are within the acceptable limits and that the charge current is less than the maximum allowable value as determined by the high-charge-limit reference. The duty-cycle required by the signal level at summing junction S_2 is greater than the duty-cycle required at summing point S_3 , thus the inputs to point S_3 will control the system operation.

The charge-current sensor applies an analog signal to the current-equalization comparator where it is compared with signals from the other battery modules. If the current level signal from the module under consideration is greater than that of the other modules, then the gating diode will be forward-biased and the higher signal will be applied to the other battery modules.

In this case the inputs to both sides of difference amplifier No. 2 are the same and there is no output and therefore, no change in the duty-cycle. If the signal level from the module being considered is less than that received from the other modules, then the gating diode is reverse-biased and an error signal is generated by difference amplifier No. 2. This causes a decrease in signal level at summing point S_3 , which results in a

decrease in the power-switch duty cycle and a corresponding increase in charge current. This adjustment process continues until all modules are carrying equal currents within an acceptable tolerance.

The duty cycle of the power switch is determined by the signal output of summing junction S_3 . The inputs to S_3 are (clockwise from output): Scanner-inhibit signal from battery-protection function, current-equalization error signal, synchronized sawtooth which determines operating frequency, and the scanner signal which determines the approximate duty cycle.

If the charge current should become greater than the maximum allowable value, as determined by the reference-level-shifter, then the current-limiting action will occur as described previously.

c. Summary

The operation under the conditions of sufficient array capability can be summarized as follows: The load demand is satisfied and the remainder of the maximum available power is used to charge the batteries. This is true, because the battery

electronics actively track the maximum point of the source and adjust the operating point to coincide with that point. This condition would normally occur throughout the major portion of the spacecraft lifetime. The MPT benefits are greatest towards the end of a mission (as the array degrades) and during those portions of the mission when the load power requirements are unusually high.

(3) Insufficient Array Capability

In this case, the source power is not adequate to supply the loads and recharge the batteries of each orbit. The maximum power point controls are operating and the source is operated at its maximum power point.

a. Control Unit

Operation of the control unit is as described in Paragraph(2)(a). The maximum power point of the source is tracked and is maintained as the system operating point.

b. Battery Module

The operation of the battery modules is controlled by the battery conditions and the power tracker control unit in the same manner as described in Paragraph (2)(b).

The significant difference between insufficient source capability and the previous cases is that the total ampere-hour discharge of the batteries is greater than the ampere-hour charge (per orbit) and the power system is not in positive energy balance.

c. Summary

The operation of the Maximum Power Tracker under the conditions of insufficient array capability is identical to that of sufficient array capability in that the power system is controlling the source operating point so that it is at the maximum power point. The difference is that energy balance is no longer positive. This condition could occur at the end of the mission (due to degradation of the array), when the load power requirements are exceptionally high, or if some failure occurred which reduced the source capability or increased the effective spacecraft load.

Note that in the above discussions of operating modes, it was assumed that the protective functions were inoperative. If at any time during the spacecraft operation, the system parameters described above are not within the established criteria, the system (or portion of the system) affected will automatically revert to the applicable protected mode.

Details of these functions and their operation are described in Paragraph 2.3.3.

2.3.3 Protection Functions

In order to ensure operation of the power system within the design parameters, certain protective functions have been incorporated into the battery module electronics. These functions automatically hold the system operation within established safe limits. Protected modes occur when certain system parameters do not agree with limiting or allowable values as determined by the system and black-box design specifications. These modes serve to protect the power system from premature failures due to improper operation.

a. Battery Voltage Limit

The maximum end-of-charge voltage characteristic of the battery and its variation with temperature are known. Sensing of the battery voltage to ensure that a maximum value is not exceeded is accomplished by temperature compensated voltage divider No. 1.

Temperature compensation (for battery temperature) is such that all points on the voltage-temperature curve of the battery appear as the same signal level at the divider output. This output is compared to a fixed reference by difference amplifier No. 3. If the battery voltage is below the maximum value, there will be no output from the difference amplifier. If battery voltage is greater than the allowable maximum, then a positive output is applied to the reference level shifter such that the shifter output senses that the maximum charge-current should be reduced to something less than the maximum rate is determined by the trickle-charge reference. System action is as previously described. The reduction in current level is controlled (as opposed to a switching operation) over a few millivolt range of battery voltages. Each battery module and battery is independent of the other modules. This function automatically resets when the battery voltage decreases below the maximum allowable value.

b. Battery Current Limit

The maximum charge current must be limited to a rate which is determined from battery considerations. The charge current is limited by the maximum current-reference signal applied through the reference-level shifter. This process has also been previously described. Each battery module has independent limiting of charge current.

c. Battery Temperature Cut-off

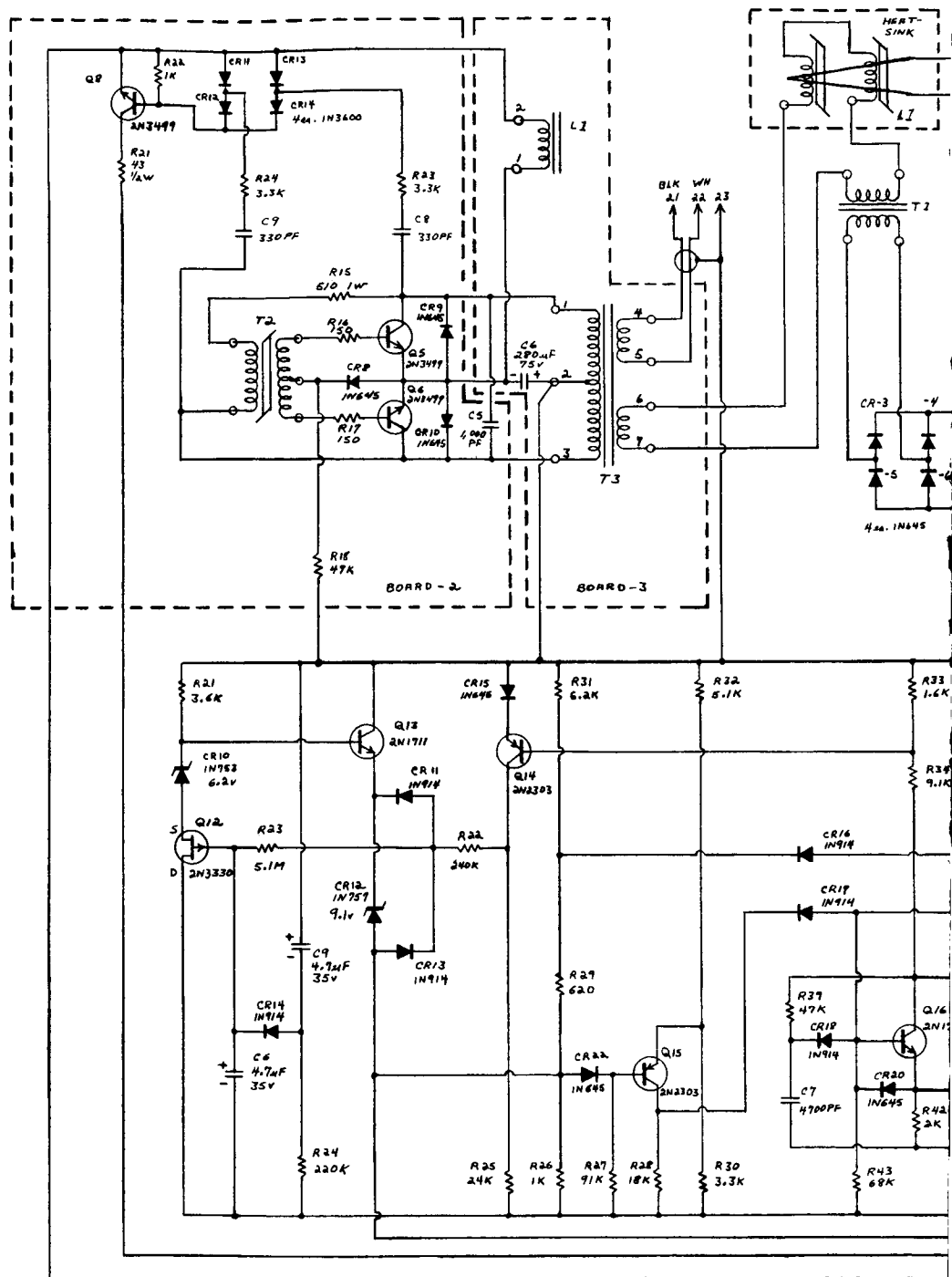
The battery charging process must be limited if the battery temperature exceeds a safe limiting value. A temperature-sensitive component of temperature compensated voltage divider No. 2 is physically located on, or near, the battery to sense temperature. If battery temperature exceeds a preset limit, the output of the divider exceeds the threshold level of the Schmitt trigger. This firing of the Schmitt trigger causes a signal to be applied to the reference level shifter which immediately establishes the trickle charge rate as the maximum allowable current. The trigger output is also applied to summing junction S_3 , to inhibit battery module operation in response to the scanner signal. The high-temperature protection function automatically resets when the battery temperature decreases below the preset safe value. A small amount of hysteresis is present to further protect the battery and prevent an oscillating condition. Each battery is independently protected.

2.4 Selected Circuit Descriptions

In addition to the maximum power tracker completed schematics, detailed descriptions of several unique circuits will be presented in this section.

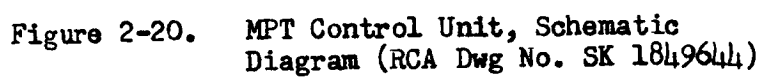
Schematic diagrams of the MPT Control Unit and a MPT Battery Module are shown in Figures 2-20 and 2-21 respectively.

FOLDOUT FRAME /



NOTES:

1. ALL RESISTORS IN OHMS $\pm 5\%$, $\frac{1}{4}$ W, CARBON COMP. UNLESS OTHERWISE NOTED.
2. \oplus BINDING POST ON FRONT OF UNIT.
3. \rightarrow XX NUMBERED PINS ON CONNECTOR SERVING A TYPICAL BATTERY MODULE. REMAINING 7 MODULES HAVE IDENTICAL BUS TERMINATIONS.
4. ALL COMPONENTS MOUNTED ON BOARD-1 UNLESS OTHERWISE NOTED.



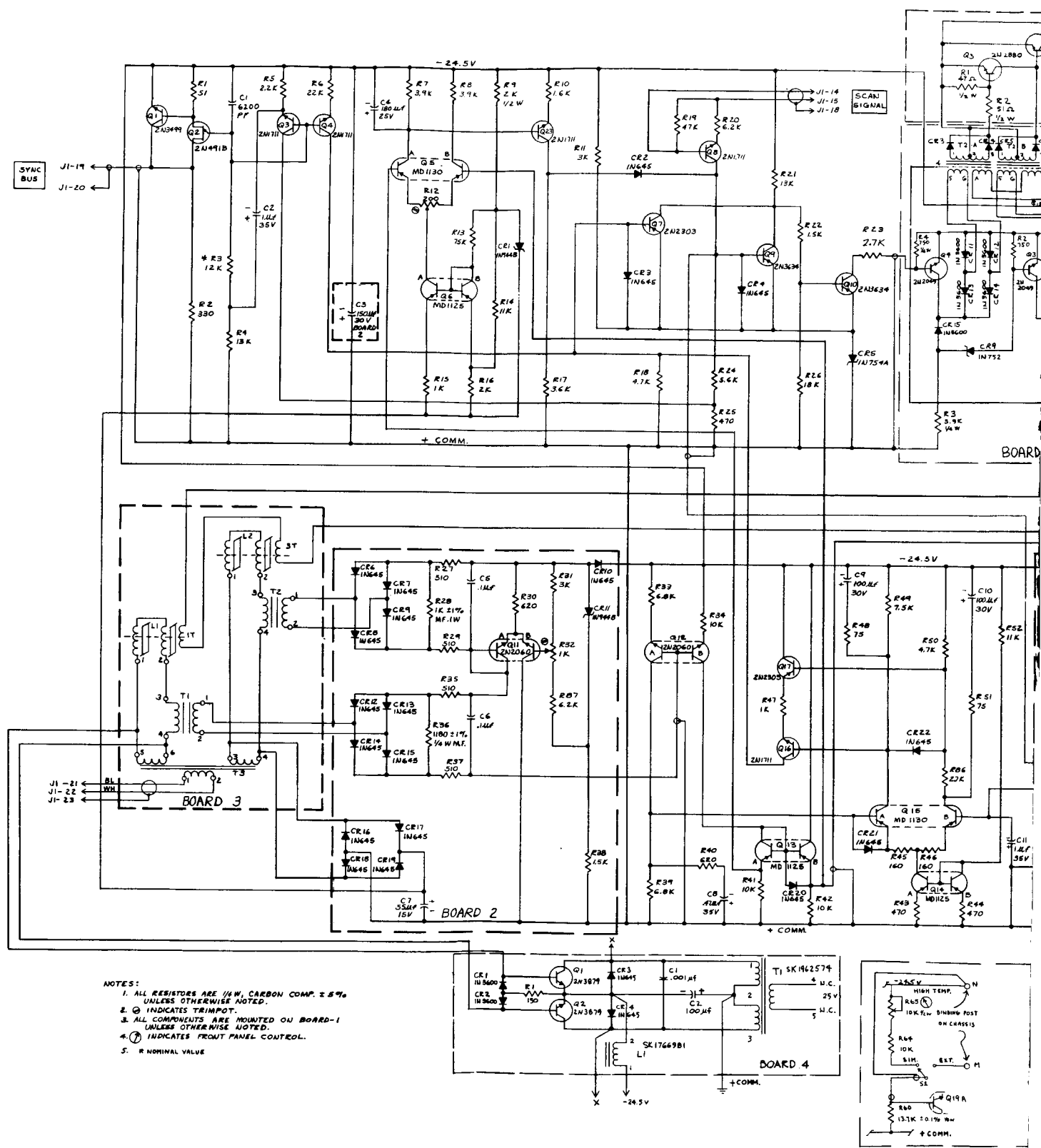
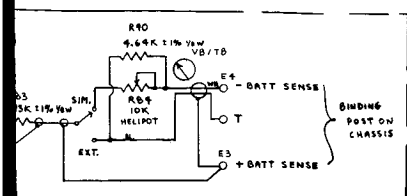
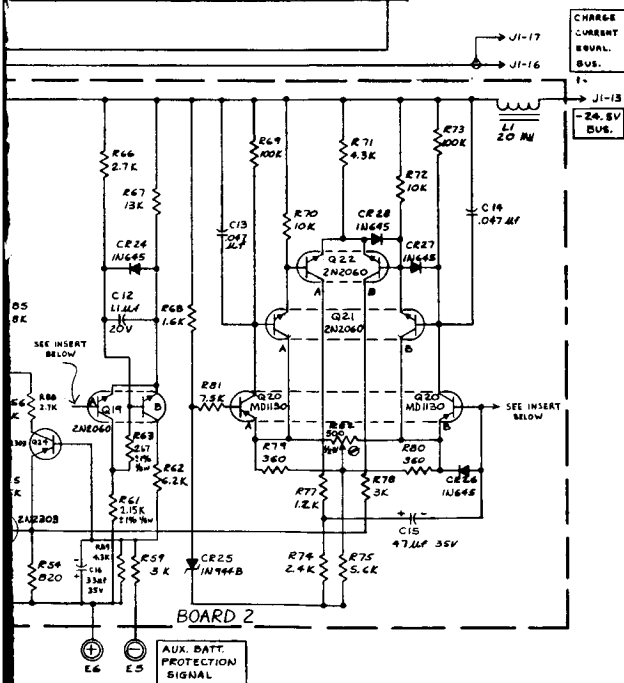
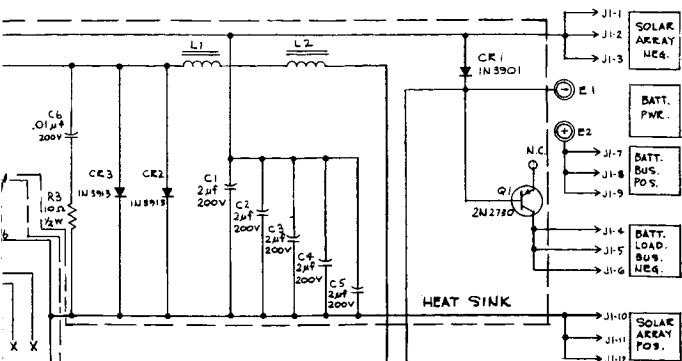


Figure 2-21. MPT Battery Module Electronics, Schematic Diagram (RCA Dwg. No. SK 1849645)



2.4.1 Power Switch Drive Circuitry

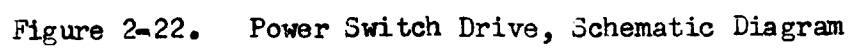
A power-switch-drive circuit capable of operation with MPT input voltages as high as 100 vdc was developed for this program.

As shown in Figure 2-22, transistors Q1 and Q2 and associated components comprise the power handling circuits.

Q1 switches load power and Q2 serves to alternately inhibit and enable Q1 as dictated by the output of the pulse-width-modulator. Base drive for Q1 and Q2 is provided by the square wave inverter circuit through transformers T1A and T1B. Resistors R2 and R3 limit base drive to transistor Q2 and R3 also serves to limit drive to Q1.

The primary windings of transformers T1A and T1B are connected in series. The voltage impressed across terminals A-B will be shared between T1A and T1B in proportion to the effective (reflected load) impedance at the respective primaries. Switching of base drive to Q1 is achieved through control of this voltage-sharing property.

Transistors Q3 and Q4 serve to short circuit windings 5-6 of T1A and T1B respectively, depending upon the state of the pulse-width-modulator output. When Q3 is saturated (Q4 Off), winding 5-6 of T1A is effectively short-circuited, thereby presenting a low impedance at the primary of T1A. Since Q4 is off, a higher impedance is presented at the primary of T1B which is equal to



the reflected load of its secondary circuits, causing the major portion of the primary voltage (V_{A-B}) to be impressed upon T1B and its secondary load. This, then, applies base current to Q1 from the inverter, causing it to turn on. Since T1A is essentially shorted, there is no drive applied to the base of Q2. Therefore, Q2 is off and its collector circuit will not divert base drive from Q1. When the pulse-width modulator changes its output state, Q3 turns off and Q4 turns on. This action diverts V_{A-B} from T1B to T1A with the net effect that Q2 is turned on and Q1 turned off.

This circuit has also been successfully applied, in this program, to a pulse-width-modulated voltage regulator capable of operation with an input of 100 volts and an output of 20 amperes at 24.5 volts. Output current limiting was also provided at the 20 ampere output level with 100 volts at the input.

Application of this circuit configuration, in place of the d-c coupled circuit, does not degrade the power transfer efficiency however, no power is dissipated in supplying drive current at the power switch high voltage level due to the magnetic-coupling provided by transformer T1. This increases the overall system efficiency, especially at high input voltage conditions.

2.4.2 Output Current Peak Detector

Control of the source (solar array) operating point so that maximum power is obtained, is accomplished by maximizing the total output current of the MPT. The peak detector circuit shown in Figure 2-23 provides this capability.

Assume the initial conditions are that C1 is charged to a low voltage so as to balance Q1A and Q1B (Q2 and Q3 are not active and Q5 is off). As the MPT scanner moves the operating point of the source towards the maximum power point, the MPT output current increases, causing the input voltage to the peak detector (which is applied to the base of Q1A) to increase. This unbalances difference amplifier Q1 causing the complementary-difference amplifier Q2 to turn on and supply charging current to C1. The voltage across C1, less the essentially constant V_{GS} voltage drop of Q3, is applied to the base of Q1B. Amplifier Q2 continues to charge C1 until the input amplifier is balanced, thus, the capacitor voltage follows the increasing input voltage. Diode CR1 and field effect transistor Q3 are used to prevent discharge of C1 through the surrounding low impedance circuits. As the source passes through its maximum power point, the MPT output current (and the peak detector input voltage) reaches a peak and begins decreasing. As this occurs, the voltage at the base of Q1A falls below that of Q1B causing the difference amplifier to forward bias Q4A and Q4B which form a complementary Schmitt trigger. The trigger action of Q4 turns on Q5 which

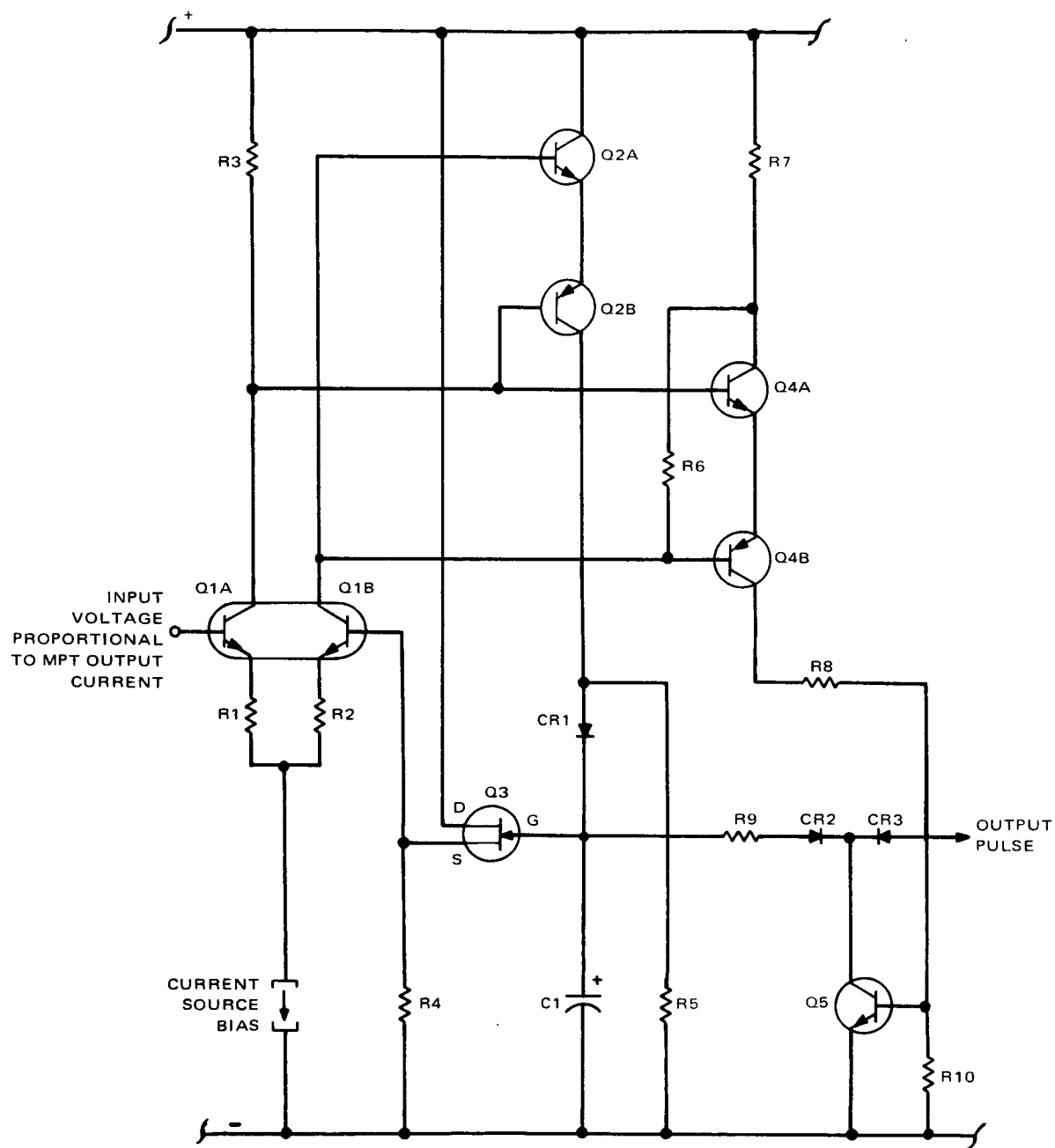


Figure 2-23. Output Current Peak Detector, Schematic Diagram

discharges C1 and supplies an output pulse. C1 is discharged until the difference amplifier Q1 becomes restored to balance which resets the Schmitt trigger. The output pulse has reversed the power point scanner so that the input voltage to Q1A is again increasing and the cycle repeats. Operation of the peak detector may begin at any point in the cycle of operation.

The sensitivity of the output current sensor/peak detector combination is the primary factor affecting tracking error. A total current decrease of 90 milliamperes is required to start the present circuit into operation.

2.4.3 Pulse Width Modulator

Conversion of the analog control signals to power switch duty cycle is performed by the pulse width modulator shown in Figure 2-24. The inputs A and B correspond to the summing points shown on Figure 2-19

The voltage reference diode VR1 and its bias resistor R1 provide a stable voltage which determines the trip points of the Schmitt trigger formed by Q1 or Q2, and Q3. With both inputs less negative than the trip level, Q1 and Q2 are off and Q3 is on providing an output signal. If either or both inputs are more negative than the trip level, Q3 is turned off and there is no output. The net effect is that of two Schmitt triggers with the outputs AND gated. To achieve duty cycle modulation, the input voltages

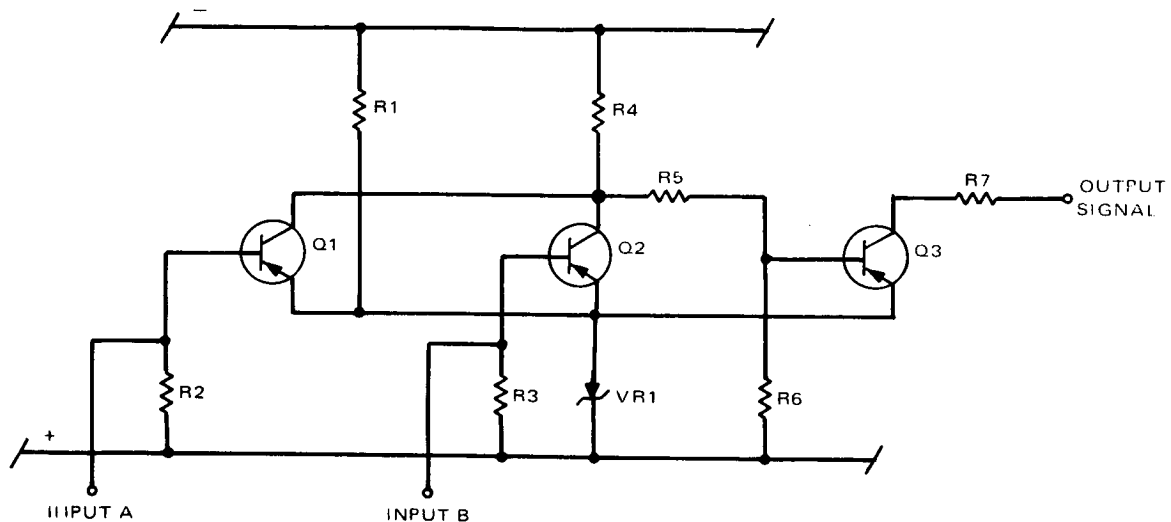


Figure 2-24. Pulse Width Modulator, Schematic Diagram

are made up of a d-c component and a sawtooth voltage at the operating frequency. Varying the d-c level then causes the desired corresponding change in the duty cycle at the modulator output.

In the MPT battery module, input A is used to provide the override control for the battery protection functions and input B is provided with a d-c level by the scanner signal and a current-sharing error signal. Extension of the above circuit to accommodate more than two inputs requires only the addition of a summing resistor and one transistor for each new input. This circuit has reduced part requirements and improved accuracy as compared with several Schmitt triggers in parallel driving an AND gate.

2.4.4 Scanner Circuits

The scanner and associated control circuits provide the signal which causes the source (solar array) operating point to be shifted. As shown on Figure 2-25, the scan generator portion of the circuitry is composed of Q1, Q2, Q3 and their associated components. A linear scan signal, or ramp, is generated by charging and discharging C1 from a constant current source. Transistor switch Q3 determines whether the ramp is positive-going (C1 charging) or negative-going (C1 discharging). When Q3 is turned on, collector current flows through R5 and R3 which results in a positive-going voltage ramp across C1. The source terminal of Q1 follows this voltage minus a small bias voltage which exists between the gate and source terminals. Diode CR3 clamps the junction of R3 and R5 to the output of the emitter follower, Q2, which is maintained at a higher voltage level by zener diode, VR1. Since the potential difference between the gate of Q1 and the anode of CR3 always remains the same, charging current flowing in R3 is constant resulting in a linear voltage ramp across C1.

When Q3 is turned off, C1 discharges through R3, R5, and R6 producing a negative-going voltage ramp. In this case, the junction of R3 and R5 is clamped by diode CR2 to a fixed voltage level, lower than the gate of Q1, resulting in a constant rate of discharge. Through the proper choice of zener diodes VR1, VR2, the charge and discharge rates can be made equal.

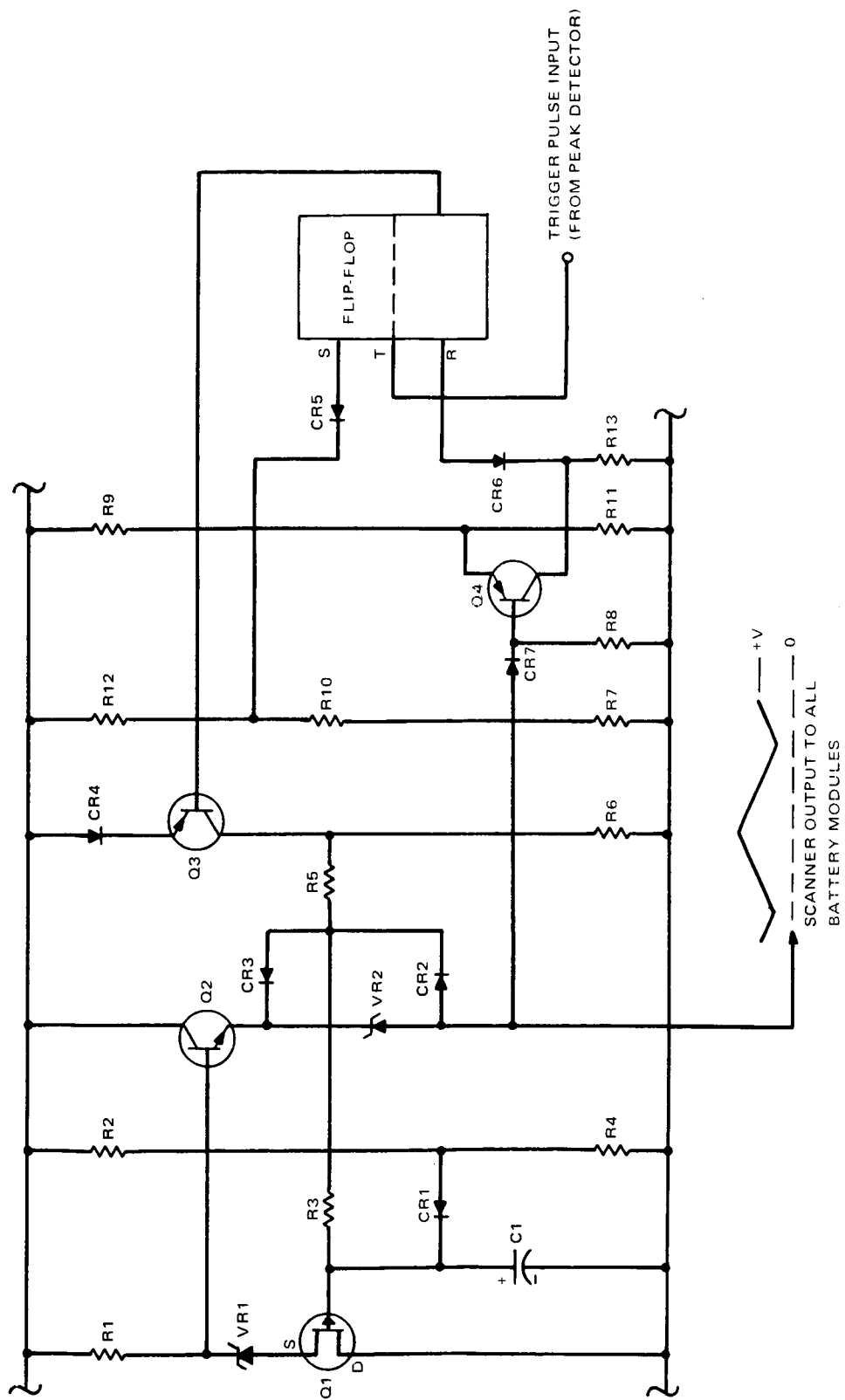


Figure 2-25. Scanner Circuit, Schematic Diagram

The network R2, R4, and CR1 provides a means of charging C1 to its lower boundary level, when power is applied to the circuit. This achieves a substantial reduction in delay time between the application of power and the appearance of a useful scanner signal level.

The status of transistor switch Q3, and therefore the scan direction, is determined by the flip-flop. The flip-flop is of the symmetrical triggering variety which changes state with each succeeding trigger pulse from the peak detector. Each change in the state of the flip-flop, changes the state of Q3, reversing the direction of the scan signal.

The two voltage dividers associated with Q4 serve to provide boundaries, or upper and lower limits, to the scanner signal. The boundaries are set to limit the scanner to the 0-100 percent duty-ratio range plus a small margin to allow for component variables. As a negative-going scan signal approaches the lower boundary, CR5 begins to conduct reversing the flip-flop, which in turn causes Q3 to turn on, thus reversing the scanner. Conversely, as the scan signal approaches the upper boundary, decreasing collector current in Q4 will cause CR6 to conduct which reverses the flip-flop causing Q3 to turn off, again reversing the scanner.

This circuit causes the generator to constantly scan back and forth in the absence of trigger pulses from the peak detector, which occurs when all battery modules are in the trickle charge mode.

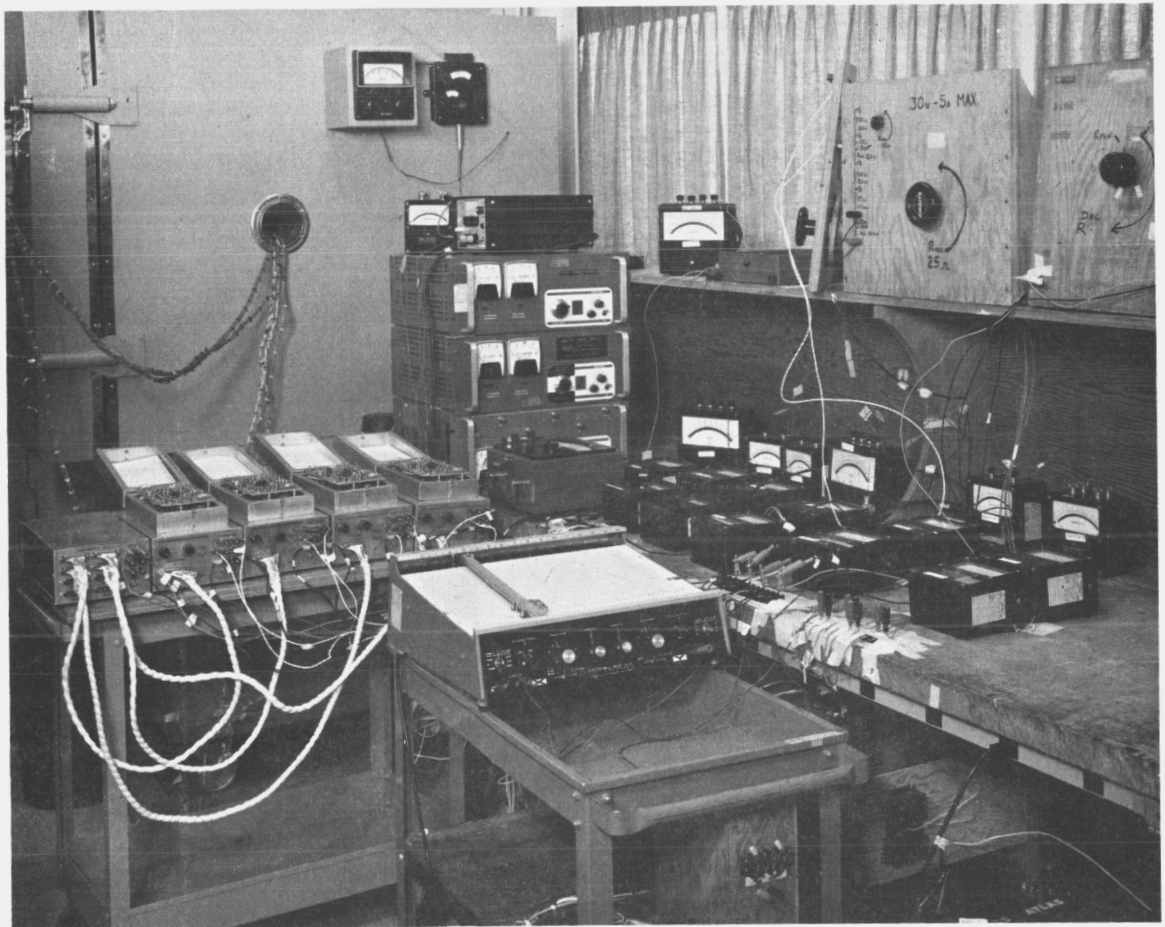
The self-reversing feature guarantees that the scanner (and the MPT system) cannot stop at either zero or 100 percent duty-cycle.

2.4.5 Other Circuits

The other circuits used are straight-forward and no description is required. The functions of these circuits have been described in Paragraph 2.3.

3.0 EXPERIMENTAL MODEL

The techniques used in the fabrication of an experimental model were chosen to closely simulate a typical spacecraft system (such as Nimbus B) and to provide maximum flexibility in the operation, testing, and development of a complete multi-channel MPT system. The laboratory testing and results were also considered. Salient points on these topics are described in this section. A typical laboratory set-up is shown in Figure 3-1.



66-9-02

Figure 3-1. MPT Breadboard Set-up

3.1 Description of Equipment

3.1.1 Basic Equipment Layout

The MPT system consists of two basic electronics components: a control unit, and eight battery modules, to approximate a Nimbus B spacecraft configuration.

The control unit is 12 inches long, 7 inches wide, and 4 inches in height, and weighs $6\frac{1}{2}$ pounds. It was designed to be the hub of the entire power tracker, containing all controls and circuitry which are common to all channels (i.e., power sensing and detection circuits, scanning controls, magnetic amplifier a-c drive, and a system synchronization generator). Connections external to the power system are made at the control unit binding posts, these include solar array input, -24.5 volt bias supply input, and load (battery) bus output. All connections to the battery modules (and between battery modules) are made via the 25-pin connectors on the control unit front panel and these include the scanning signal, synchronization, source power, bias power, a-c drive, and charge-current-sharing signals. The control unit shown on Figure 3-2 may be used with up to eight battery channels.

The dimensions of each battery module is 12 x 7 x 7 inches and weighs 11 pounds. Each is designed to provide a complete set of controls for one battery. The module contains all circuitry necessary to operate one battery channel including power handling circuits, pulse-width modulators, current-equalization circuits,



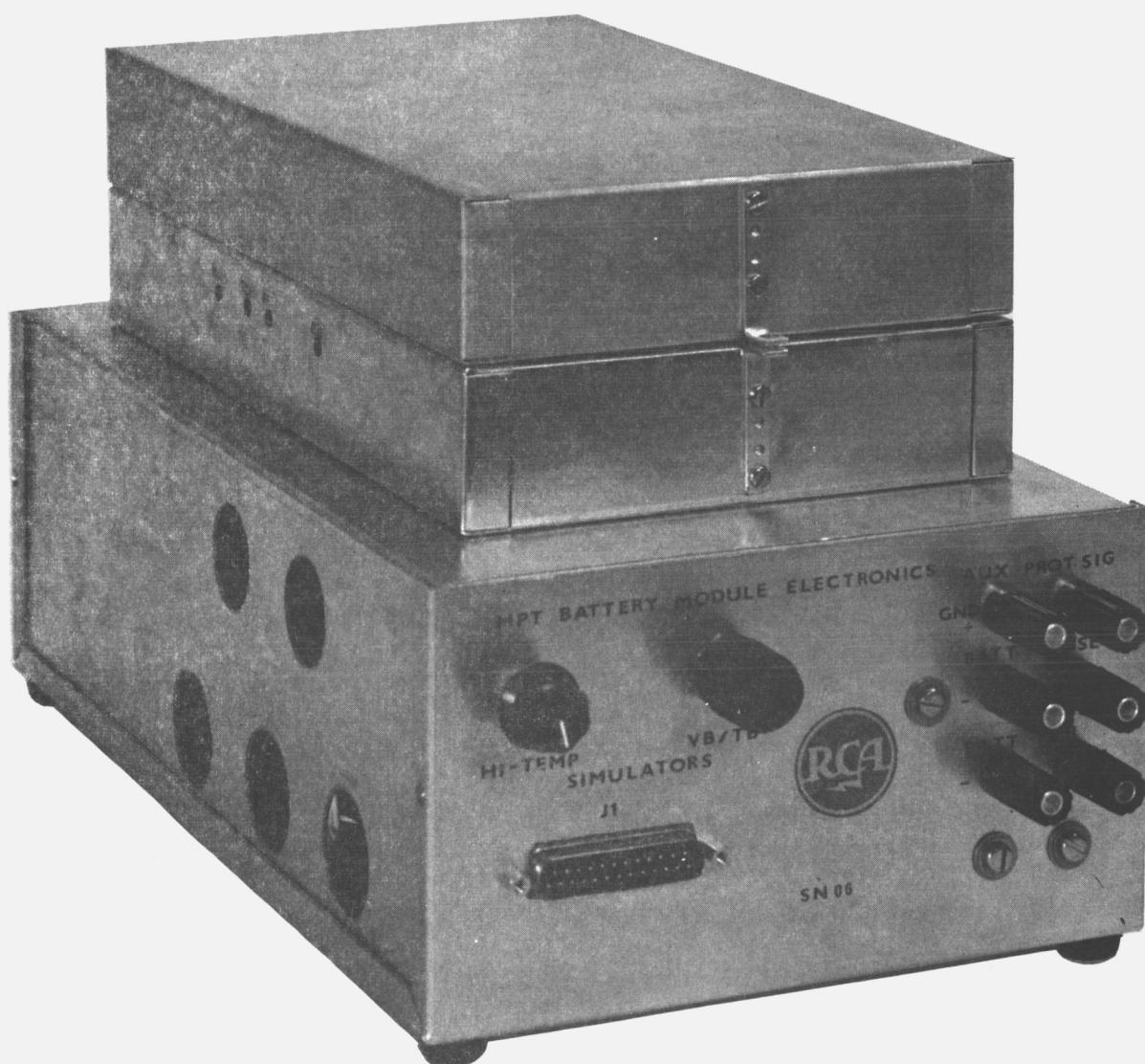
66-3-15

Figure 3-2. - MPT Control Unit

and battery protection circuitry. Binding-post connections are provided for battery power (MPT output power) and sensing leads. A 25-pin connector is provided to make all connections to the control unit.

Input terminals for auxiliary battery protection permit ground command, third electrode, or other signals to be used to activate the battery protection feature. Manual simulation controls for the battery-high-temperature and overvoltage protection features, and connection points for battery-mounted thermistors to permit

functional use of the battery protection functions are provided. Transfer from the simulated mode to the operational mode is made using the switches provided. Figure 3-3 is a photograph of a battery module.



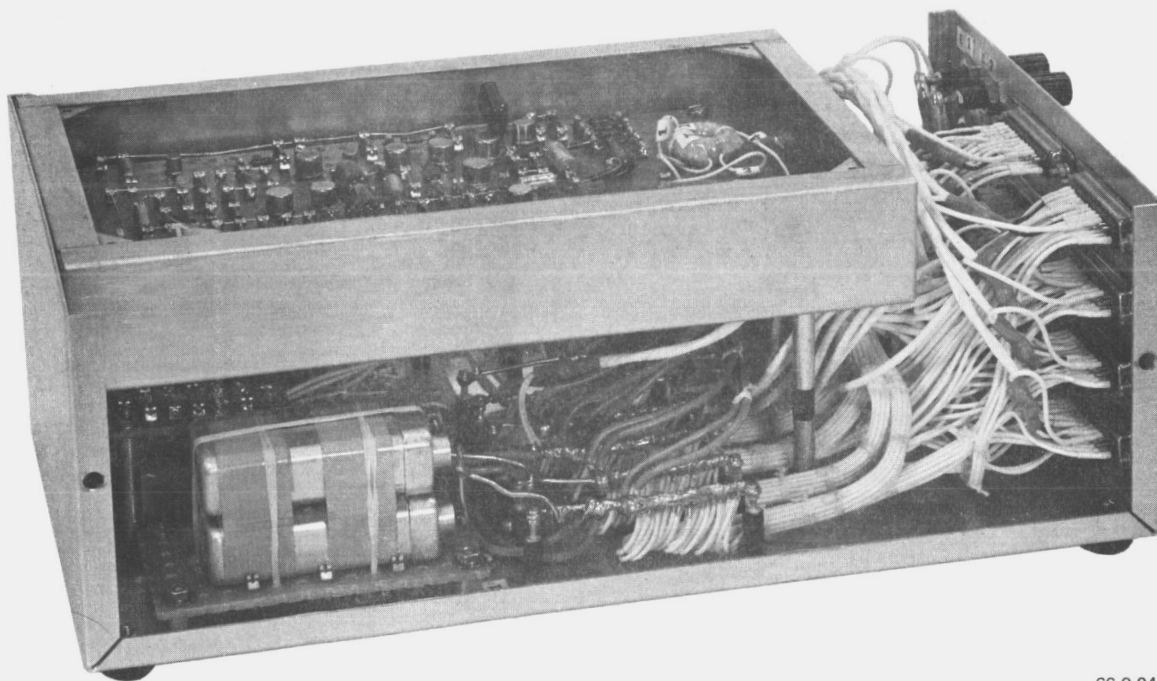
66-9-03

Figure 3-3. MPT Battery Module, Exterior View

3.1.2 Construction Techniques

Construction was limited to methods utilizing standard laboratory materials and hand-tools wherever possible. The outer housings of both the control unit and battery module are aluminum chassis boxes. Circuits are handwired on vector-type circuit boards.

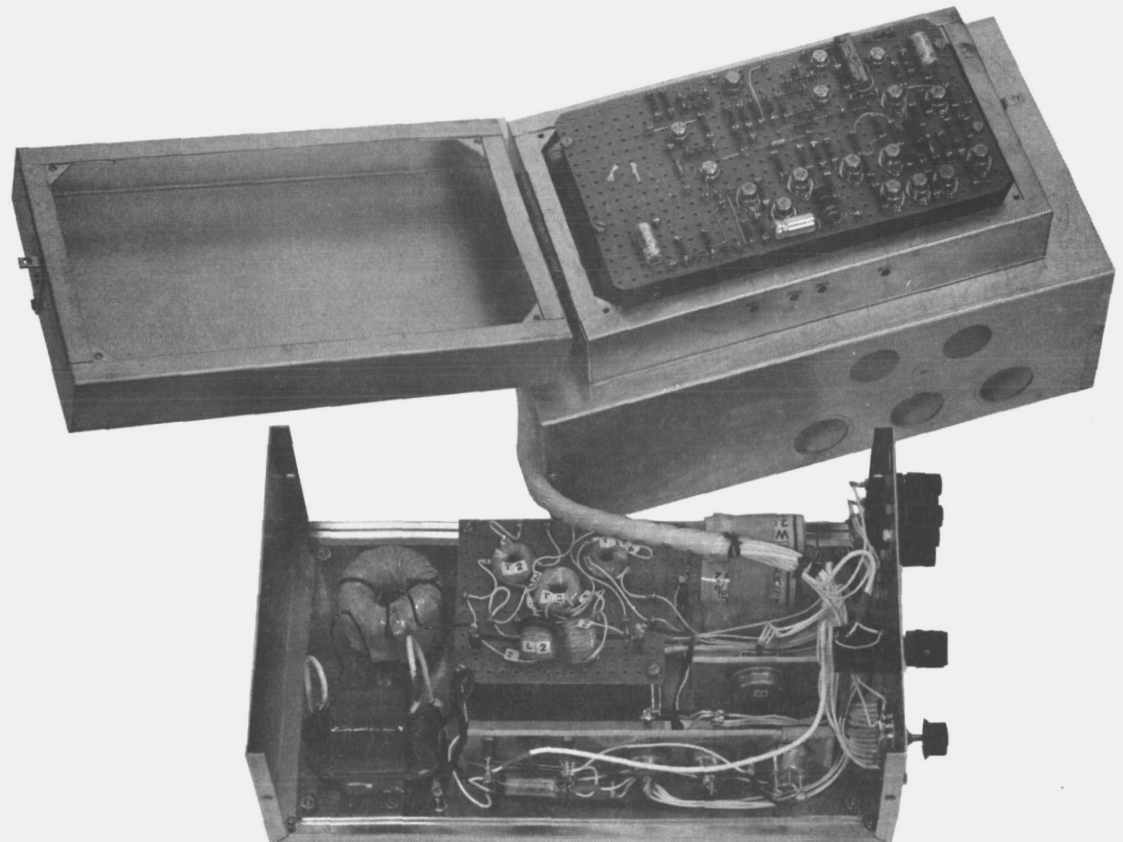
Figure 3-4 shows an interior view of the control unit. The heavy bus-wires at the center are the common tie-points for all eight battery modules. Each of the eight output connectors is identical and serve one battery module. Parts of the output-current peak detector and the scanning signal generator are visible on the top board, which is mounted in a steel enclosure to provide shielding against EMI. The input-filter capacitors are at the lower left corner and the magnetic amplifier circuits are behind them.



66-9-04

Figure 3-4. MPT Control Unit, Interior View

The battery module interior is shown in Figure 3-5. A 1/4" aluminum baseplate is mounted to the outer box to act as a heat sink and provide structural support. Dissipating components are mounted to aluminum angles which are fastened to the baseplate. The filter chokes are secured directly to the base. Low-level control circuitry is contained in the top compartment which is made from steel chassis boxes to provide EMI shielding. Vent holes have punched in the main enclosure to increase convection cooling of the heat sink.



66-9-06

Figure 3-5. MPT Battery Module, Interior View

3.1.3 Filtering and Noise

The physical layout of the experimental model and the sensitivity required of the control circuitry result in a condition where transients and noise could severely restrict system operation. The primary source of noise is the power switches in the battery modules which cause high-current pulses, with extremely fast rise and fall times, to be drawn from the source via the MPT harness and internal wiring. The measures taken to control this noise are described below:

a. Array Filter

A capacitive filter, located in the control unit, is used to supply the current pulses to the battery modules. This allows the array to operate at an average condition rather than in a pulsed mode.

b. Input Filters

Capacitive filters (using high Q, high frequency, capacitors) located in each battery module are used to reduce high frequency noise generated by the power switching circuits.

c. Output Filters

The output inductor in each battery module is used to average the battery charge (or load) current.

d. Power Supply Decoupling

The -24.5 volt auxiliary power for the low-level circuitry is decoupled in each module by series inductors and bypass capacitors. This prevents any noise which is picked up on the power bus from interfering with the control functions.

e. Shielding

To reduce the noise susceptibility of the equipment, shielding was provided for the low-level circuits of both control unit and battery modules by steel chassis boxes. Internal wiring for low-level circuits was made using shielded wiring to minimize noise pick-up.

f. Synchronization

To reduce the interactions which would be caused by each battery module having a free-running power switch, system synchronization was provided. This is necessary to implement the current sharing feature which requires controlled-interaction between battery modules.

Inclusion of the above described functions resulted in an experimental model which was adequate to satisfy all its performance goals.

3.1.4 Harnessing and Cabling

The cabling considerations were basically the same within the harness as they were within each module. Shielded cables are used for control functions to minimize induced noise. Power cables use

several No. 20 AWG stranded wires in parallel to lower resistive losses.

The complete MPT harness consists of eight identical cables, each about four feet in length. Each end is terminated in a 25-pin connector (female) which mate with the front panel receptacles (male) on either the control unit or battery modules. These cables are constructed so that either end may be connected to any connector on the control unit and the other end to any battery module.

For laboratory tests, connections between the solar array, -24.5 volt power supply, and the MPT control unit are made with No. 14AWG wire. Power connections between the batteries and the battery modules were made with two No. 14 AWG wires in parallel, however, battery sensing connections consist of No. 20 AWG shielded wires.

3.1.5 System Losses

The MPT system experimental model power losses were investigated in order to recommend methods of improving efficiency and reducing shunt losses. The results are presented below for both efficiency and shunt loss improvement.

a. Transfer Losses

Power transfer efficiency is determined by the losses in the power switch, filters, and drivers. The loss is proportional to the output current consisting of both fixed-voltage drop ($I-V$) and resistive I^2R components.

The loss in the power switch was high because the switch was operated in a non-saturating mode. This was found to be necessary to avoid long storage times which prevent use of small duty cycles (i.e., high input voltage operation). The loss could be reduced by allowing the switch to saturate and providing a means to rapidly turn it off. This has been accomplished by incorporating a magnetically-coupled, power switch drive circuit capable of operation at 100 volts.

The losses in the filters and wiring were mainly resistive. These can be reduced by increasing the conductor sizes in the chokes and harnesses and by good package design to reduce lead length. Experimental model harness and wiring lengths were unavoidably long due to the requirement for flexibility during the development phase. Implementation of this reduction would not only result in an overall increase in efficiency but would also serve to reduce the decrease of efficiency with high output current. The loss in the flyback diode becomes significant at high output current levels. Reduction could be accomplished by selecting components for low forward voltage drop or by paralleling two devices.

The shunt current losses for the d-c driver configuration were relatively small and constant regardless of terminal conditions. A magnetic a-c coupled base drive circuit for the power switch has been incorporated which should provide a small increase in efficiency. The reduction of the drive losses is primarily dependent upon the increase of current amplification (h_{fe}) of the power-switch which is a device limitation.

b. Shunt Losses

Shunt loss is the power from the -24.5 volt power supply required to operate the MPT sensing and control circuits. This loss is essentially constant and represents from one to two percent of the source power for the present MPT system configuration. The following three approaches to the problem were evaluated:

- (1) The present circuit configuration shunt loss could be reduced by redesigning all sensing and control circuits at a higher impedance level. This approach would create several problems. The MPT control circuitry is very sensitive to small variations of certain parameters as it must be to closely regulate and control these parameters. At higher impedance levels, the circuitry will be more susceptible to noise and transients. Also, the a-c stabilization of the system would become more difficult and critical. Implementation of this method was not considered to be a feasible approach.

- (2) The inclusion of a day-night switch in order to reduce the MPT shunt losses. The switch would be placed in series with the -24.5 volt supply and would remove bias power from the MPT control and sensing circuitry when the tracker is not required (i.e., during orbital night when there is no source power available).

The value of this switching arrangement would be greatest in a low altitude satellite system where the dark portion of the orbit may be as much as 40 percent of the total period. In considering the incorporation of the day-night switch, the effect on overall reliability caused by the placement of the switch in series with the MPT system as well as the increase in required circuit complexity must be weighed against the shunt loss reduction. A detailed trade-off study considering orbit, inclination, source capability, mission length, etc. would have to be performed, to determine the suitability of the day-night switch for a particular spacecraft.

- (3) A third approach to the reduction of shunt losses is conversion of the MPT system to integrated circuits. All circuit functions can be categorized such that implementation of integrated circuit technology is feasible.

Both analog and digital integrated circuits are presently available which can probably be used to perform most of the control and sensing functions. Also available, from several manufacturers, are custom monolithic and hybrid circuits which may prove useful where standard circuits are not feasible or practical. Investigations of performance with respect to temperature, noise susceptibility, efficiency and stability may be performed in converting to integrated circuitry.

Other advantages of using integrated circuits include increased reliability, reduced weight, and reduced size. It appears that integrated circuits offer the most promising approach to improved performance and shunt loss reduction.

3.2 Laboratory Testing and Results

3.2.1 Test Objectives

The test program was designed to allow testing of the Maximum Power Point Tracker System over a range of system parameters similar to the Nimbus satellite requirements. The tests were sufficient to permit detailed evaluation and study of the system performance at the black box level and the generation of parametric data useful for spacecraft level systems evaluation.

The tests were conducted in such a manner that a direct comparison between the established design and performance goals and the experimental results would be obtained.

3.2.2 Test Conditions

An MPT System employing four battery channels connected as shown in Figure 3-6 was used for the performance testing.

The performance testing was performed with the system modules in temperature chamber at temperatures of +25, -10, and +60°C.

3.2.3 Performance Test Results

The test results are given below as related to the established performance criteria.

a. Power-Transfer Efficiency

The efficiency of the MPT System in transferring power from the source to the load was measured under various conditions of array power, battery voltage, and temperature.

The solar array was imulated by a N.J.E. Simulator over the range of 510 to 820 watts. A plot of power-transfer efficiency vs. array power is shown in Figure 3-7 for the case with 25°C ambient temperature. Figure 3-8 shows the overall effects of all the test parameters.

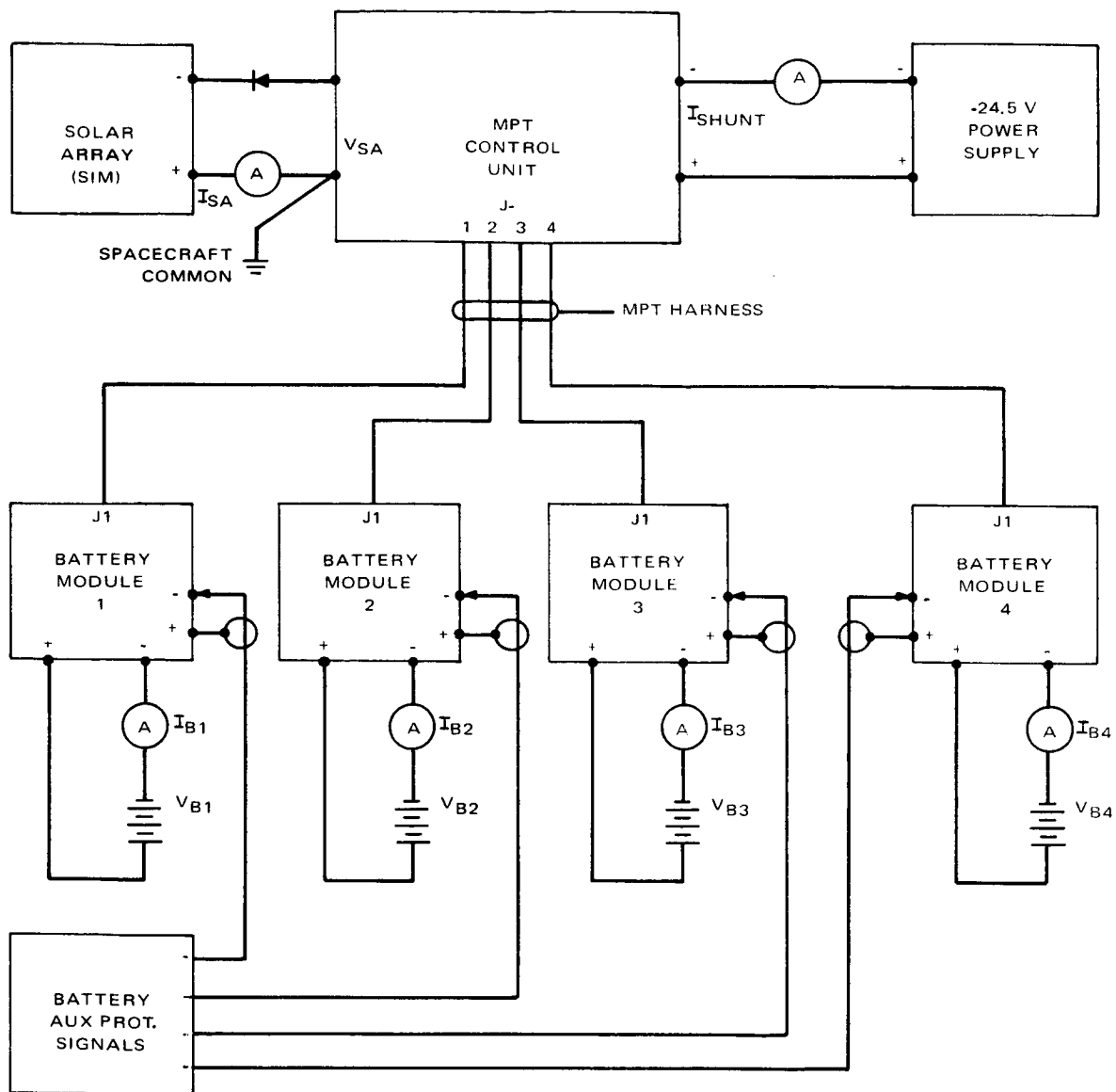


Figure 3-6. MPT Performance Test Configuration

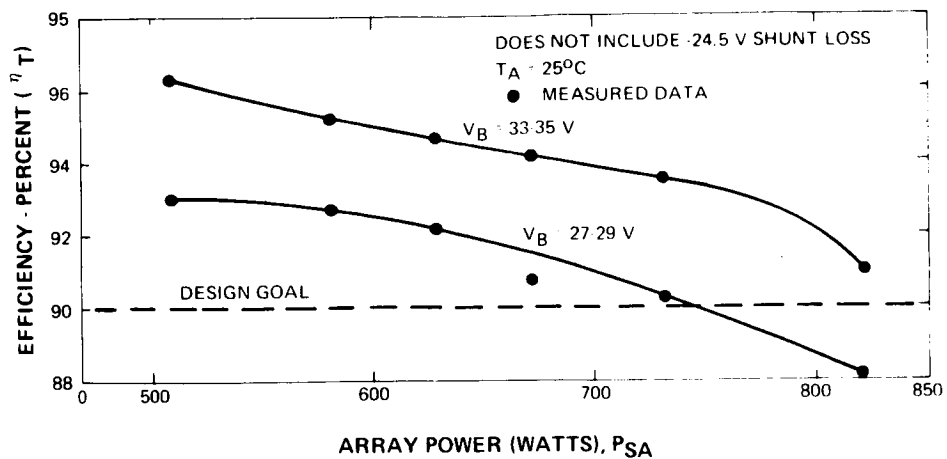


Figure 3-7. MPT System Power Transfer Efficiency vs. Array Power

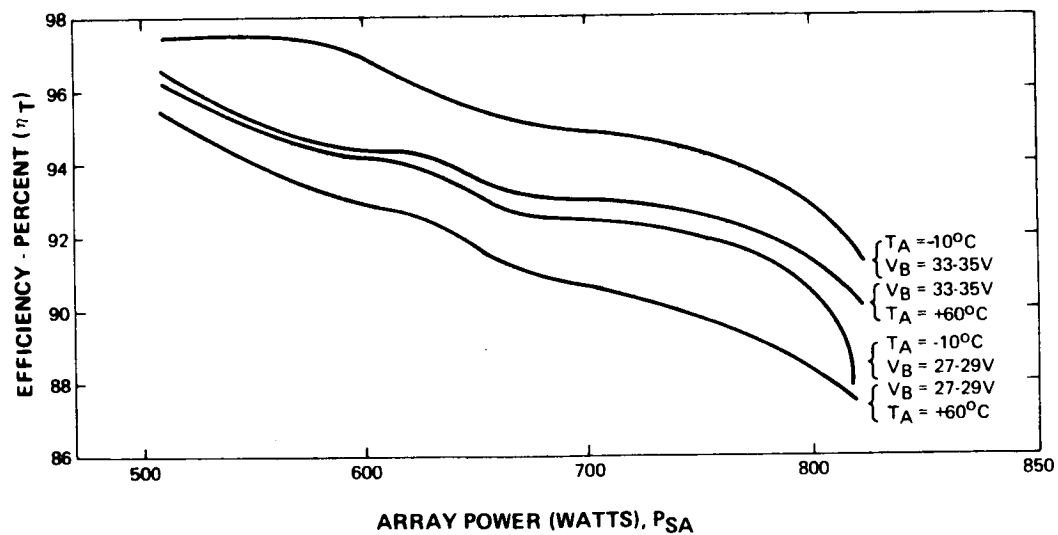


Figure 3-8. MPT System Power Transfer Efficiency vs. Array Power

The power transfer efficiency is dependent upon both array power and battery voltage as can be seen from Figures 3-7 and 3-8. There are several well defined losses which account for this phenomenon.

(1) Dissipation Losses

The major losses are series losses which are directly dependent upon the magnitude of the output current.

These losses are dissipation in the power-switch (which was operated in a non-saturating mode in the d-c coupled drive circuit) and the wire losses (including the chokes). Note that at any given array power, the output current is larger when the battery voltage is lower. This implies lower efficiency at the low battery voltages due to the resistive losses, which is substantiated by the data. The efficiency at high array power level is also reduced by increased switching losses in the power-switch transistor.

(2) Flyback Diode Losses

Another major loss occurs in the flyback diode. This loss is dependent upon the output current and the power-switch duty cycle (losses occur during the OFF period of the power-switch). At any fixed array power, reduction of battery voltage causes an increase of battery current and a reduction of power-switch duty cycle, both of which cause increased losses in this diode.

All the above losses are essentially series losses. The loss due to shunt current is relatively fixed and is approximately two watts per battery module. The power dissipation associated with the shunt current has been reduced by the ac-coupled drive circuit previously described. The shunt loss drawn from the -24.5 volt supply is treated separately in Paragraph 3.2.3e.

A major factor causing the decrease in transfer efficiency at high output currents was the resistive loss in the leads. In flight type equipment, this loss would be reduced by maintaining short lead lengths (the battery modules located physically close to the batteries) and by custom designing the output filter chokes with this factor in mind. For the experimental model system, more than three percent of the array power was dissipated in the interconnecting wiring and the filter chokes, which caused the efficiency to fall below the 90 percent design goal for the case of an 820 watt array and low battery voltage.

b. Charge Current Sharing

The data obtained for all conditions of battery voltage and ambient temperature was reduced to obtain the worst-case deviations as a function of array power. These results are shown as a percentage of the average battery current in Figure 3-9. The design goal of +10 percent is also shown for comparison purposes.

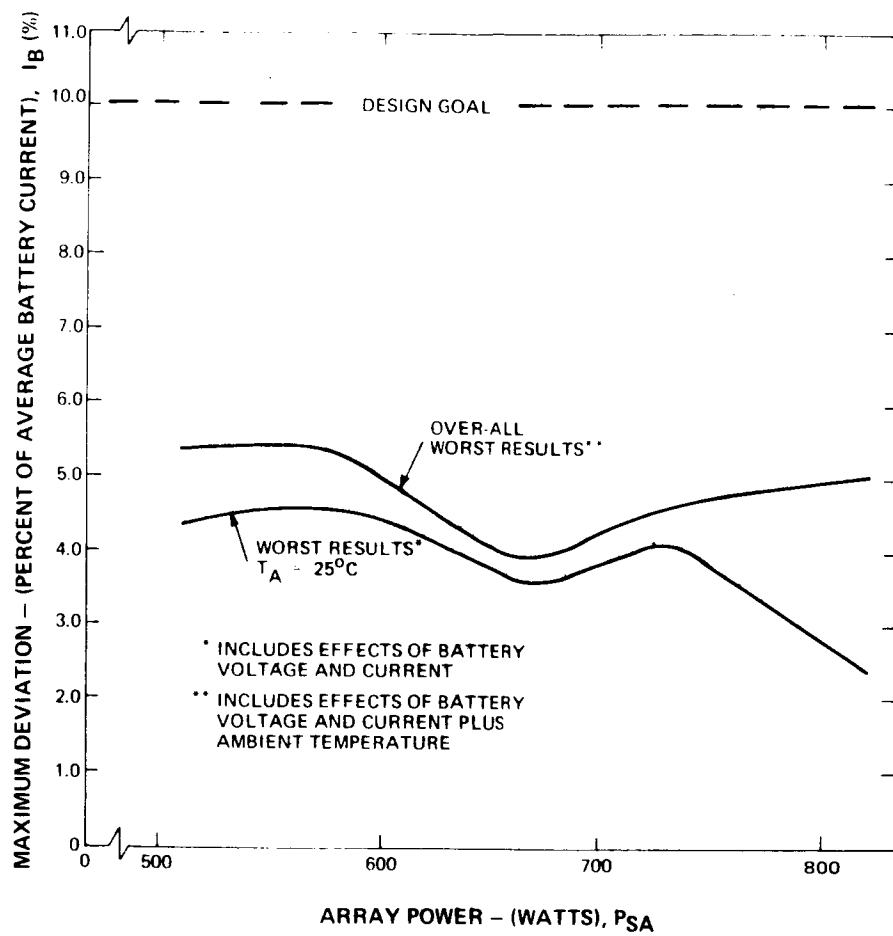


Figure 3-9. MPT System Charge Current Sharing vs. Array Power

The precision of the current sharing is limited by several factors. This is directly affected by the sensitivity of the comparison amplifiers and the current sensing circuits. For example: The current sensor output voltage swing is approximately 5 volts for the range of battery currents from 0.5 amperes to 15 amperes or 0.34 volts per ampere. Using $P_{SA} = 820$ watts at 25°C , the current sharing has less than three percent deviation from the average ($I_{Bave} = 5.48$ amperes). This reduces to $\Delta I_B = 160$ milliamperes corresponding to ΔV at the sensor of approximately 55 millivolts or 1.1 percent of full scale.

Also, it must be considered that the current sensor output contains some ripple, due to the ripple in the battery current, and also due to current sensor generated noise. Since the batteries are not all at the same voltage, the duty cycles of the battery modules differ. This causes the ripple in one module to be slightly out of phase with the ripple in another. Hence, voltages from different modules, each carrying equal currents, may not appear equal at the point of comparison.

Another factor influencing this accuracy is the calibration of each battery module. This item will be discussed in Paragraph 3.2.3h.

c. Maximum Charge Rate

The level at which each battery module limits charge current was also measured for all conditions of battery voltage and ambient temperature. The array powers used were the extremes, 510 and 820 watts. Current limiting was within 250 milliamperes of the nominal setting for 12.0 amperes. This is a combined effect of 2.08 percent, as shown in Figure 3-10.

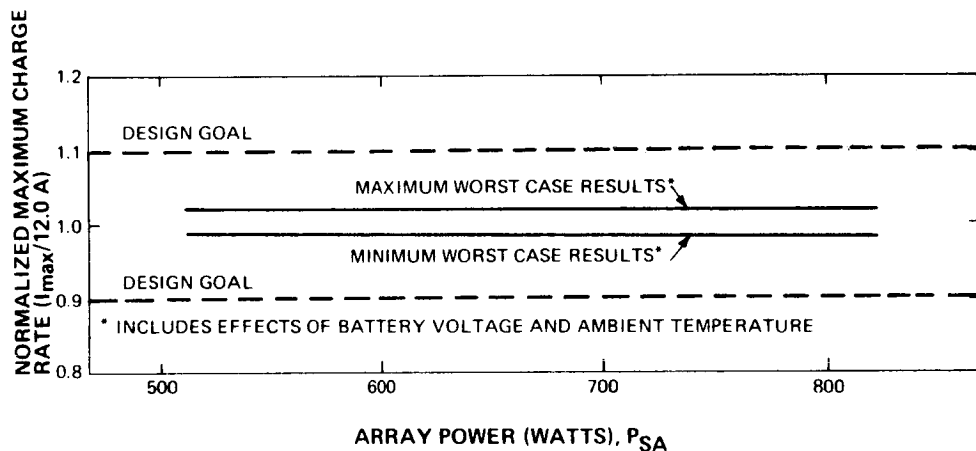


Figure 3-10. MPT System Maximum Charge Rate vs. Array Power

The largest change in maximum charge current, for either array power only or battery voltage only, was ± 100 milliamperes for any battery module. Similarly, the largest change due to temperature was ± 200 milliamperes. The above deviations are individual cases and may not coincide with the overall worst case results. All modules were within 200 milliamperes of nominal at the first measurement.

The stability of the maximum charge rate is mainly dependent upon the accuracy of the initial calibration, the current sensing circuits, and the stability of the voltage reference. The discussion of Paragraph b is applicable to these measurements.

d. Trickle Charge Rate

The trickle charge current was measured for each battery module under all conditions of battery voltage, array power, and ambient temperature. The results were all within 40 milliamperes of the 300 milliampere nominal current or 13.3 percent. The results are shown in Figure 3.11, as is the design goal.

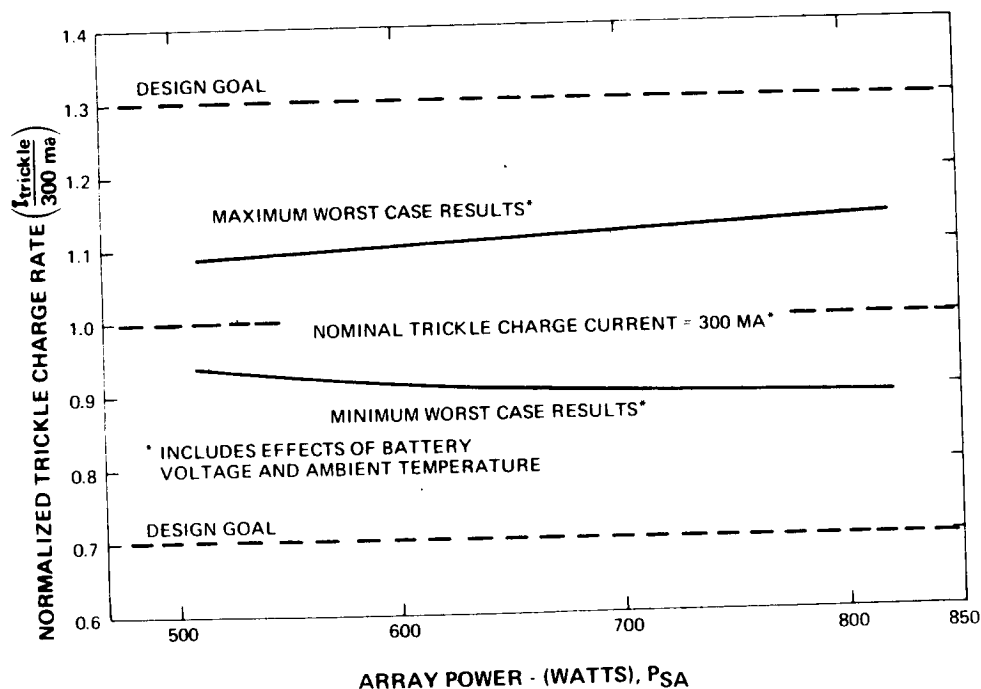


Figure 3.11. Trickle Charge Rate vs. Array Power

The change in the trickle charge rate due alone to battery voltage, was typically 30 milliamperes. Change due to array power variations was no greater than 20 milliamperes, while variations due to temperature were as high as 70 milliamperes. These deviations are the worst individual occurrences and may not coincide with the overall worst case data. All modules were within 10 milliamperes of nominal at the first measurement.

The precision of the trickle charge rate is dependent upon the accuracy of the initial calibration, the current sensor accuracy, and the stability of the zener diode reference. These errors closely parallel the maximum-charge-rate errors because the same control functions are being used.

e. Shunt Loss

The shunt loss is defined as the power drawn by the MPT from the -24.5 volt supply. The magnitude of the loss is approximately 10 watts and is essentially constant for all conditions of battery voltage, array power, temperature, and mode of operation. Typical and worst case losses are shown in Figure 3-12. Relative losses are approximately two percent at an array power of 510 watts and one percent at 820 watts.

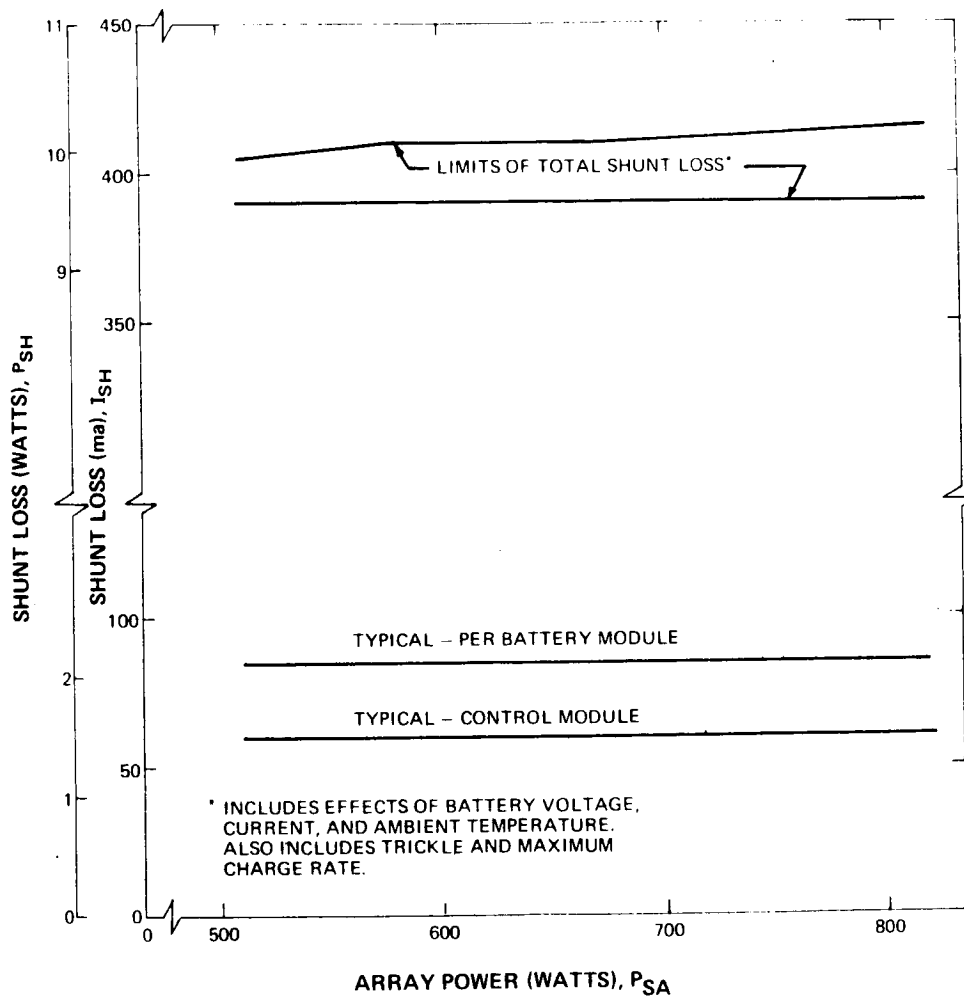


Figure 3-12. MPT System Shunt Loss vs. Array Power

The power consumption is essentially constant with array power, due to the use of magnetic amplifiers for current sensing in place of d-c amplifiers. This allows the -24.5 volt power supply to operate into a relatively fixed load which can lead to higher auxiliary power supply efficiency.

f. Tracking Error

The tracking error is a measure of the ability of the MPPT to fix the system operating point at the maximum power point of the source. This value can be meaningfully expressed as a percent of the maximum power.

The tracking error may be defined as follows:

$$\frac{\Delta P_S}{P_{SM}} = \frac{\Delta I_o V_B}{\eta_T P_{SM}} \quad (3.1)$$

where:

- ΔI_o = the maximum deviation from peak output current
(measured value)
- V_B = the battery voltage which is assumed constant for
a 90 milliampere current change (measured value)
- η_T = the power transfer efficiency (calculated from
measured data)
- P_{SM} = the array power at the maximum power point
(calculated from measured data).

It is apparent that the maximum tracking error is obtained when $\Delta I_o V_B$ is largest, and $\eta_T P_{SM}$ is smallest.

For

$$\begin{aligned}\Delta I_o &= 90 \text{ milliamperes} \\ P_{SM} &= 510 \text{ watts} \\ V_B &= 33.7 \text{ volts} \\ \eta_T &= 96.3\%\end{aligned}$$

then:

$$\frac{\Delta P_S}{P_{SM}} \% = \frac{0.09 \times 33.7}{0.963 \times 510} 100 = 0.62\%$$

$$\text{or } \Delta P_S = 3.16 \text{ watts}$$

The smallest tracking error is obtained for the opposite conditions:

$$\begin{aligned}\Delta I_o &= 90 \text{ milliamperes} \\ P_{SM} &= 820 \text{ watts} \\ V_B &= 27.5 \text{ volts} \\ \eta_T &= 88.2\%\end{aligned}$$

then:

$$\frac{\Delta P_S}{P_{SM}} \% = \frac{0.09 \times 27.5}{0.882 \times 820} 100 = 0.34\%$$

$$\text{or } \Delta P_S = 2.81 \text{ watts.}$$

These results are in agreement with the measured data which also indicates a power error of approximately 3 watts.

g. Interaction of Variables

Tests were run to demonstrate that MPT performance was not degraded by large differences in battery voltage and battery protection function operation.

Note that in the normal operation of a satellite power system, the batteries will not normally be identical nor will they all operate at the same voltage and current levels. It is necessary to provide for the independent operation of each battery channel to account for battery differences. The MPT was designed to incorporate this practical feature and the purpose of this test was to demonstrate its capability.

The precision of the current sharing and trickle charge rate were in agreement with results reported in Paragraphs 3.2.3b and d. Shunt losses from the -24.5 volts supply remained constant. The power transfer efficiency decreased under this test due to the higher currents supplied to the batteries. Tracking accuracy remained nominal.

Behavior of the MPT during this test was as predicted.

h. MPT Calibration

A major factor which affected the performance tests results is the variation between various MPT units and modules. Each module was calibrated separately and this calibration shifted

when several modules were connected together. This was caused by the shift in the operating switching frequency of each battery module, except the one which runs naturally at the highest frequency and which was used to synchronize the entire MPT system.

The frequency dependence of the MPT is primarily in the magnetic-amplifier type current sensors. The current sensor output is controlled by the volt-second area of the applied drive. The square wave oscillator which supplies this drive was synchronized by the battery module having the highest natural operating frequency. This increases the square wave frequency and decreases the output volt-second area.

This problem has been corrected by using the square wave oscillator in the control unit as the synchronizing source for the system. This results in all battery modules being calibrated and operated at the same frequency.

3.2.4 System Test Results

System tests were conducted in which the MPT was connected into a typical space power system with a solar array simulator, four lead-acid batteries, and a Nimbus B PWM regulator with simulated load. One result of these tests was to highlight a few basic problems and limitations of the proposed MPT configuration.

a. Auxiliary Power Supply

To demonstrate that the external bias required by the MPT is not a limiting factor, the -24.5V power was supplied from three different sources: a -24.5V power supply, the -23.5V auxiliary regulator, and the PWM regulator output. No problems were encountered in operating from any of these sources.

b. System Configuration A

The PWM Regulator was connected in parallel with the solar array at the array terminals of the MPT control unit. The system configuration was as shown in Figure 3-13, with the MPT current sensor sensing the total-battery-current.

Charge current sharing was maintained and the power point was successfully tracked with this configuration.

One problem found was that the MPT erroneously detected the peak power when load current transients were induced at the PWM regulator output. The tracker re-acquired the maximum power point on the next scanner cycle.

In applying the maximum power tracking concept to an actual spacecraft, the following conditions can exist and be serious problems:

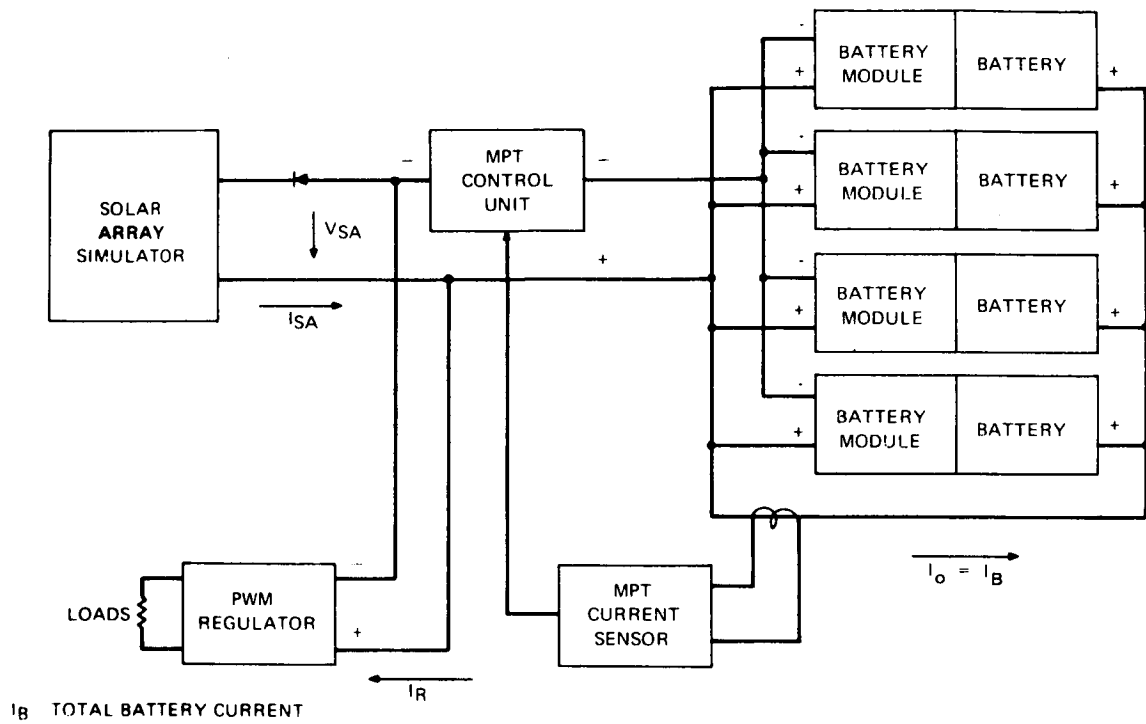


Figure 3-13. MPT System Test Configuration A

- (1) The existing MPT system may become biased away from the P_{max} point due to repeated, low energy, transients occurring at the PWM regulator input. This can be caused by fluctuating (a-c) loads, or by normal load switching or sequencing. This is due primarily to the fact that the MPT system senses load input current (total battery current) as being proportional to delivered array power.
- (2) Rapid fluctuations of the array due primarily to fluctuations in illumination and/or projected area may cause the MPT to "off-bias" from the P_{max} point due to the relatively slow speed-of-response of the system. This slow response is a result of the slow scan rate and filtering requirements of the current sensors throughout the MPT system.

The problem described in (1) above may be alleviated by implementation of a direct, source-power sensing scheme. However, heavy load fluctuations and/or the condition stated in (2) above would still create problems of off-biasing due to the slow system response. Heavy load transients would cause fluctuations in array operating point which the system could not follow.

There appear to be several plans of attack on this problem:

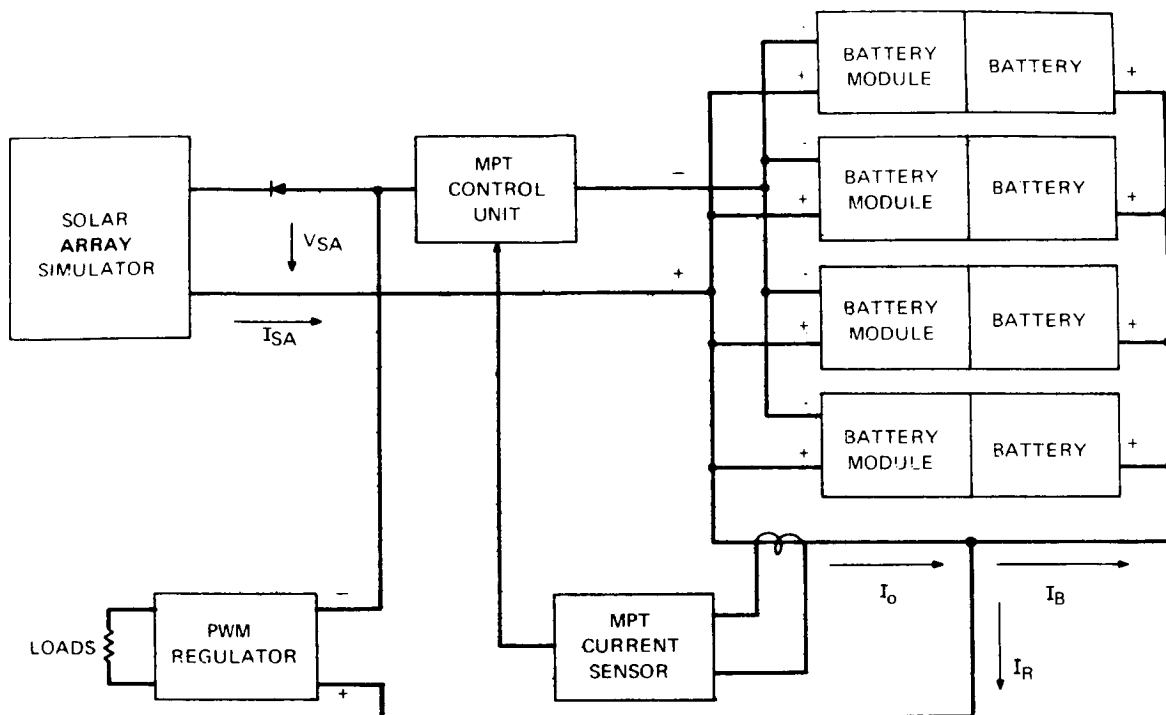
Through more or less brute-force techniques, render the system incapable of recognizing these fluctuations,

i.e.: either filtering the fluctuations before they reach the array bus or slowing the system response still further. This method could probably be made to work through judicious circuit design. However, increased load filtering bears a significant weight penalty and perhaps a transient response penalty for the load regulator. Slowing the system response may create too large a phase error between the actual and the sensed states of the array. This could result in excessive off-biasing of the array indicating less than optimum array-power utilization.

It must be noted that an off-bias condition from which the existing MPT system can recover satisfactorily is one where the interval between transients is much greater than the scan rate.

c. System Configuration B

To alleviate the transient susceptibility problem encountered in Paragraph b, above, the PWM regulator was connected between the negative array terminal and the positive battery terminal on the control unit. The system configuration is as shown in Figure 3-14 and the total output current (total of battery plus PWM input currents) is sensed as the indication of maximum power. This change reduced the transient susceptibility problem, but then the MPT became biased away from the array maximum-power-point as PWM regulator load current was increased. The following graphical analysis clearly shows the reasons for the improper MPT operation.



I_B = TOTAL BATTERY CURRENT
 I_R = REGULATOR INPUT CURRENT
 I_O = TOTAL OUTPUT CURRENT
 $I_O = I_B + I_R$

Figure 3-14. MPT System Test Configuration B

The nature of the PWM input I-V characteristics caused the total output current to deviate from a well defined relationship to the MPT output power. In the configuration shown, the two parameters of interest are the array voltage (which is also the input voltage to the PWM regulator) and the total output current. A set of input characteristics for the PWM regulator are constructed in Figure 3-15. For the batteries, the characteristics of battery current versus array voltage are constructed in Figure 3-16 as follows:

Curve 1 is the solar array I-V characteristic and line 1 is a typical battery characteristic. The intersection of curve 1 and line 1 at point A is the operating point if the battery were connected directly across the array as in Figure 3-17A. The curve of array power versus array voltage is curve 2 (using the vertical scale of power drawn on the left) which is constructed by graphing the locus of the voltage-current products for all points on the array characteristic, curve 1. Some device such as the (MPT) is now assumed to be interposed between the array and the battery (Figure 3-17B), which can vary the voltage operating point on the array characteristic, while maintaining the battery at 30 volts. For simplicity, assume the device is lossless and that all the power output of the array appears as input power to the batteries. Rearranging the equation of Figure 3-17B so that:

$$I_B = \frac{P_{SA}}{V_B} \quad (3.2)$$

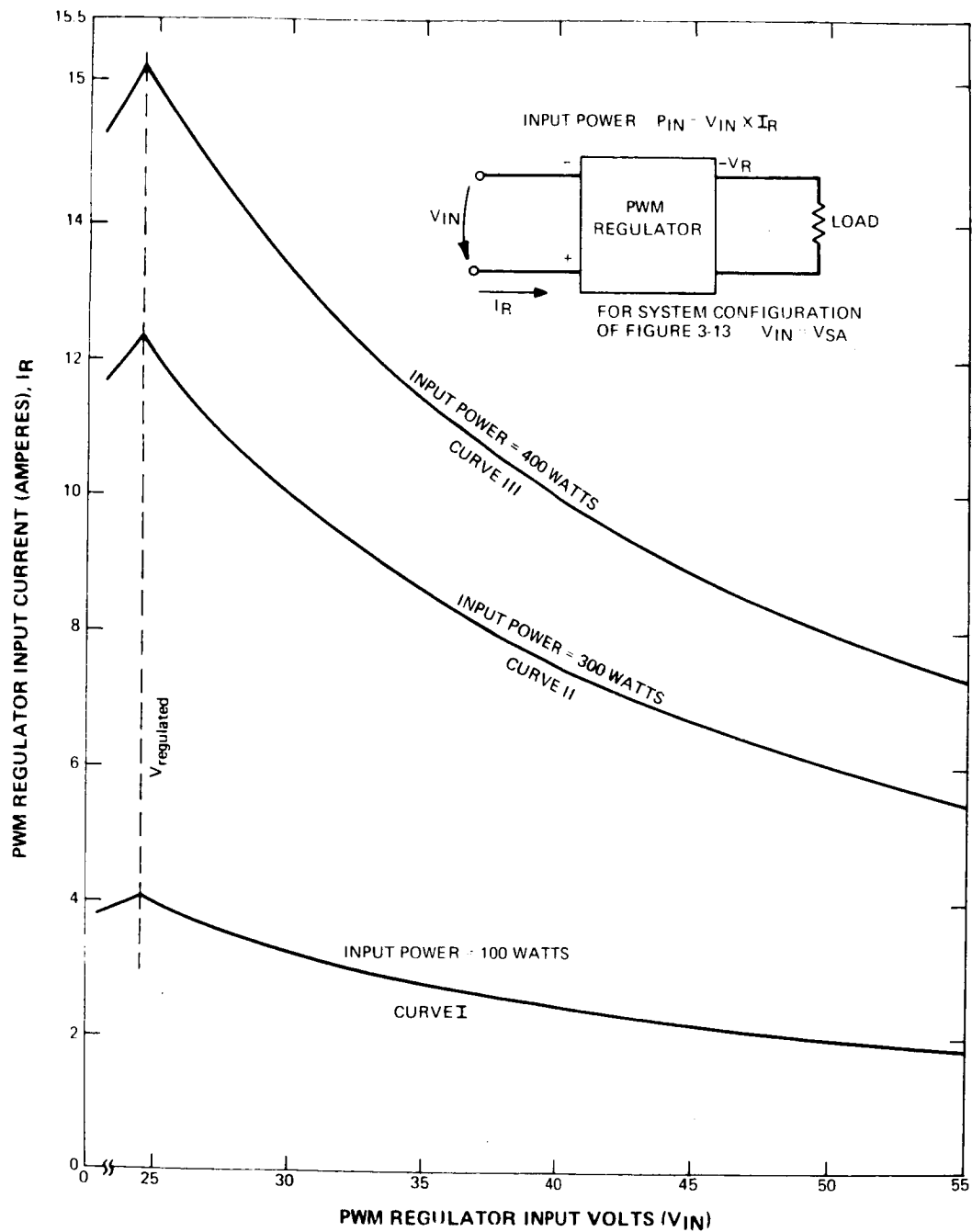


Figure 3-15. PWM Regulator Input Characteristics

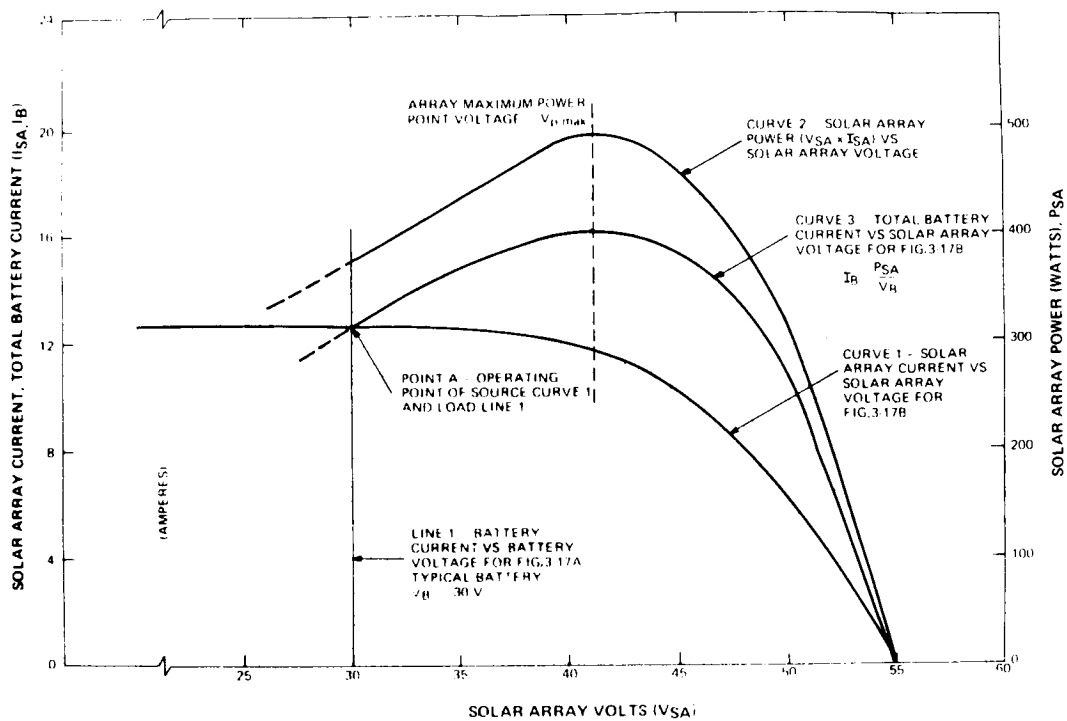


Figure 3-16. Solar Array I-V Characteristic and Load Lines for Battery

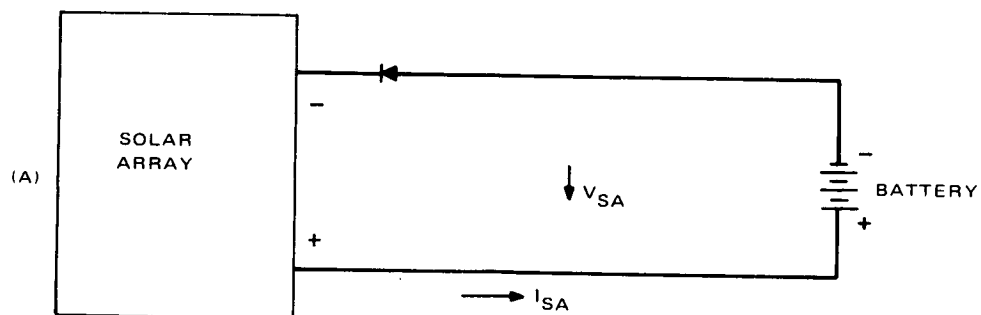


Figure 3-17A. Solar Array/Battery System

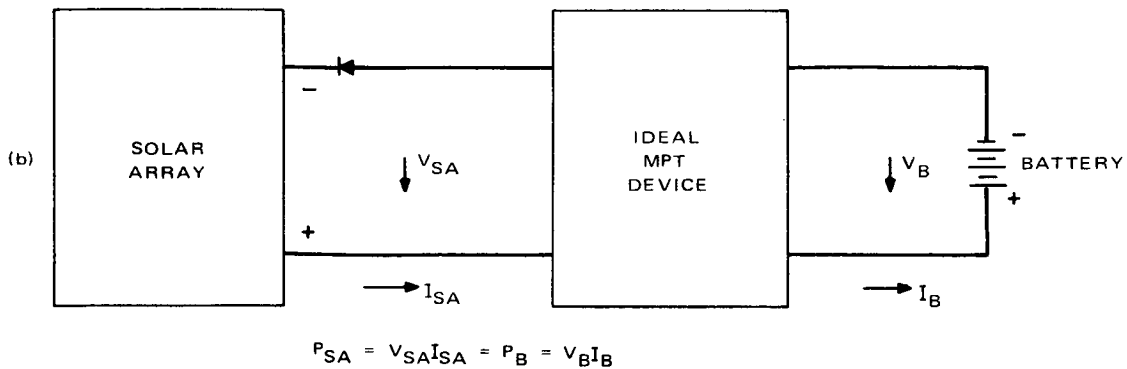


Figure 3-17B. Solar Array / MPT/Battery System

Curve 3, which is the characteristic of battery current vs. array voltage for the given system, can now be constructed. Note that the point of maximum current on curve 3 occurs at an array voltage (which is defined as $V_p \text{ max}$) corresponding to the array maximum power point.

Since both the MPT and the PWM Regulator are in parallel in Figure 3-14 the input voltage to both must be equal and must be equal to the array voltage, V_{SA} . The MPT current sensor measures a current which is the sum of the battery currents

and the PWM regulator input current. From Figures 3-15 and 3-16 the characteristic of the total output current (I_o) vs. the solar array voltage, can now be constructed as shown on Figure 3-18. Note that as the input power to the PWM regulator is increased, the peak current point becomes less defined and is shifted so that it no longer corresponds to the maximum power point voltage. Since the current sensed is no longer a valid indication of the output power, the tracker cannot track the maximum power point of the array.

d. Availability of Solutions

It appears that solutions do exist for specific problems. However, a single solution which will not compromise performance in other respects does not appear readily available so long as the system retains the basic operating principle of slowly varying a power switch (or switches) duty-cycle and searching some parameter such as load current or source power for a maximum.

3.2.5 Conclusions

a. Design and Performance Goals

The design and performance goals which were established for the MPT system are compared with the results of the performance tests as follows:

(1) Power Transfer Efficiency

The power transfer efficiency was generally greater than the 90 percent, which was the desired result.

The system failed to reach this performance goal only under the combined conditions of low battery voltage

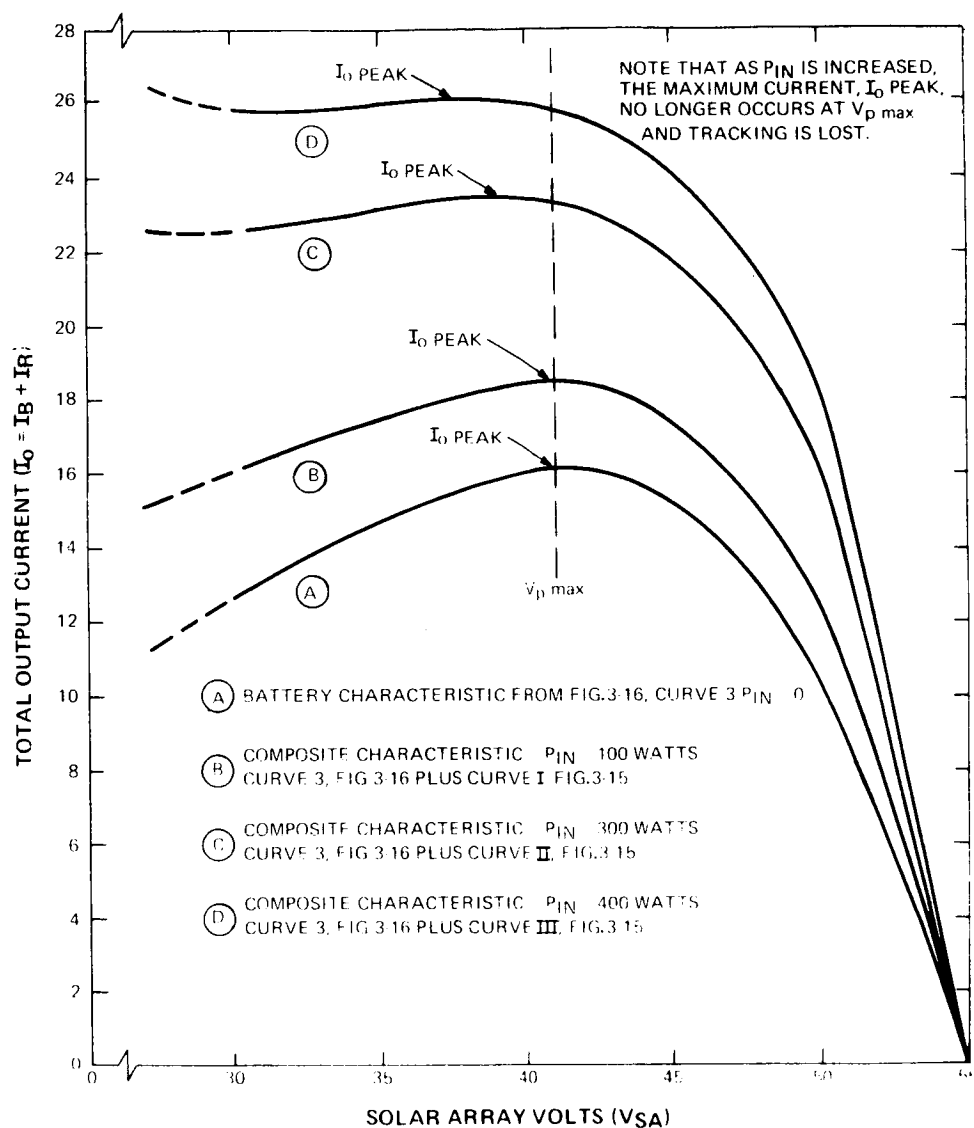


Figure 3-18. Composite I-V Characteristics, I_o vs. V_{SA}

and high array power (greater than 730 watts). From the analysis of the major losses, it appears that this condition could be improved by merely repackaging the system.

(2) Charge Current Sharing

The degree of current sharing achieved was approximately +5 percent as compared with the +10 percent design goal. Analysis of the behavior of the MPT control circuitry indicates that some slight improvements could be obtained, but the conditions previously described appear to limit the capability of the present control circuitry.

(3) Maximum Charge Rate

Maximum charge rate was maintained within +2 percent of the nominal value. The design goal was +10 percent. This accuracy also appears to be approaching the maximum capability.

(4) Trickle Charge Rate

The precision of trickle-charge rate was approximately +13 percent as compared to the +30 percent design goal. This accuracy also appears to be approaching the maximum capability.

(5) Shunt Loss

The shunt loss was approximately two percent (maximum) of the array power and is considered to be relatively nominal.

(6) Tracking Error

The MPT system maintained the array operating point within 0.62 percent of maximum power which is well within the +2 percent performance goal.

(7) Summary

The MPT experimental model has demonstrated that all the established design goals have been achieved or exceeded. The feasibility of a multiple battery maximum power point tracking system has been demonstrated.

b. System Interface and Application

The operation of the MPT experimental model in a typical space power system has highlighted several limitations of the basic operating concept used. Therefore, application of this first generation power tracker is necessarily limited by the type of system in which it is employed. Although solutions to specific problems may be found, general solutions are not feasible with the present operating concept.

3.3 Summary

The feasibility of a Maximum Power Tracker of multiple battery capability has been demonstrated by the construction and test of an experimental model. Included in this system are battery protection functions for voltage, temperature, and third electrode, or other auxiliary protection functions. The present MPT system has met or exceeded all the design goals which were established. This system can be used with power sources other than solar arrays by extending the present concept and providing proper interfaces. Successful operation with higher source voltages (up to 100 volts dc) has been achieved. Operation with low voltage sources requires application of other voltage-conversion techniques.

4.0 SECOND GENERATION MPT SYSTEM

4.1 Reasons for a New Concept

During the development of the low speed MPT system, as described in Paragraph 1.0, several system problems and interactions were discovered which severely restrict MPT operation. The problems which came to light during the system testing phase are described below:

With the MPT connected in a typical space power system configuration, load transients caused the MPT to falsely detect maximum power. This could result in the system operating at other than the maximum power point of the source if the transients repeated at a sufficiently rapid rate. This effect is primarily due to the use of the output (battery) current as an indication of source power, and the slow speed of response of the MPT system.

The MPT system was also unable to track the source maximum power point if the load return was connected to the battery return. This effect was due to the use of the total output (battery and load) current as an indication of source power. In this configuration, the PWM regulator caused the load current to be directly unrelated to the source power and the MPT was unable to maintain operation at the maximum power point of the source.

Both the above phenomena are direct results of the basic concept used to develop the low-speed MPT system. A single solution which will not compromise system performance does not appear readily available if the basic operating principle of slowly varying a power switch

duty-cycle and searching some system parameter, such as load current or source power for its maximum is retained.

An alternate approach to the existing low-speed MPT system would be to speed up the system response by increasing the rate at which duty-cycle is scanned. This method has been applied with some measure of success⁽²⁾. However, in order to avoid interaction between the scanning frequency and the power-switch/pulse-width-modulator frequency, a large separation between these frequencies was wisely maintained. If (in view of the state-of-the-art of power-switching components and efficiency) the highest acceptable power switch frequency is limited to the region of 10-20 kHz, it appears that the conclusions reached in the referenced investigation, concerning the scanning or hunting frequency, are quite reasonable (i.e. limited to about 300 Hz for a power switch frequency of 10 kHz).

It would, however, be desirable for the MPT system to be able to respond to transients as rapidly as does the source. Impedance measurements of typical solar panels (Nimbus) reveal a load change response, which begins to appear capacitive in the region of kHz. A ratio of maximum scan frequency to array response of between 3 and 5:1 (for purposes of faithfully following array variations) would yield a scan frequency of 15 to 25 kHz for the Nimbus array. Smaller arrays would require higher frequencies.

(2) NAS 5-9210, "Nondissipative Solar Array Optimum Charge Regulator" performed by Hughes Aircraft Company.

Separation between power-switch frequency and scan frequency (neglecting interference effects) would have to be at least one octave, in order that control might be exercised. This would result in a power switch frequency of 30 to 50 kHz, which is clearly excessive. It may be noted that a scan frequency, this much in excess of the array response, would cause a phase error between the system duty cycle and the actual array operating point. This would result in less than optimum power transfer.

4.2 Second Generation System Concept

Derivation of a high-speed maximum power tracking system concept must, as a result of the problems and limitations previously described, represent a departure from the constant-frequency, variable-duty-cycle methods heretofore employed. The second generation MPT system is based on an extension of the concepts and techniques developed for the ripple-controlled PWM regulator during the initial phases of this contract.

4.2.1 Basic System Operation

The basic system as shown in Figure 4-1 only includes the functional elements required for the power tracking mode of operation. The characteristics of some of the functional elements are as follows:

a. Source Characteristics

Figure 4-2 presents the source characteristics which must be obtainable at the highest switching frequency of the system.

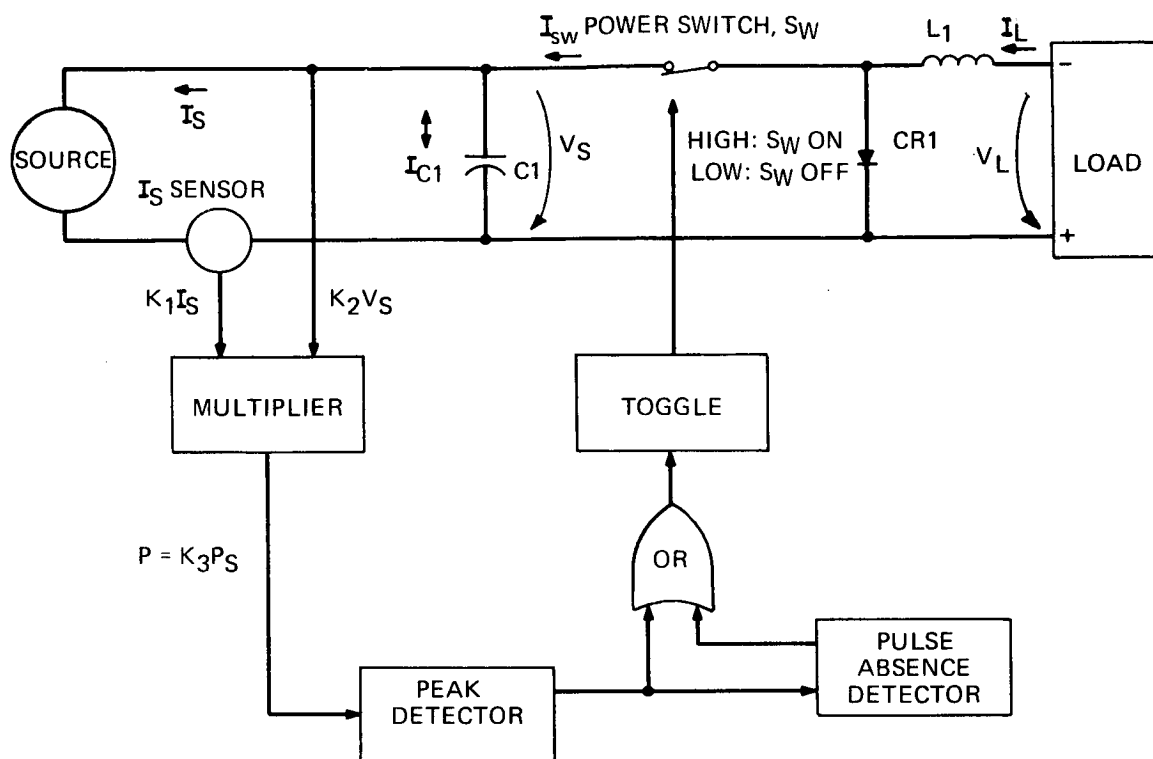


Figure 4-1. Basic System Diagram

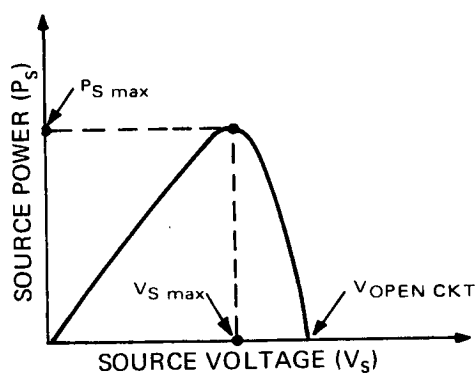


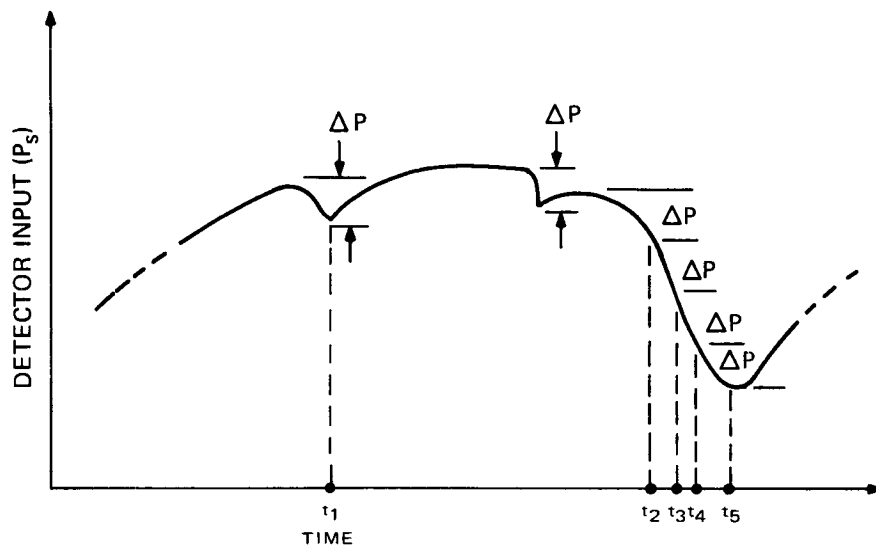
Figure 4-2. Source Characteristics

b. Multiplier

The input signals are instantaneous source-voltage and current. The output signal is proportional to instantaneous source power being delivered. Response times of this system compatible with the maximum operating (or switching) frequency of the system.

c. Peak Detector

The input is a signal proportional to instantaneous source power. The output is a pulse whenever the input signal decreases by a small amount, ΔP , from the previous value. (See Figure 4-3.)



- (1) ΔP IS PEAK DETECTOR SENSITIVITY
- (2) PULSES GENERATED AT t_1, t_2, t_3, t_4, t_5

Figure 4-3. Peak Detector Characteristics

d. Pulse Absence Detector (PAD)

The PAD generates an output pulse similar to the peak-detector output whenever the period between peak-detector output pulses exceeds some predetermined time. The purpose of this function is to avoid a situation whereby the system might "hang-up" in an undesirable state with the power switch either full on or full off.

e. Toggle

This is a bistable device which changes states with each input pulse. In one state, the toggle drives and holds the power switch on; in the other, it drives and holds the switch off.

f. Load

The only restriction placed upon the load is that it must be capable of absorbing maximum source power at some voltage, V_L , which is lower than that at which the source delivers its maximum power, $V_{max}^{(3)}$.

Operation of the basic system in the power tracking mode is as described below.

-
3. This voltage requirement is a function of the power switch/inductor (L1)/flyback-diode (CR1) configuration, only. Other voltage relationships could be incorporated by utilizing the same basic concept and other voltage conversion circuitry.

Assume the system is at rest with $V_S = V_{C1} = V_{SOC}$ circuit and the power switch is open. The opposite assumption, i.e. that the switch is closed and $V_S = V_{C1} = V_L$, can also be made with the result that the system will start and continue to operate properly. This assumption then, in no way limits the generality of the description. The PAD will issue a pulse since the peak detector cannot detect with the system at rest since the source power cannot change. This will then turn on the switch and the switch current, I_{SW} , will begin to flow, increasing at a rate dependent upon V_S and V_L (for a given value of $L1$). The source voltage will begin to decrease and the source current to increase. In effect, the source operating point will move over the $P_S - V_S$ characteristic toward the P_{max} point. Note that during this time, I_{SW} is composed of I_S and I_{C1} and is greater than either. Note also, that the period of time throughout which this entire action occurs is consistent with and dependent upon the circuit constants, $L1$ and $C1$, and the existing voltage levels. This indicates that the action can be designed to take place in tens or hundreds of micro-seconds providing the source can accommodate such operating speeds.

As the source operating point traverses the $P_{max} - V_{max}$ point, the source power peaks and then falls off. When P_S decreases from P_{max} by an amount, ΔP , the peak detector issues a pulse which reverses the toggle and thereby changes the state of the power switch (i.e. turns it off).

At this point in the cycle, two things occur: (1) the current flowing in L_1 tends to continue flowing, due to its inductance and, as a result, a flyback action occurs causing C_{R1} to conduct. (2) Source current will be diverted from the power switch and will flow into the capacitor. This will charge the capacitor and cause its voltage (and the source operating point) to rise towards the source open circuit voltage, V_{soc} . As V_S traverses V_{max} , source power will peak (note that P_S is being delivered to the capacitor) and when the power decrease (ΔP) is traversed, the peak detector again issues an output pulse. This pulse causes the power switch to turn on again and the hunting action continues as before. Note that if L_1 has a sufficiently large inductance, it will maintain conduction of C_{R1} through the entire off period of the power switch, although this is not a necessary condition for operation of the system.

This MPT concept will allow maximum power to be drawn from the source, regardless of variations in source characteristics over a wide range of source variation rates. For example, the high-speed MPT then has applicability where a solar array has a rapidly fluctuating output as is the case for a spin-stabilized spacecraft with a body-mounted solar array which might exhibit ripple in the array power-time characteristic due to the spacecraft rotation. Source fluctuations due to loading at the source terminals (other than the MPT loading) might also be followed in a stable manner if the MPT system operating frequency is sufficiently in excess of the transient rates.

4.2.2 System Protective Mode Operation

In order to apply the basic MPT concept to an operating system, the inclusion of system protective functions is required. These include battery voltage and current limiting, battery high-temperature cut-off, and battery current-sharing controls. The complete system functional diagram including the protection features is shown in Figure 4-4. Operation of these functions is as follows:

The power switch may be turned on by the flip-flop (toggle) in the control unit. This is done in order that all battery modules operate in step regardless of their respective modes of operation (i.e. overcharge protection, current sharing, or actively tracking the P_{\max} point). Assuming battery protection to be inactive, the system will be tracking the P_{\max} point.

When the system is tracking, the current sharing controls will allow all the power-switches to turn on together when the output of the control unit toggle presents a positive-going output voltage. When the array operating point passes the P_{\max} point, the peak detector issues an output pulse which reverses the toggle.

At this point, the power switch in the battery module passing the highest current will turn off. The remaining battery modules (having lower output currents) will have a positive current-sharing error signal, ϵ_3 (this is the same error signal generating mechanism that was used in the low-speed MPT system). If ϵ_3 is sufficiently large, a positive-going signal, u_3 , will be

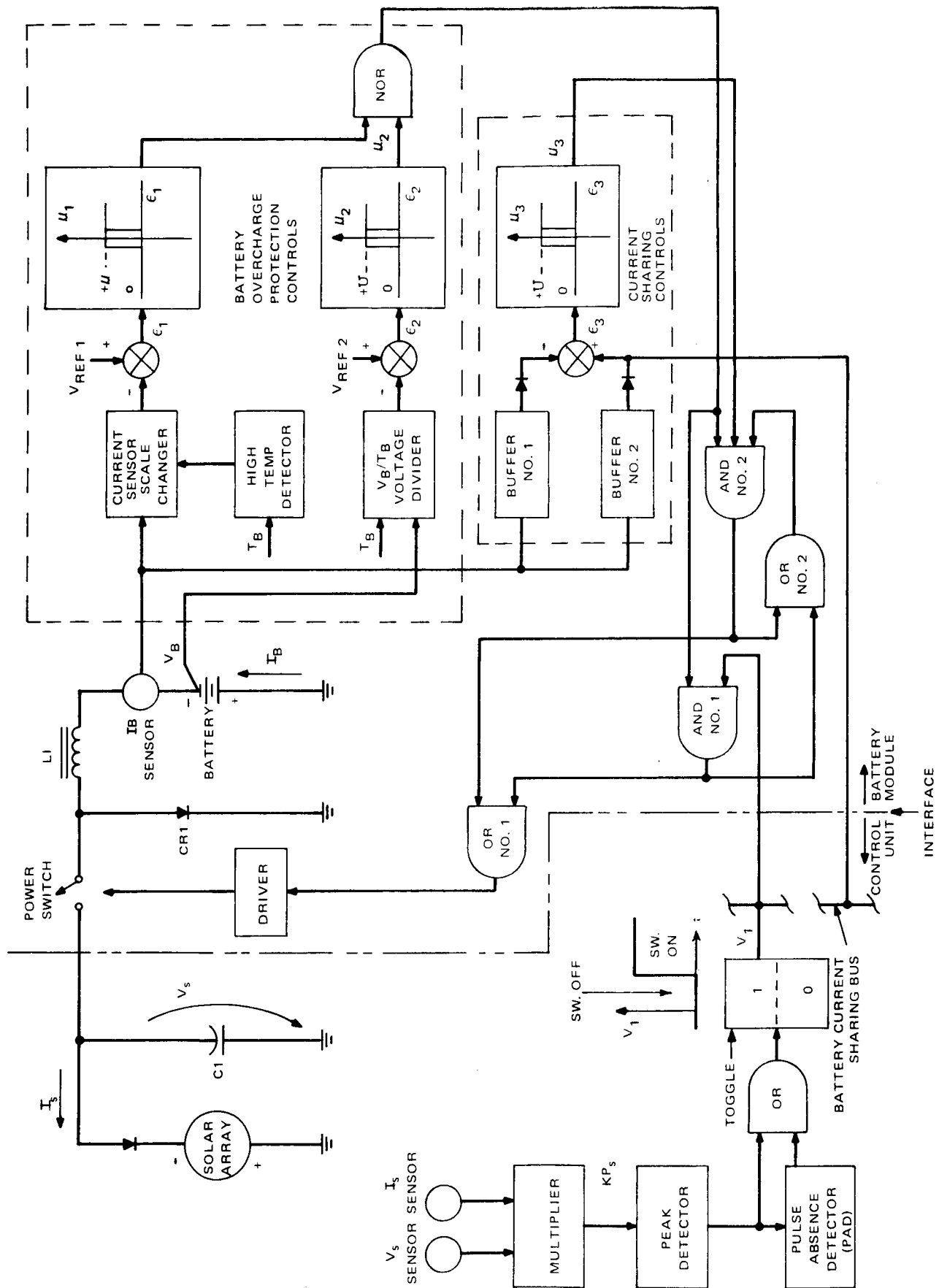


Figure 4-4. Functional Diagram, High Speed MPT System

applied to AND gate 2 which will act to hold the corresponding power switch on until the current increases. This cause ϵ_3 to reverse polarity by some small amount. At this point, u_3 becomes zero, releasing AND gate 2 and the power switch turns off. This action will effectively cause the lower-current battery modules to have larger duty cycles than the highest current module, but at the same operating frequency. In effect, the low-speed system performs in the same manner in this mode.

Battery protection controls function in just the opposite manner. An error signal ϵ_1 is generated if the battery current exceeds a predetermined maximum value, and current limiting action is initiated. If the battery temperature increases above a predetermined maximum limit, the high-temperature detector senses the fault and causes the current sensor scale-changer to increase the effective current sensor gain. Thus the current limiting action will occur at a lower current level as determined by the scale-changer characteristics. Similarly, if the battery voltage and temperature increase above a predetermined characteristic, then an error signal ϵ_2 is generated. Existence of a large error signal (ϵ_1 and/or ϵ_2) will cause the NOR gate output to be zero (it is positive for negative values of ϵ_1 and ϵ_2) thereby inhibiting AND gates 1 and 2. This action will turn the power switch off if it is on, or will inhibit turn-on if it is off. This action effectively reduces the duty cycle and will continue until the battery protection error(s) are reduced to acceptable values.

Note that the transition from the normal tracking mode to a protected mode, and between the various protective modes, is automatic and is performed continuously.

4.3 High-Speed MPT Circuits

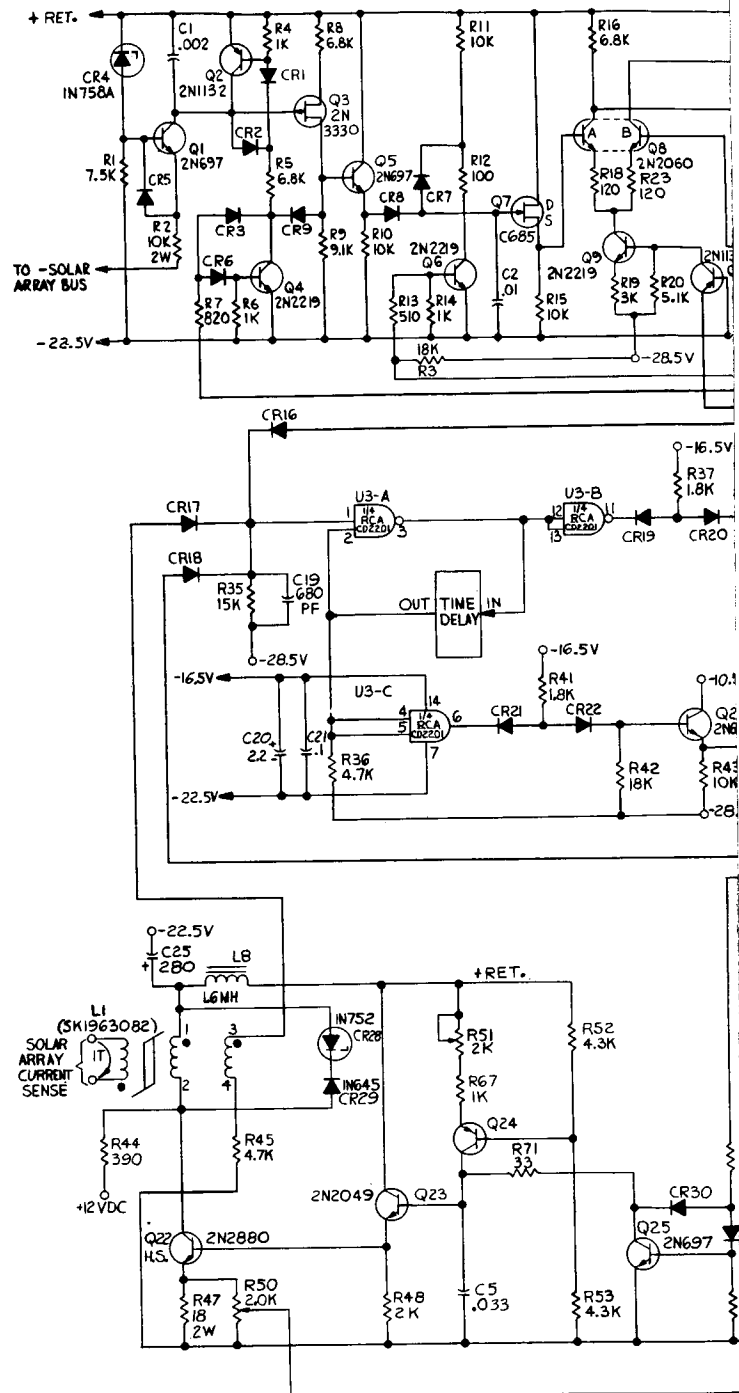
The implementation of the high-speed MPT concept required that many different control circuits be developed. The schematic diagrams for the high-speed MPT Control Unit and Battery Module are shown in Figures 4-5 and 4-6 respectively.

Some circuits used in the low-speed system have been carried over with little or no changes (e.g., the power switch drive circuitry is almost identical to that used in the previous system). Selected circuits from the high-speed MPT system are described below. Deviations from the low-speed circuits are noted when applicable. It should be noted that the implementation of the second generation MPT concept was designed to demonstrate feasibility and that the results may not reflect the optimum circuit configuration.

4.3.1 Power Sensor Circuit

One of the more significant requirements placed on the MPT system is that of having the capability of sensing and producing a signal proportional to instantaneous array power, with a response time compatible with system speed. While there is no severe accuracy requirement, the power sensor output must be monotonically related to its input and must operate

FOLDOUT FRAME



NOTES:
 1. UNLESS OTHERWISE SPECIFIED:
 ALL DIODES ARE IN914
 ALL RESISTORS ARE CARBON COMPOSITION 5% 1/2 W.
 ALL CAPACITORS IN MICROFARADS, RESISTORS IN OHMS.
 2. 1/4 IC IS (1) PACKAGE.

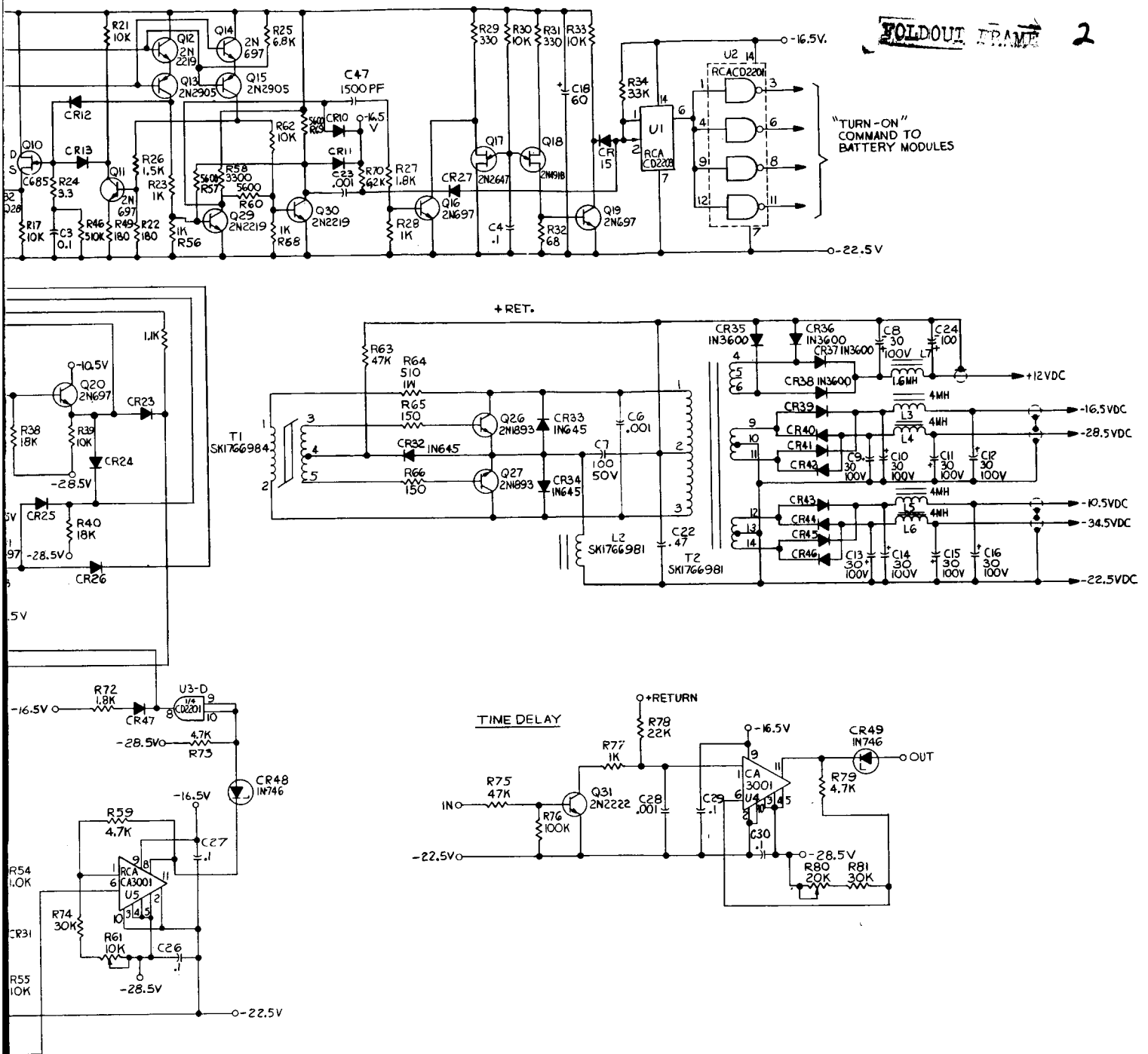
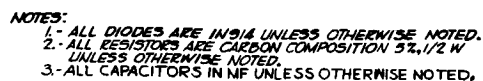
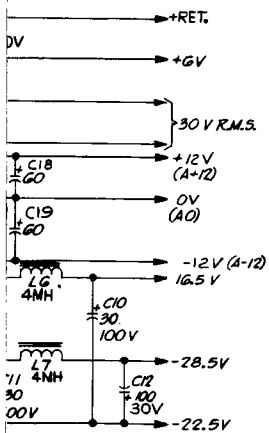
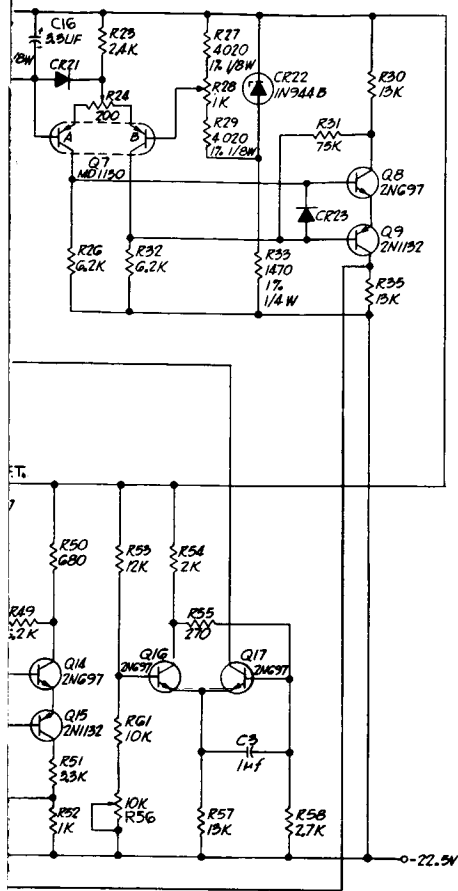


Figure 4-5. High-Speed MPT Control Unit, Schematic Diagram (RCA Dwg. SK 1975689)



4-14

2



efficiently in that insertion and operating losses must be small relative to the measured power.

There were basically two schemes considered for this purpose which appear capable of fulfilling the basic requirements. Hall effect circuits appear well suited to such an application. Hall multipliers are available with isolated inputs, frequency responses through 100 kHz and reasonable specifications of residual outputs and temperature coefficients. Units are available as off-the-shelf items with current ratings through 40 amperes and low insertion losses. In order to sense voltage, a resistor would be connected in series with the Hall element, directly, and the combination connected between the array terminals. The penalty to be paid in this case for such a simple arrangement is the relatively high Hall-element current required. For a full-scale output of 60 millivolts, a Hall element current of about 300 milliamperes is required. Assuming this loss to occur at maximum array power which would occur near maximum array voltage, a power loss of 30 watts would occur for a maximum power voltage of 100 volts. This is clearly excessive for array powers much less than 30 kilowatts.

The scheme implemented is one which takes advantage of the fundamental relationship between the voltage on a capacitor and the current and time required to develop that voltage. A means for implementing a d-c power sensor in this manner is explained below.

Figure 4-7 shows a Functional Diagram of this scheme.

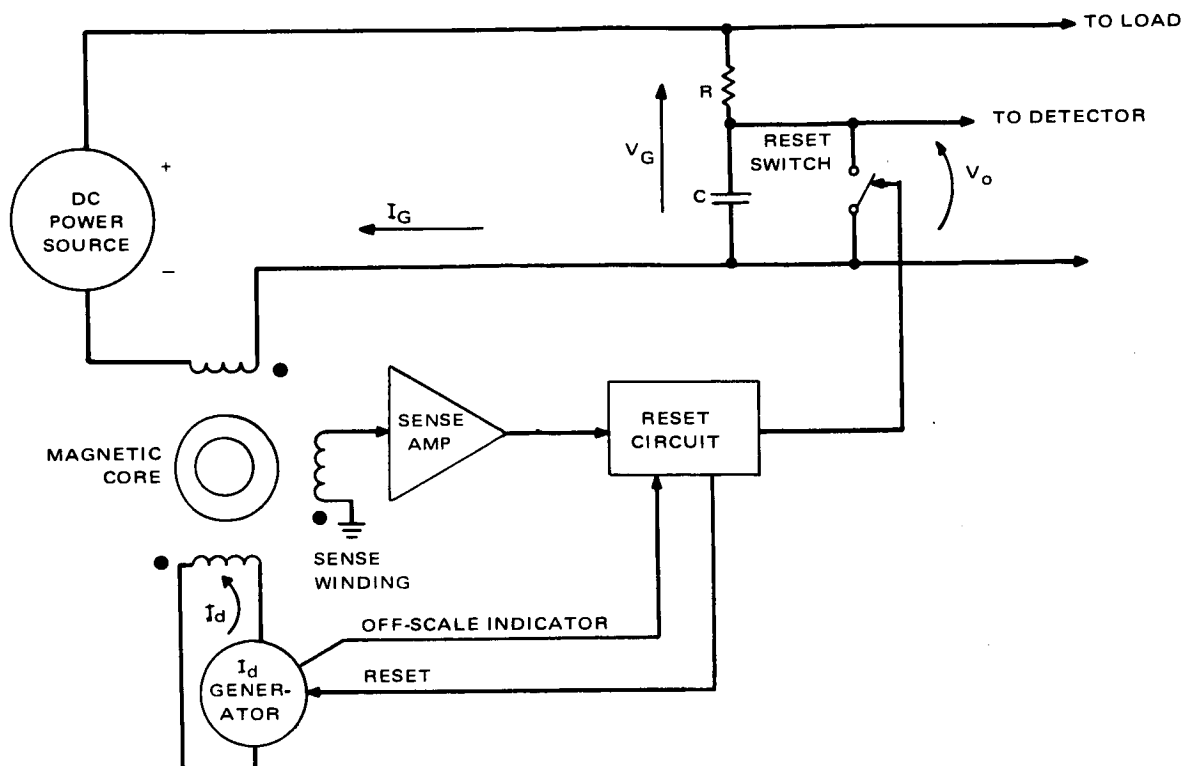


Figure 4-7. DC Power Sensor Functional Diagram

Circuit action is assumed to begin with the reset circuit action which opens the RESET SWITCH and initiates the I_d generator.

The voltage, V_o , is the output of the indicated R-C network and may be expressed in terms of the Laplace transform after the reset switch is opened at $t = 0$ as:

$$V_o(s) = \frac{V_G(s)}{1 + SRC} \quad (4.1)$$

In the time domain (considering $V_G \approx$ constant over the sampling interval).

$$V_O(t) = V_G \left[1 - e^{-t/RC} \right] \quad (4.2)$$

For period of time, t_1 , much smaller than the time constant, RC , results in the linear approximation,

$$V_O(t = t_1) \approx \frac{V_G t_1}{RC} \quad (4.3)$$

If the remaining circuitry, indicated in Figure 4-7, satisfies the relationship,

$$t_1 = K_1 I_G, \quad (4.4)$$

then

$$V_O(t = t_1) \approx \frac{V_G}{RC} K_1 K_G = \frac{K_1}{RC} P_G \quad (4.5)$$

where

K_1 is a proportionality constant.

P_G is the generator power to be measured.

t_1 is the time at which reset circuit action occurs.

The output voltage waveform will appear as shown in Figure 4-8.

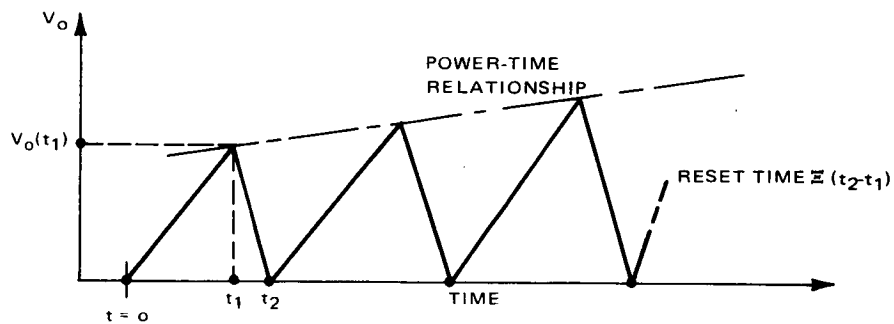


Figure 4-8. Output Voltage Waveform

The dashed line in Figure 4-8 represents the sensed Power-time relationship. If

$$(t_2 - t_1) \ll t_1, \quad (4.6)$$

then the average voltage also is proportional to the power which indicates that an ordinary, average reading voltmeter may be employed as a readout device.

The manner in which the current-to-time conversion as described by equation (4.4) is achieved is as follows.

For $I_d = 0$, the state of the magnetic core (indicated in the schematic diagram) is described by Figure 4-9.

This causes an increasing magnetic field intensity (H_d) in the core in a direction opposite to that of $-H_G$. This field intensity adds algebraically with $-H_G$. The direction of H_d is indicated in Figure 4-9 as is the resultant field intensity, H_c .

Figure 4-11 shows the various field intensities described above as a function of time.

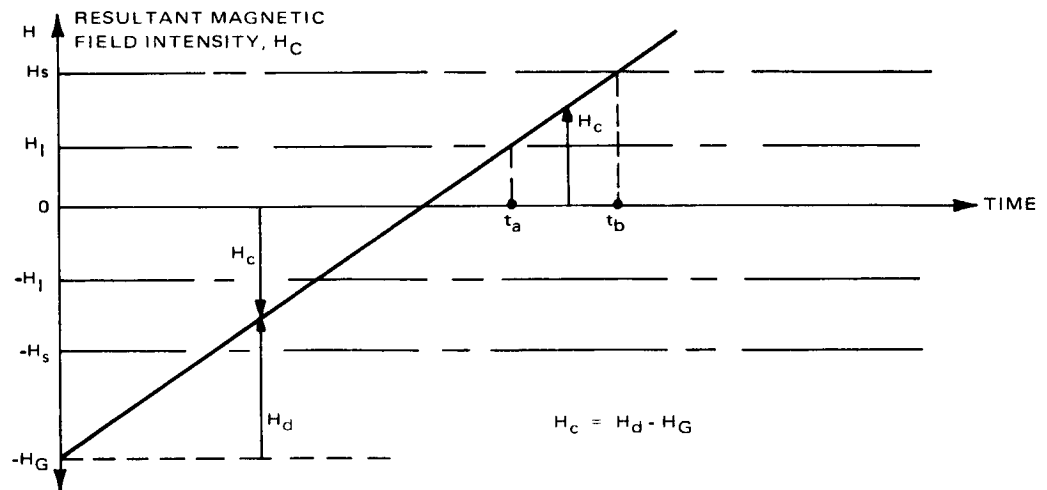


Figure 4-11. Core Field Intensity vs. Time

As the resultant field intensity becomes equal to $+H_l$ at ($t = t_a$) and the core becomes unsaturated, a voltage is induced in the sense winding of the core which can be sustained until $H_c = +H_s$ at ($t = t_b$). This voltage is amplified and used to initiate reset circuit action.

This action is such as to: (a) momentarily close the reset switch thereby discharging the capacitor, C , to zero voltage and (b) to reduce I_d to zero current. It is assumed that the time required for reset action is small. It is further assumed that reset action occurs at $t = t_a$, therefore, t_a is the same as t_1 in equation (4.4).

In this case, then, t_a will vary with and be approximately proportional to the magnitude of H_G and, therefore, I_G . This approximation will improve in terms of sensor accuracy as the ratio of H_G to H_1 increases.

The I_d generator is actually a current sawtooth oscillator whose maximum current amplitude related by the magnetic circuit to the maximum current (I_G) to be expected in a particular situation. This oscillator may be reset to zero at any time by the reset circuit action as already described. When the generator current, I_G , is zero or in the wrong direction, the current sensor will not operate as described. Additional logic circuits would be required to hold the reset switch closed forcing V_o to zero.

The need for this logic is eliminated by placing an appropriate bias on the core by modifying the I_d generator such that it contains adequate negative bias in its waveform. This is illustrated in Figure 4-12.

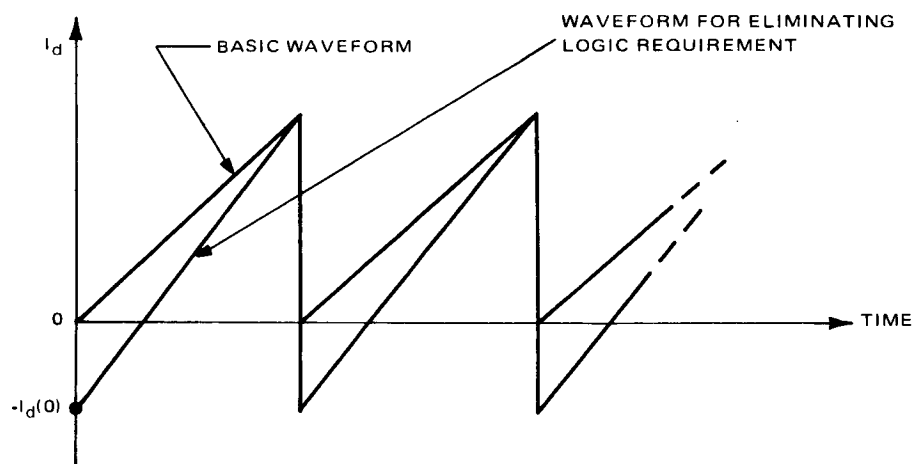


Figure 4-12. Practical I_d Generator Characteristic

In this case, $-I_d(0)$ must be sufficient to reset the core to an operating condition more negative than $-H_s$ enabling the generation of sense pulses for conditions of zero I_G . The zero I_G condition results in a zero or minimum indication at the power-sensor output. Conditions of excessive I_G or of I_G in the wrong direction result in an off-scale indication to the detector or readout device.

4.3.2 Peak Power Detector Circuit

The high-speed MPT system requires a peak-detector circuit which performs the same basic functions as were required in the low-speed system. However, the high-speed circuit must perform these operations within a short sampling-

interval. A power comparison and either information storage or peak detection is performed within a five microsecond sampling time. The circuit is shown in Figure 4-13.

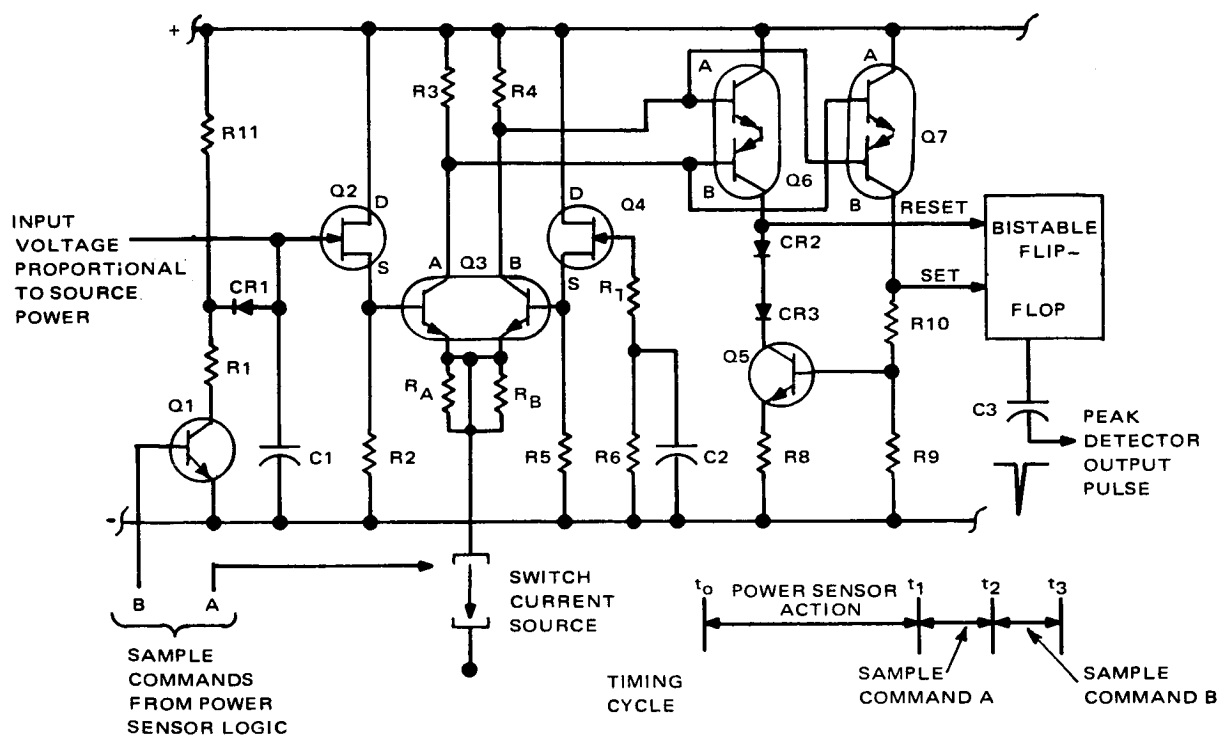


Figure 4-13. Peak Power Detector Circuit

Before a description of circuit operation is presented, the functions of the various circuit elements will be described. A switched current source, which is controlled by sample command A from the power sensor logic, provides the bias current to turn difference amplifier Q3 on or off. Capacitors C1 and C2 are used as memory devices for instantaneous source power information. Field-effect transistors Q2 and Q4, and diodes CR1, CR2, and CR3, are used to maintain high circuit impedance preventing unwanted loss of capacitor charge which is equivalent to storage of inaccurate information. Transistors Q1 and Q5 are used to discharge C1 and C2 at the appropriate time in the operating sequence. To ensure that instantaneous source power must alternately increase and decrease, a bistable flip-flop is included. This eliminates erroneous peak detector output pulses which can occur as a result of source power phase lag.

The sequence of operation is as follows:

Assume initially that capacitors C1 and C2 are discharged and transistors Q1, Q3, Q5, Q6, Q7 and the current source are turned off. At time t_0 , the source power increases and a proportional voltage from the power sensor charges C1 during the time $t_1 - t_0$. At time t_1 , sample comand, A, is received from the power sensor logic turning the difference amplifier bias current source on. Since the voltage on C1 is greater than that on C2, difference amplifier Q3 is unbalanced causing complementary difference amplifier Q6 to conduct,

charging C2 until its voltage equals that on C1 and Q3 is restored to balance. Thus, the instantaneous source power information is transferred from C1 to C2 which acts as a memory element. When amplifier Q6 conducts (which indicates an increase in source power) a reset input is provided to the bistable flip-flop. At time t_2 , sample command A is removed, turning difference amplifier Q3 off. Also at time t_2 , sample command B is applied which turns on Q1, discharging C1 in preparation for the next power sensor sample cycle. At time t_3 , sample command B releases and the cycle repeats beginning at time t_0 . If source power continues to increase each power sensor sample period, the circuit operation continues as described. Assume now that the source power decreases. Thus, at time t_1 , capacitor C1 is charged to a voltage which is less than that of C2. Sample command A turns on difference amplifier Q3 which is again unbalanced but in the opposite manner causing complementary difference amplifier Q7 to conduct. This action turns on Q5, discharging C2 and resetting the peak detector. Capacitor C2 is discharged to a voltage level equal to that of C1 and Q3 is again restored to a balanced condition. Q7 also provides a set input signal to the bistable flip-flop which issues a peak detector output pulse. The action between times t_2 and t_3 is as previously described for increasing power operation. Further decreases in source power are rejected as errors by the peak detector until a power increase to reset the flip-flop occurs.

4.4 Working Model

The fabrication of a working laboratory model was undertaken to demonstrate the feasibility of the high-speed MPT concept. The methods and techniques employed in this breadboard set-up which can have significant effects on the system operation are described below.

4.4.1 Basic Equipment Layout

The high-speed MPT system breadboard consists of a control unit (CU) and a battery module (BM) as shown in Figure 4-14. An open style layout was used to facilitate circuit testing and debugging.

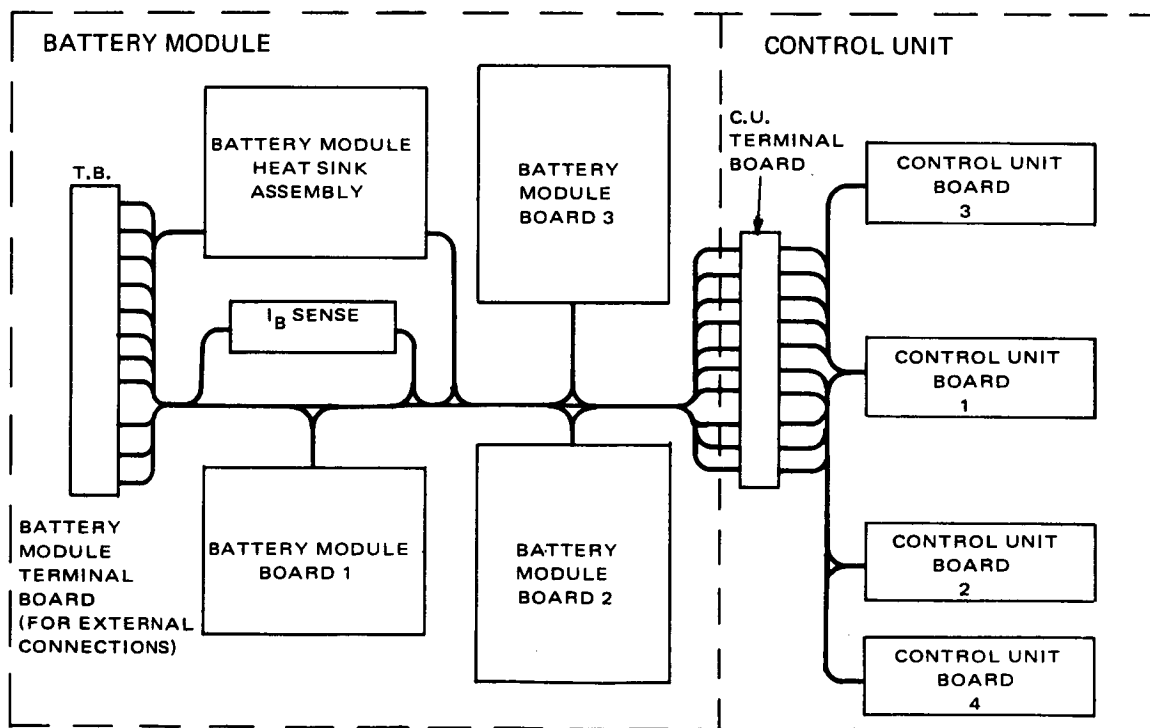


Figure 4-14. High Speed MPT Working Model Layout

Control circuits are constructed on vector-type circuit boards and the circuits are generally functionally grouped. For example, board 3 in both the control unit and battery module each contain the complete internal power supply for the generation of integrated circuit bias voltages and square-wave a-c drive voltage. The heat-sink assembly is similar in construction to that in the low-speed MPT system and includes the power-switching transistor, its driver circuits, the array capacitor, and the output filter inductor.

A terminal-board is provided in the battery module section to facilitate the connection of the solar array, battery power, and battery sensing wires. A second terminal board in the control unit section serves to interconnect the two MPT sections and is also used as the input point for control-circuit bias power.

4.4.2 Grounding and Noise Suppression

As a result of the high operating speeds of the tracker control circuitry, the problems associated with grounding and noise are more critical than was the case in the low-speed system. The grounding plan adopted is shown in Figure 4-15. This scheme and a few filters reduced the ripple and noise on the bias power busses to tolerable levels. Shielded cables were used for power distribution to reduce the effects of radiated noise.

The major source of EMI is the power switching network which is located on the heat sink assembly. To reduce

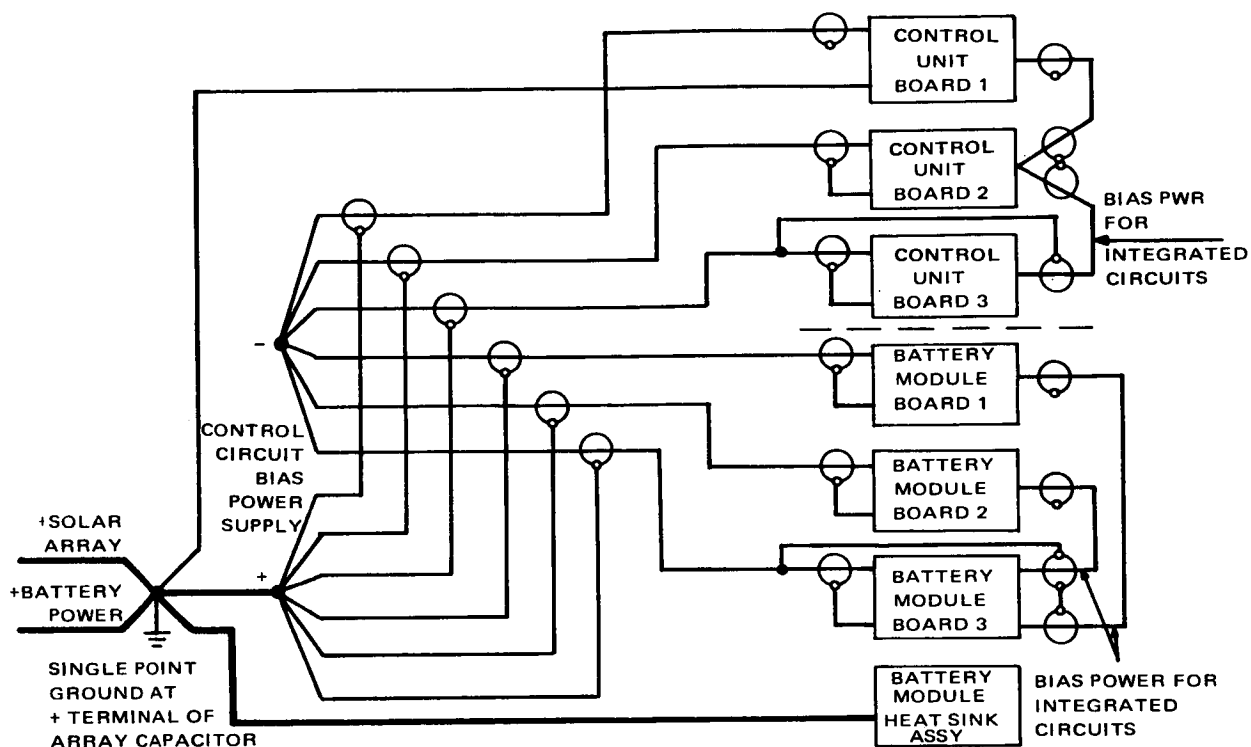


Figure 4-15. Working Model Ground Plan

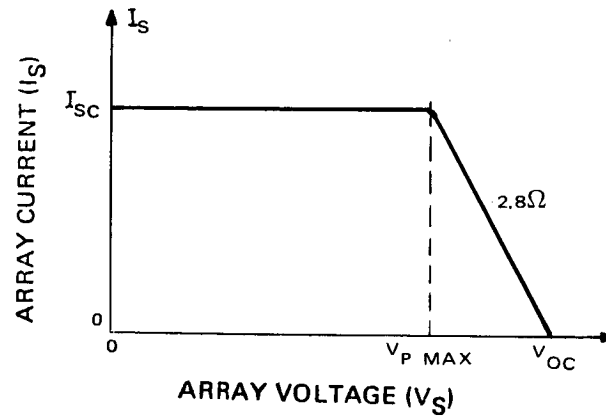
the effect of this noise on the low-level circuitry, the heat sink assembly was enclosed in an aluminum enclosure.

4.5 Laboratory Evaluation

To demonstrate the validity of the high-speed MPT concept, and the feasibility of the proposed control circuits, a series of laboratory tests were performed. These tests were designed to measure the performance capabilities of the second generation system (as incorporated in the working model) and provide a comparison using the low-speed system performance as a base-line. The system tested was made up of a control-unit, one battery module, lead-acid batteries,

and an adjustable solar array simulator. The simulated solar array I-V characteristic is as shown in Figure 4-16.

a. I-V Curve



b. Typical Parameters:

I_{SC} (Amperes)	V_{OC} (Volts)	$V_{P MAX}$ (Volts)	P_{max} (Watts)
4.0	60	48.8	195
4.0	90	78.8	315
6.0	60	43.2	259
6.0	90	73.2	439
8.0	60	37.6	301
8.0	90	67.6	541

Figure 4-16. Simulated Solar Array Characteristics

4.5.1 Power Transfer Efficiency

The power transfer efficiency is defined as the ratio of average MPT output power to average input power expressed as a percentage.

$$\eta_T = \frac{V_{B\text{AVE}} \times I_{B\text{AVE}}}{V_{S\text{AVE}} \times I_{S\text{AVE}}} \times 100 \quad (4.1)$$

Figure 4-17 for a range of array powers. The efficiency was found to decrease for array characteristics having lower short circuit currents. This is a result of the power sensor full-scale range of 1500 watts (100 volts and 15 amperes) being much greater than the

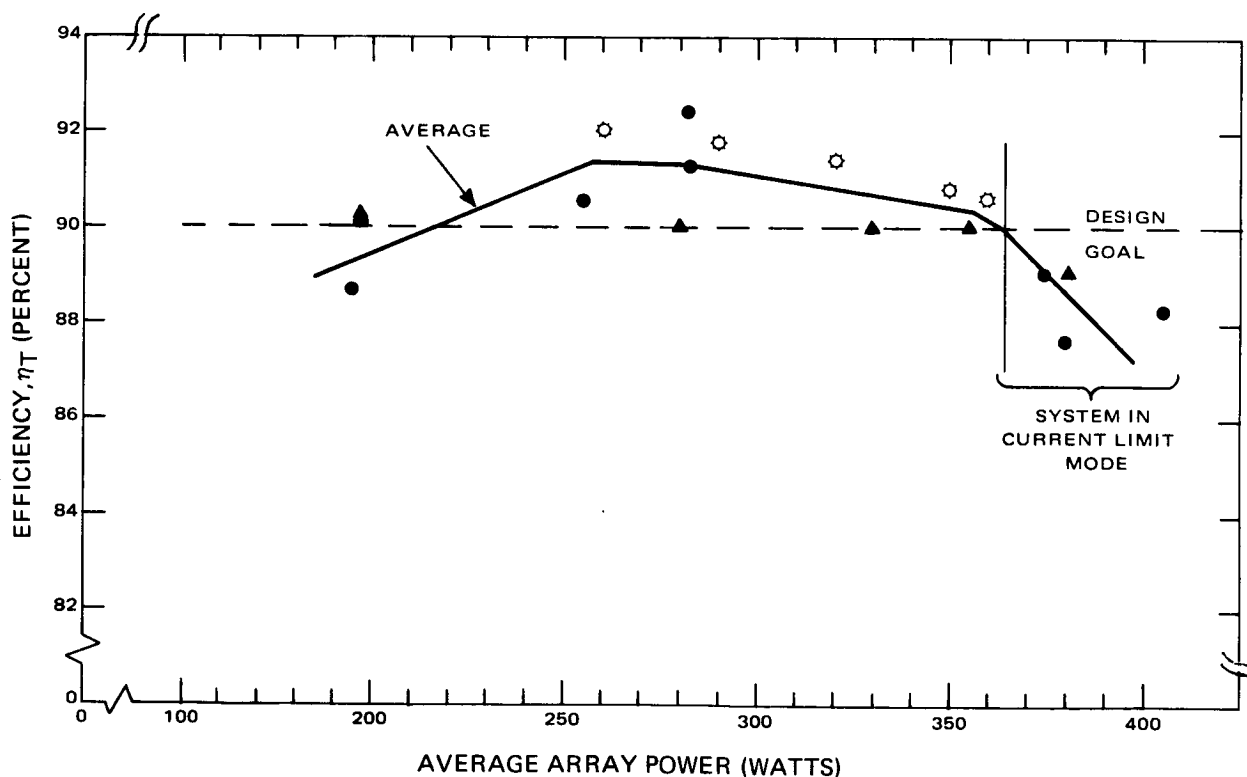


Figure 4-17. High Speed MPT Power Transfer Efficiency

operating power levels, and the decrease in current sensor sensitivity at low current levels. Generally, the results are comparable to the low-speed system performance and satisfy the 90 percent design goal.

4.5.2 Charge Current Sharing

No results are available for this parameter since only a single channel system was constructed. The current sharing circuit performance has not been verified.

4.5.3 Maximum Charge Rate Control

The maximum-charge-current-limit function was set to operate at 11 amperes. Limiting action appeared to be satisfactory on an average basis, however, the circuit action is dependent on the state of the turn-on command (toggle output). For the single channel system of the working model, the pulse absence detector operates when a protection feature is initiated and the power maximizing controls are inhibited. The current-limit control circuits operate only during one half-cycle of the PAD. Thus, in a multiple battery channel system, the current limit level will tend to be input voltage (duty cycle) dependent. Additional logic will be required to overcome this short-coming.

4.5.4 Trickle Charge Rate Control

The trickle charge current regulation function was set to about 300 milliamperes for the working model. This mode of operation occurs when the battery voltage,

battery temperature, or both, exceed safe limits as determined by battery considerations. The same difficulties as occurred in the maximum charge current limit controls also apply to the trickle charge rate controls since much of the sensing and control circuitry is common to both functions. Thus the additional logic described in section 4.5.3 will provide a solution for both problems.

4.5.5 Shunt Loss

The shunt loss is the power which is required by the sensing and control circuits from the external -22.5 volt power supply. The shunt loss vs. array power is shown in Figure 4-18. In comparing these results to those for the low speed system, it should be noted that the drive power for the power-switching network

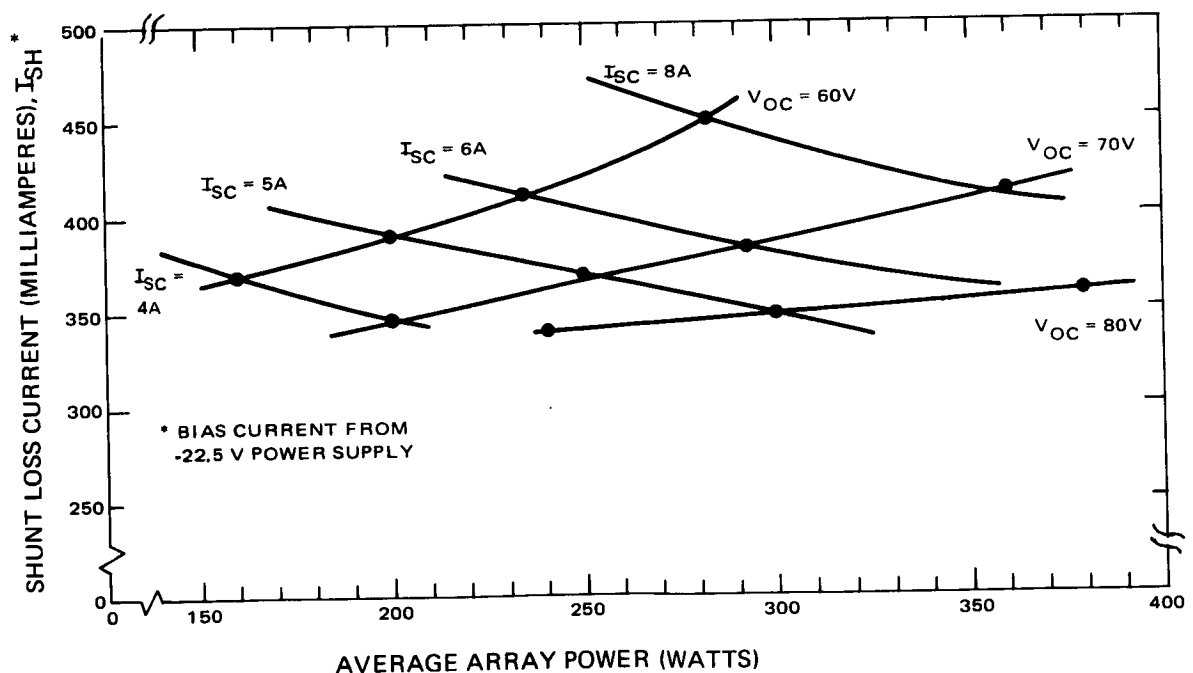


Figure 4-18. Shunt Loss Current vs. Array Power

is included as part of shunt loss in the high-speed system and as part of power-transfer loss in the low-speed system. Power-switch drive requires approximately 160 milliamperes from the bias power supply when the transistor switch is operating at 50 percent duty cycle. Thus, shunt loss will decrease for higher source voltages. Similarly, the shunt loss will increase for increasing array current due to the current-sweep generator in the power sensor.

4.5.6 Tracking Error

For the high-speed MPT, tracking error is best found by comparing the average power delivered by the source (as determined from average voltage and average current meter readings) to the known source power at the maximum power point. Tracking error is directly proportional to the sensitivity of the peak detector circuit which does not vary as a function of array power level.

Average tracking error is defined as:

$$E_T = \frac{P_{\max} - P_{\text{Save}}}{P_{\max}} \times 100 \quad (4.2)$$

The maximum tracking error was 14.3 percent which occurred at an array maximum power of 230 watts and the minimum was 5.6 percent at 380 watts. This error is larger than that experienced for the low-speed system because the peak detector circuit sensitivity was reduced to eliminate the effects of noise and spurious signals. The increased susceptibility to noise is a

direct result of the extremely wide bandwidth circuits which are required by the high operating speed of the MPT system.

Again, the effects of operating over a small portion of the power sensor range (as described in section 4.5.1) are evident. The source power change necessary to operate the peak detector was: $\Delta P = 28$ watts for an array short-circuit current of $I_{SC} = 5$ amperes, $\Delta P = 22$ watts at $I_{SC} = 6$ amperes, and $\Delta P = 20$ watts for $I_{SC} = 8$ amperes. The variation in ΔP is due to the power sensor characteristic and not a change in peak-detector sensitivity. Some improvement in sensitivity could be obtained either by increasing the array power level or reducing the full scale range of the power sensor circuitry.

4.5.7 Load Transient Susceptability Problem

To simulate a spacecraft power system configuration, a PWM regulator and load were connected in parallel with the MPT as shown in Figure 4-19. Transients were

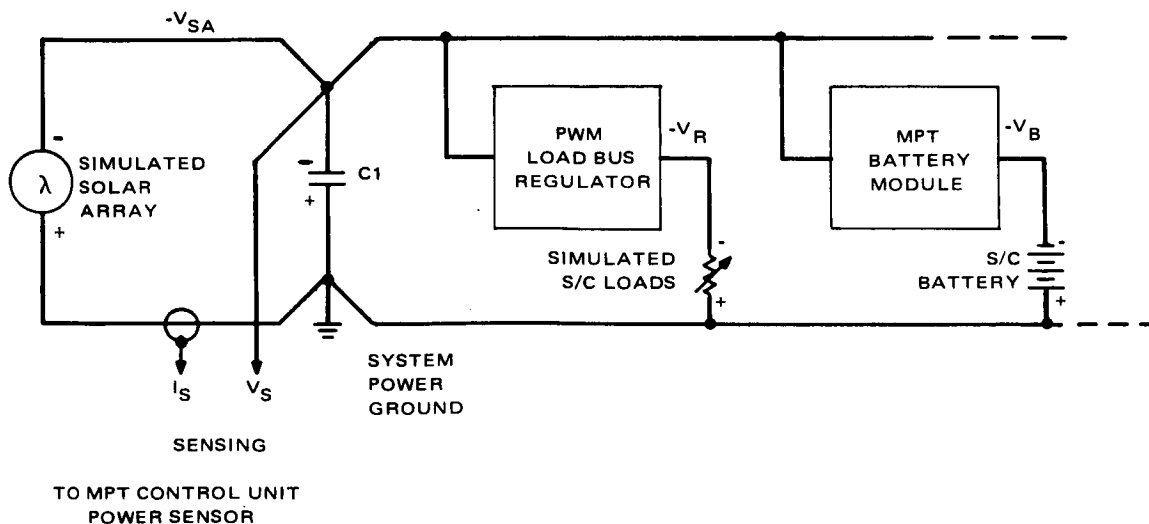


Figure 4-19. MPT System Test Configuration

induced at the output of the PWM regulator to ascertain the response of the MPT controls to load transients. The effect of load transients on the tracking operation was considered for transients up to 6 amperes. Sometimes, depending on the instant of application of the transient, the system became biased off the source maximum power point but tracking operation was restored by the pulse absence detector within 0.5 milliseconds. This is a significant improvement over the low-speed system where the maximum restore time could be one scanner cycle (about 15 seconds) and a 1-ampere load transient was not tolerable. The low-speed MPT problem was described in section 3.2.4.b). When the PWM regulator load current was increased beyond the point where the array could meet the demand, the system reverted to a battery-discharge mode and exhibited the hysteresis effect which is characteristic of part-time parallel power trackers. This effect was described in section 2.1.2.c).

4.5.8 Off-Bias Operation Problem

When the high-speed MPT is operated in parallel with the PWM load bus regulator, as in Figure 4-19, no interaction effects, which cause the disabling of the tracking function, are experienced. The low-speed system interaction problems which were encountered in this mode of operation were described in section 3.2.4.c).

One effect of the PWM regulator connection could be the reduction of the operating frequency of the MPT power switch due to the capacitance of the regulator

input filter being in parallel with the array capacitor in the MPT. Although this does not present any critical problems, the capacitance of the PWM regulator and the MPT must be designed with this effect in mind in order to control the operating frequency of the MPT. This effect was experimentally verified.

A second possible interaction occurs when an L-C input filter is used on the PWM regulator. This two-section filter introduces undesired resonances which can cause the cessation of tracking operation. This interaction was also experimentally verified.

The PWM Regulator as used in the testing of the high-speed MPT had no input filtering in order to avoid the interactions described above.

4.5.9 Rapidly Varying Solar Array

To demonstrate the applicability of the high-speed MPT to spacecraft with rapidly varying solar array characteristics (e.g. spin-stabilized spacecraft with body-mounted solar arrays), the solar array simulator characteristics were varied. Fluctuating array characteristics of this sort are caused by shadowing and variation of the angle-of-incidence of solar energy, both of which primarily affect the short-circuit-current level.

These effects were simulated by sinusoidally varying the short-circuit currents of the array simulator. Successful tracking of the maximum power point was

maintained for a ± 50 percent current variation at frequencies up to 200 Hz.

Thus, the high-speed MPT has demonstrated not only conceptual feasibility but applicability to a wide variety of missions.

4.6 Summary of Results

As a result of the severe limitations inherent to the first-generation (or low-speed) MPT system, a second-generation concept was developed to provide a more widely applicable system. The high-speed system retained all the performance features which had been incorporated into the low-speed system.

A working laboratory model of the high-speed MPT was constructed and evaluated. Laboratory results demonstrated that the basic concept was indeed feasible and that the observed performance was comparable to that of the first generation system. It should be noted that the goal of the working model was to demonstrate feasibility of the concept and that the results are not representative of optimized circuits in an optimum configuration. It must be recognized that circuit improvements will be required in the future.

The most significant of the results is the elimination of the restrictions of the low-speed system. The presence of load transients and the non-linear input characteristic of a PWM voltage regulator did not cause the MPT to become

biased off the source maximum power point. In addition, the high speed MPT system was able to maintain system operation at the maximum power point for a rapidly fluctuating array characteristic (as would be the case for a spin stabilized spacecraft with a body-mounted solar array).

The second-generation MPT system provides a means of efficient power conditioning which can result in significant increases in space power system capability. Of additional importance is the applicability of the basic technology to all types of spacecraft, and the wide variety of power system configurations with which the high-speed MPT system concept may be used.

5.0 PROGRAM RECOMMENDATIONS

Consideration of the test results and the circuit details of the high-speed MPT system provides several areas in which re-evaluation and improvement could be made in the future.

5.1 Battery Current Controls

The addition of logic functions to enable full time control of the battery current (in current-limit or trickle-charge modes) by closed-loop regulator techniques is desirable. This circuitry may take the form of either an enable/disable or a modulator function. Inclusion of this recommendation in a multi-channel system may be necessary to ensure proper operation and prevent interaction between battery modules.

5.2 Power Sensor Circuit

The present power sensor circuit samples source power at rates between 30 and 100 kHz which necessitates the use of wideband control circuits in the control unit. A method of decreasing this bandwidth requirement, thereby reducing tracking error by permitting increased peak detector sensitivity, is desirable. One possible method is to incorporate a power sensor having a continuous analog output in place of power sampling scheme. It is recommended that an investigation be made to devise a way to do this, possibly using a Hall-effect multiplier if the insertion power loss as described in section 4.3.1 can be reduced to acceptable levels.

5.3 Multiple Battery Channel Operation

The MPT working model as constructed is comprised of a control unit and one battery module. This system does not demonstrate multiple-battery channel operation or permit evaluation of the current sharing controls. Therefore, a system of several battery modules (in a modular form) should be built to serve as an experimental system model to demonstrate the full capabilities of the high-speed MPT.

5.4 System Operating Frequency

In the design and development of the high-speed MPT as described in this report, the effects of the array capacitor and the output inductor have been both observed and nominally designed. However, on the basis of the system tests and performance evaluation, the methods for the selection of the optimum-values for these components should be investigated in detail. A derivation of an analytical expression for the scan frequency and the tracking error would be required to insure proper tracking operation, adequate design margins in the control and sensing circuits, and provide a satisfactory range of operating frequencies for both nominal and worst-case design philosophies.

6.0 REFERENCES

- 6.1 Nekrasov, P., "System Comparison and Analysis of Tracking and Non-Tracking Space Power Supplies," presented at the 4th Space Congress, April 3-6, 1967, Coco Beach, Florida.
- 6.2 MacKenzie, C.M.; Greenblatt, R.C.; Cherdak, A.S.; "Nimbus Power Systems (1960-1969)"; presented at the Aerospace Electronic Systems Convention, October, 1966, Washington, D.C.
- 6.3 Advance Voltage Regulator Research and Development Program, Final Report, 6 March 1963 through 1 August 1964, Contract NAS 5-3248, Prepared for NASA-GSFC by RCA-Astro-Electronics Division.
- 6.4 Non Dissipative Solar Array Optimum Charge Regulator, Final Report, July 1966, Contract NAS 5-9210, Prepared for NASA-GSFC by Hughes Aircraft Co.
- 6.5 Bolton, C.N. of GSFC and Nekrasov, P.S. AED; "Analysis of the Advanced Nimbus Power System", July 1967, by Goddard, X-716-67-350

APPENDIX I

POWER TRACKER PERFORMANCE ANALYSIS

A. INTRODUCTION

The comparison of three power-tracker configurations presented in Paragraph 2.1.2 is based on the assumption that the most desirable performance is achieved when the battery charge is maximized. A detailed analysis of the reasons for this assumption is presented herein. The values of shunt losses and line drops used in this analysis are assumed and are considered typical of solar-array power subsystems like Nimbus B. The parameters and assumed values are shown in Table I-1.

TABLE I-1

PARAMETER	VALUE ASSUMED	COMMENTS
Array Output	Worst-Case at End of Life (12 Months)	Solar-Array I-V Characteristic
Storage Cell Output at +25°C and 95% State of Charge	Worst-Case at End of Life (12 Months)	Storage-Cell I-V Characteristic
Number of Batteries	8	23-Cells per Battery
Shunt Losses at: PWM Load-Bus Regulator Output Series-Tracker Output or Parallel-Tracker Input Unregulated Bus	5 watts 0.176 ampere 0.176 ampere	Fixed At Unregulated-Bus Voltage Level Battery Voltage (during charge)
TOTAL (During Charge)	0.352 amperes	At Unregulated Bus
Line Drops Array-Blocking Diode Path (D1) Battery-Output Isolation-Diode Path (D2) Line-Isolation Diode Path (D3)	1.8 volts 0.45 volt 0.35 volt	
Efficiency Factor	0.9	Fixed for all PWM devices (Series Tracker, Parallel Tracker, Load-Bus Regulator, and Discharge Regulator)

B. ANALYTICAL CALCULATIONS

The following paragraphs of this Appendix contain step-by-step calculations for the Series-configuration Power Tracker. These calculations are typical of the analytical method used to evaluate any of the power-tracker configurations studied. The calculations shown in B.9 through B.14 are based on a battery-discharge condition.

1. Input Parameters

Assuming equilibrium array temperature, the tracker input parameters for the array output at 40°C (P_{\max}) are as follows:

$$V_{\max} = 38 \text{ volts}$$

$$I_{\max} = 9.52 \text{ amperes}$$

The tracker input voltage is given by

$$V_{\text{in}} = V_{\max} - V_{D1} = 38.0 - 1.8 = 36.2 \text{ volts}$$

The tracker input power (P_s) is

$$P_s = V_{\text{in}} I_{\max} = 36.2\text{V} \times 9.52\text{A} = 345 \text{ watts}$$

2. Output Power

The tracker output power (P_T) is the total of all tracker modules.

It is determined, using efficiency factors, as follows:

$$P_T = P_s \eta_T = 345\text{W} \times 0.9 = 310 \text{ watts}$$

3. Charge Current

A total charge current (I_{ch}) of 4 amperes was used.

4. Battery Charge Voltage

Battery I-V characteristics were used to determine the battery charge voltage (V_{BC}). A value of 31.42 volts at a charge current of 4.0 amperes was used.

5. Output Current

The total tracker output current (I_T) was calculated as follows:

$$I_T = \frac{P_T}{V_{BC}} = 9.86 \text{ amperes}$$

6. Load-Bus Regulator Input Current

The PWM load-bus regulator input current (I_o) was determined by:

$$I_o = I_T - I_{ch} - I_{sh} = 5.51 \text{ amperes}$$

where

$$I_{sh} = 0.352A$$

7. Load-Bus Regulator Input Voltage

The PWM load-bus regulator input voltage (V_o) was calculated as:

$$V_o = V_{BC} - V_{D2} = 30.97 \text{ volts}$$

where

$$V_{D2} = 0.45 \text{ volts}$$

8. Load-Bus Regulator Output Power

The PWM load-bus regulator output power to spacecraft loads (P_L) was as follows:

$$P_L = V_o I_o \eta_c - 5W = (30.97V) (5.51a)(.9) - 5 = 148.5 \text{ watts}$$

where

$\eta_c = 0.9$ and 5 watts is the shunt loss at V_R . The results of this calculation ($I_{ch} = 4$ amperes, $P_L = 148.5$ watts) are shown in Figure 2-6 for the series tracker.

9. Battery Discharge Current

A total battery discharge current (I_{Bd}) of 2 amperes was assumed.

10. Battery Discharge Voltage

Using battery I-V characteristics, the battery discharge voltage (V_{BD}) was found to be 29.64 volts for a battery discharge current of 2 amperes.

11. Output Current

The tracker output current (I_T) was calculated as follows:

$$I_T = \frac{310 \text{ watts}}{29.64a \text{ MP}} = 10.44 \text{ amperes}$$

12. Load-Bus Regulator Input Current

The total PWM load-bus regulator input current (I_o) was:

$$I_o = I_T + I_{Bd} - I_{sh} = 12.09 \text{ amperes}$$

where

I_{sh} is the total of the shunt loss currents.

13. Load-Bus Regulator Input Voltage

The PWM load-bus regulator input voltage (V_o) was determined as:

$$V_o = V_{Bd} - V_{D2} = 29.19 \text{ volts}$$

14. Output Power

The PWM load-bus regulator output power to spacecraft loads (P_L) was as follows:

$$P_L = I_o V_o \eta_c - 5W = 312 \text{ watts}$$

The results of this calculation ($I_{BD} = 2$ amperes, $P_L = 312$ watts) for the series are shown in Figure 2-6 for the series-tracker configuration.

APPENDIX II

GRAPHICAL ANALYSIS OF MPT SYSTEM OPERATION

A. GENERAL

A graphical approach for ascertaining instantaneous behavior of a power tracker system is discussed in the following paragraphs. This analysis is presented in addition to and in contrast with the analyses of Section 2.2.

The method of graphical analysis of the MPT system may be derived through consideration of the fundamental power relationships which exist in the system. The analysis is primarily concerned with a part-time parallel tracker, however, the effects of the series vs. parallel and full-time vs. part-time configurations will be pointed out.

Neglecting losses, a basic power equation describing the system is:

$$p_s = p_L + p_b \quad (\text{II-1})$$

where:

p_s is instantaneous source or array power

p_L is instantaneous load power

p_b is instantaneous battery power where

(+) indicates charging,

(-) indicates discharging.

Figure II-1 is a unidirectional graph of equation (II-1).

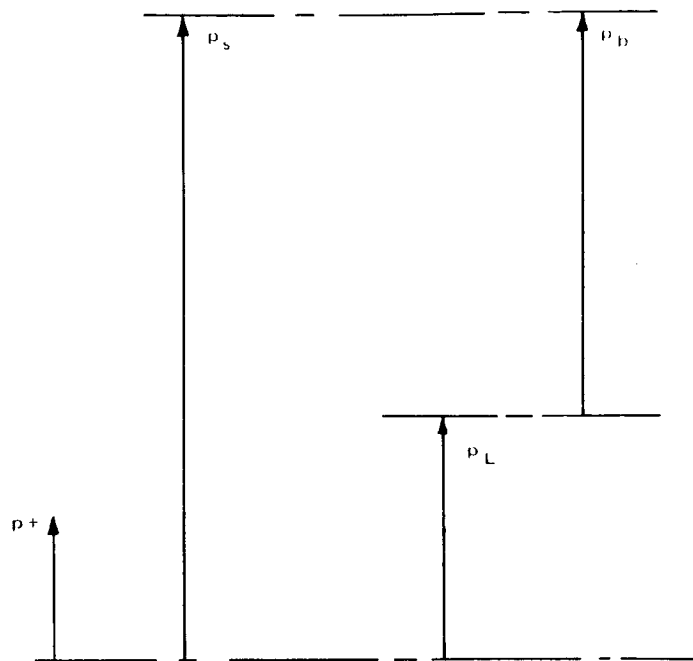


Figure II-1. Graph of Equation, $p_s = p_L + p_b$

This graph, alone, is inadequate to describe the desired relationships between the terms for variations in array, load, and battery. Additional dimensions must be included. Both current and voltage are directly involved in the power system analysis. However, since knowledge of any two of the parameters (p, v, i) uniquely determines the third, there is little to be gained in employing all three. Voltage is generally employed as a common denominator in system analysis, and, inasmuch as the power system output is a regulated voltage rather than a regulated current, this parameter will be employed here.

The solar array $p_s - v_s$ characteristic is shown typically in Figure II-2. The maximum power point coordinates are delineated as p_{sm} and v_{sm} for power and

and voltage respectively. This is a graph of power available from the array as related to its terminal voltage.

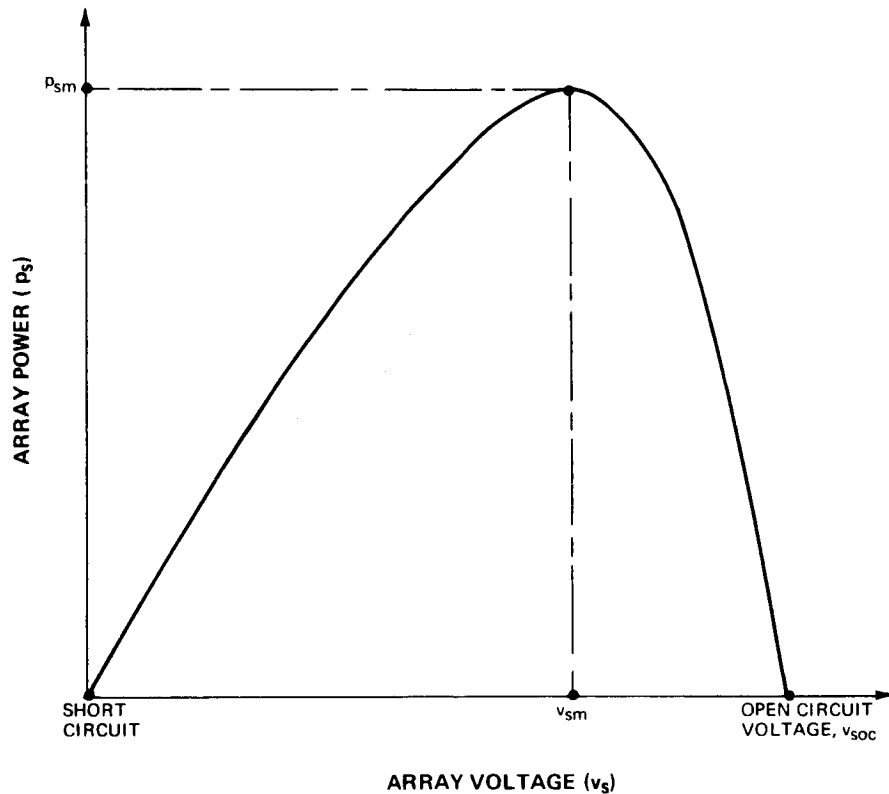


Figure II-2. Typical Solar Array p_s - v_s Characteristic

Load power may be related to the PWM regulator input voltage as shown in Figure II-3. This graph shows an ideal regulator with a pure resistive load, R_L . It is obvious that v_s must always be greater than v_{rb} in order to preserve the regulated system output.

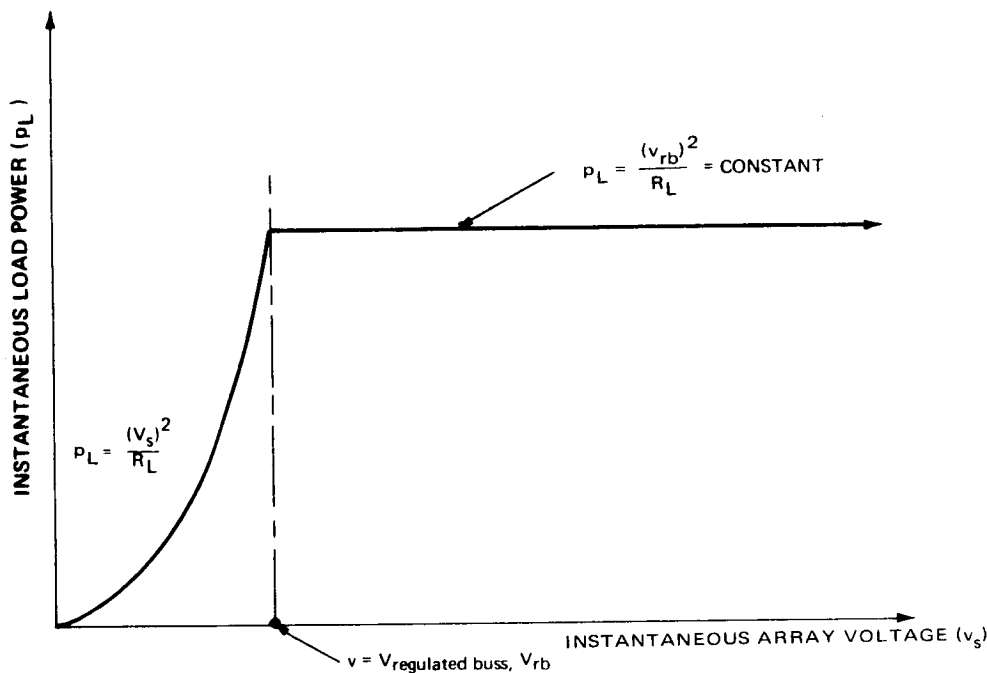


Figure II-3. Load Power-Regulator Input Voltage Characteristic

The battery p_b - v_b relationship is shown in Figure II-4(a). Here power may be battery input (charging) or battery output (discharging). This graph shows instantaneous power transfer for some arbitrarily chosen state-of-charge and lifetime. The graph should be made to follow normal battery behavior with a shift to the right as the state-of-charge increases and to the left as it decreases. In addition, V_{BC} and V_{BD} will diverge as operating life proceeds. A reasonable linear approximation to the p_b - v_b characteristic is shown in Figure II-4(b).

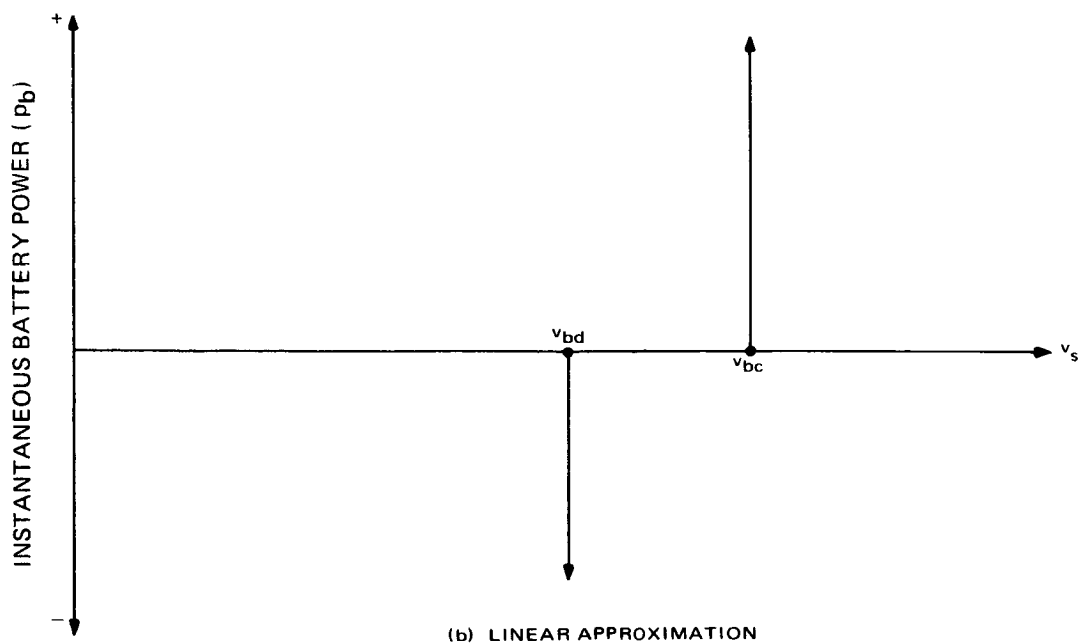
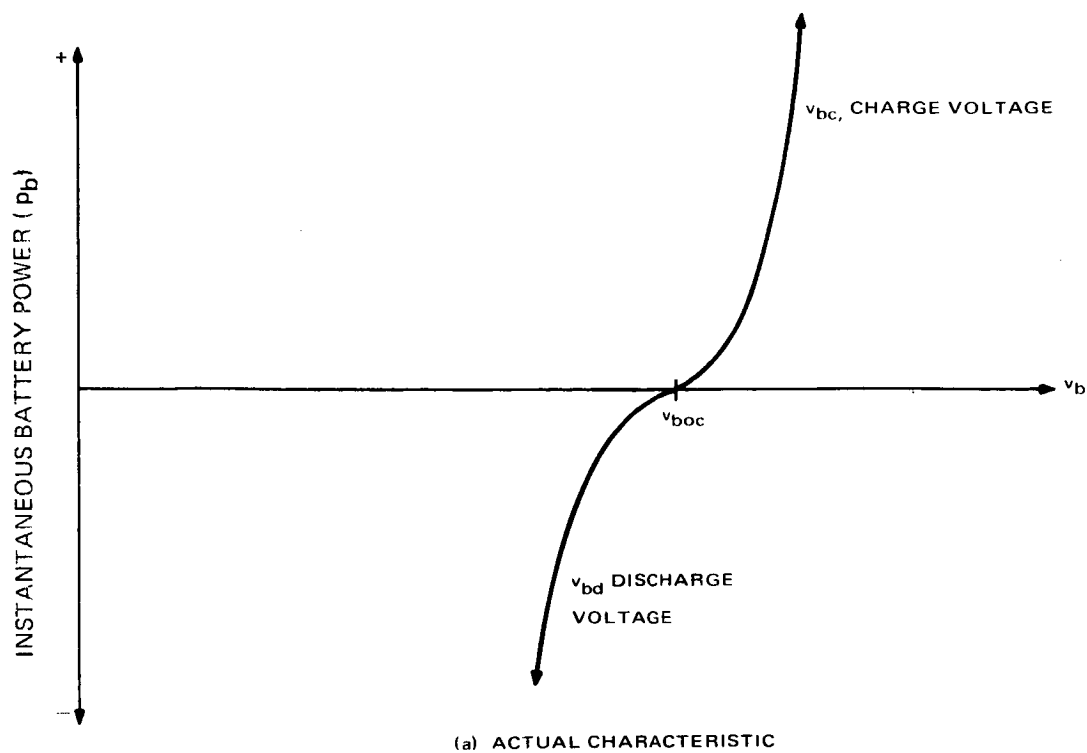


Figure II-4. Battery $p_b - v_b$

The assumption must be made that the system voltage level constraints:

$$\left. \begin{array}{l} v_{bd} > v_{rb} \\ v_{sm} > v_{bc} \end{array} \right\} \quad (II-2)$$

are satisfied.

B. ANALYSIS BY OPERATING MODES

The overall operation of the MPT is non-linear but may be considered in three operating modes.

1. Discharge (Night) Mode

Battery discharge during spacecraft night is represented by equation (II-1) with

$$\begin{aligned} p_s &= 0, \text{ or} \\ -p_b &= p_L \end{aligned} \quad (II-3)$$

This indicates that the load power is being supplied by the battery. The graphical representation is found by summing the p-v characteristics of the battery and the load as is shown in Figure II-5. Note that the battery discharge equals the load power as indicated by the intersection of the v_{bd} line with the p_L line. This analysis is valid for both series and parallel tracker configurations.

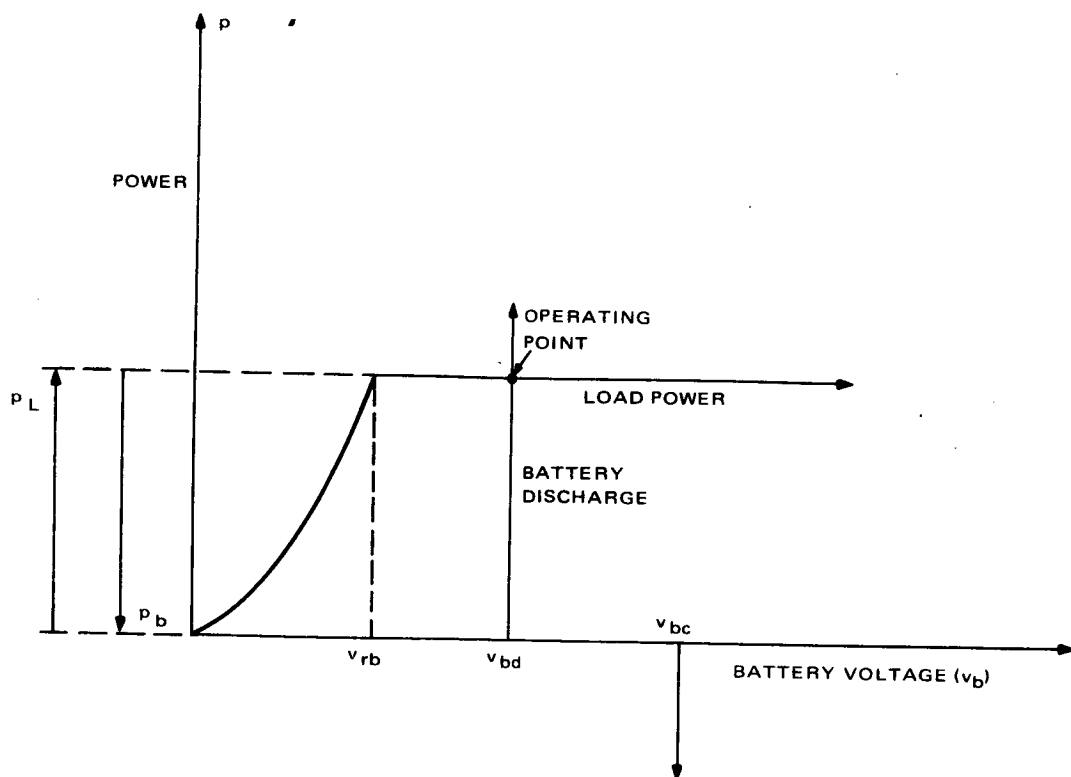


Figure II-5. Operation Point for Battery Discharge ($p_s = 0$)

2. Normal Tracking (Day) Mode

The second mode of operation is the normal or tracking mode. The MPT switching action causes the array operating point to be at or near the maximum power point. The parallel tracker configuration will be analyzed.

Full graphical evaluation of Equation (II-1) requires a conversion of the coordinates of Figure II-2, II-3 and II-4, in order to make them

compatible. The ordinates of these figures are expressed in terms of power and will need no transformation since it is assumed, for purposes of this analysis, that losses in the MPT are negligible. The abscissas, on the other hand, are in terms of battery and array volts. For convenience, the abscissa of Figure II-4 (in terms of battery volts) will be transformed to array volts. The resulting battery characteristic will be equated to the array and load characteristics and a graphical solution to Equation (II-1) will be evaluated.

The battery voltage, v_b , and the array voltage, v_s , are related by the MPT power switch duty-cycle as:

$$v = \frac{v_b}{\alpha} \quad (\text{II-4})$$

where:

α is the power switch duty cycle

The abscissa of Figure II-4 is divided by α and the composite p-v characteristic of battery and load vs. array voltage is constructed as shown in Figure II-6. Note that this characteristic is only a valid model when $p_s > p_L$ and the battery is not discharging. The other cases will be considered in Paragraph B.3.

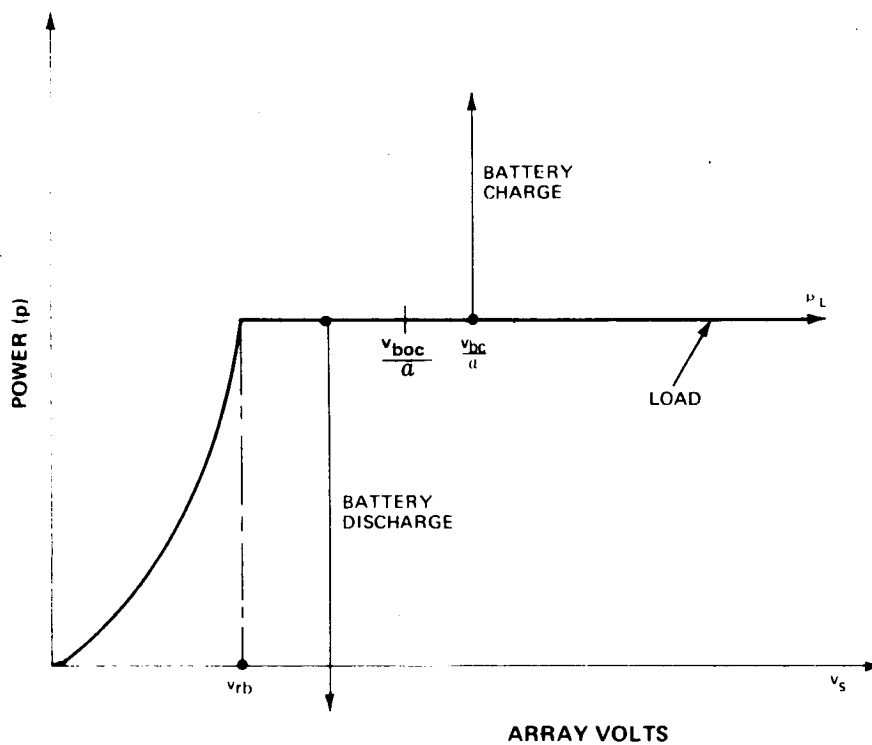


Figure II-6. Graph of $p = p_L + p_e$

Figure II-7 is a complete graph of Equation (II.1) with the solution indicated as that intersection of the array and load-battery characteristics which satisfies the equation. Note that variation of α will vary the load-battery characteristic abscissa and that maximum battery charging power will be obtained for the condition,

$$\frac{v_{bc}}{\alpha} = v_{sm} \quad (II-5)$$

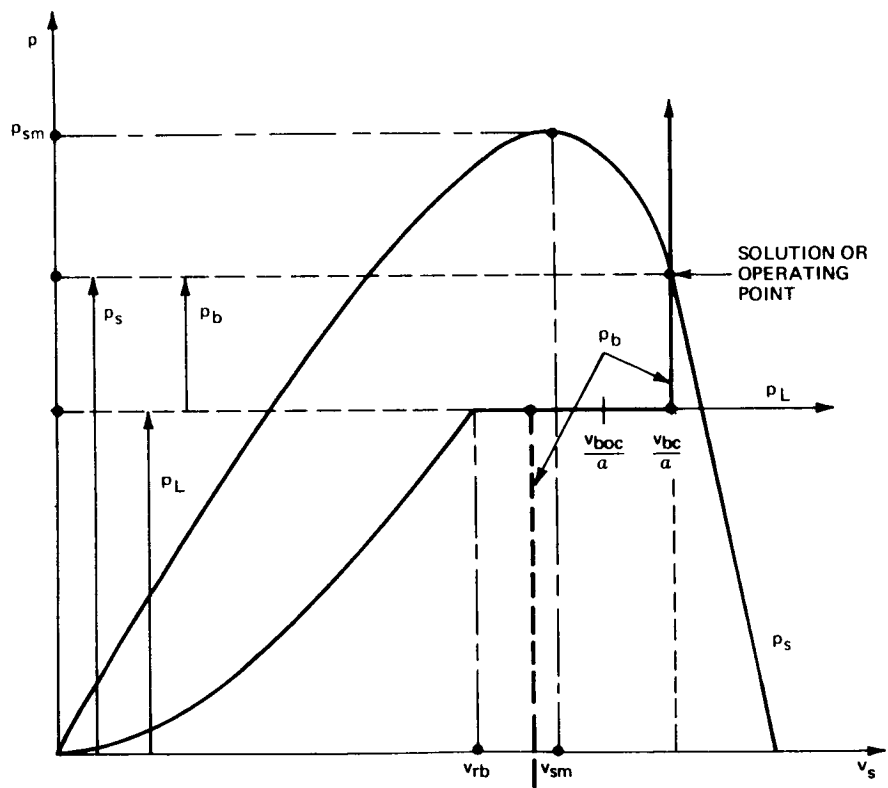


Figure II-7. Graph of $p_s = p_L + p_b$ versus v_s

It must be noted that the battery always clamps the MPT output and the regulator input when $p_s < p_L$. This being the case, the load-battery characteristic may exist only between V_{boc} and V_{bc} , including the battery charge characteristic as shown on Figure II-8. There are several cases of general interest for which this analysis becomes limited.

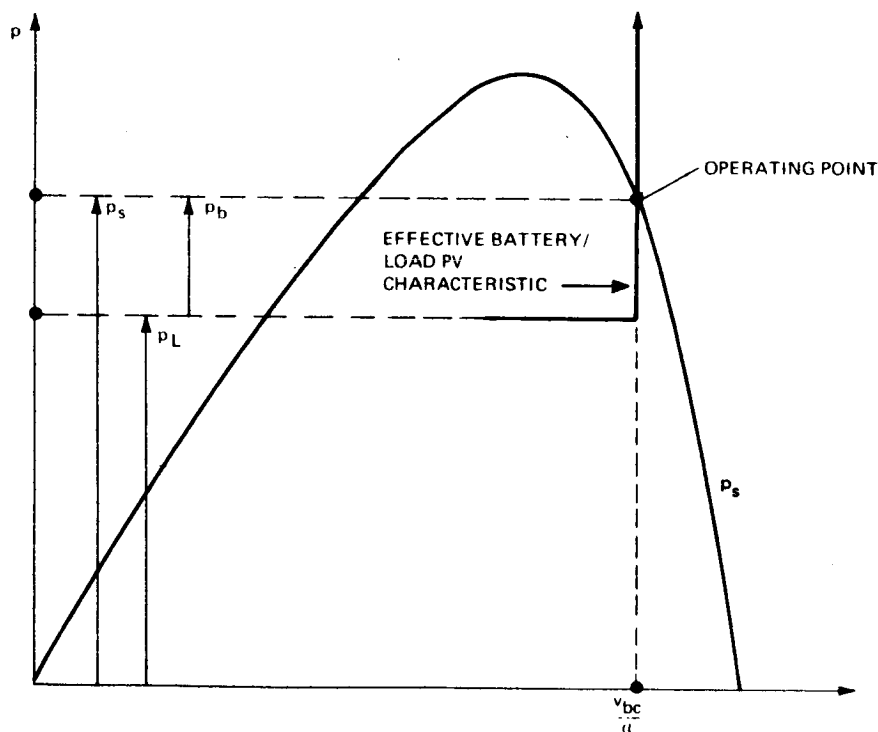


Figure II-8. Simplified Graph of $P_s = P_L + P_b$

For small values of α , the load-battery characteristic is shifted to the right causing V_{boc}/α and v_{bc}/α to diverge. This condition is shown on Figure II-9 for the actual battery power curve. As the operating point (O.P.) approaches V_{boc}/α , the battery approaches zero charge current, and the relationships derived for the part-time MPT are not valid and therefore do not apply. For a full-time tracker the analysis remains valid with the battery discharging. As the operating point approaches V_{soc} , the battery assumes more and more of the load and within the limits, when v_{bd}/α equals V_{soc} , the battery supplies the entire load. The analytical relationships are not applicable for operation when $\frac{v_{bd}}{\alpha} > V_{soc}$ which is an impossible operating point. These conditions occur, however, well above normal array operating points since the MPT will maintain operation at or near the maximum power (p_{sm}) point, except under certain transient conditions.

For large values of α (approaching 1.0), there exists a possibility of multiple operating points for full-time trackers as indicated in Figure II-10. Here, there are three possible operating points indicated for one condition of battery, load and array characteristics. However, since this is not within the normal region of operation and might occur only under transient conditions it is not of primary concern. In addition, the MPT circuitry will not allow continued operation at any of these points since the array would not be operating at its maximum power point.

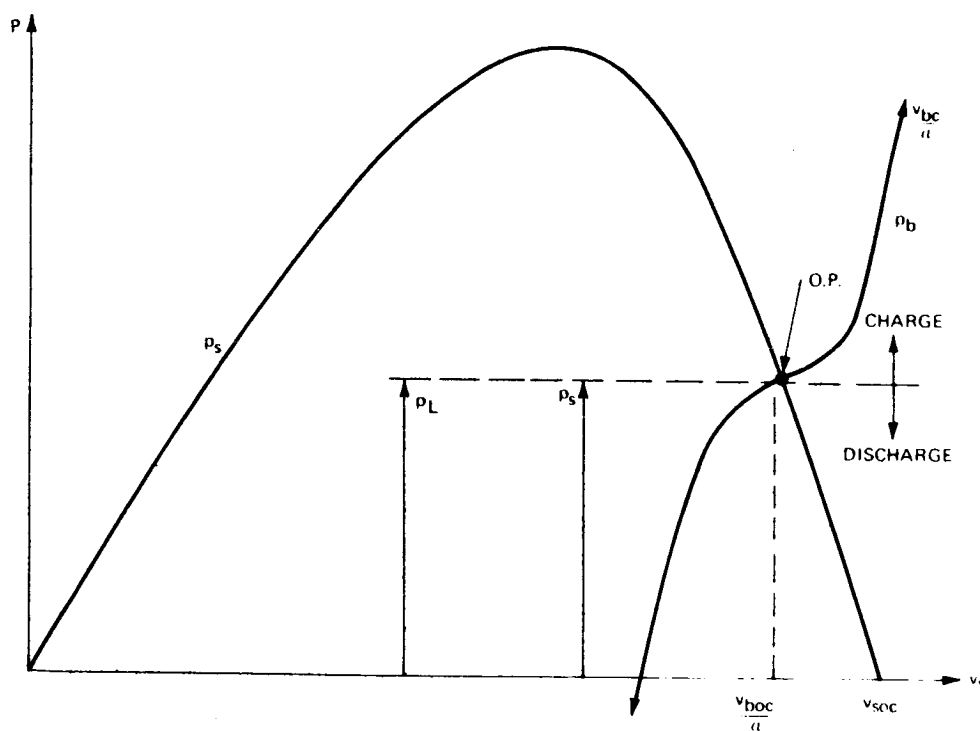
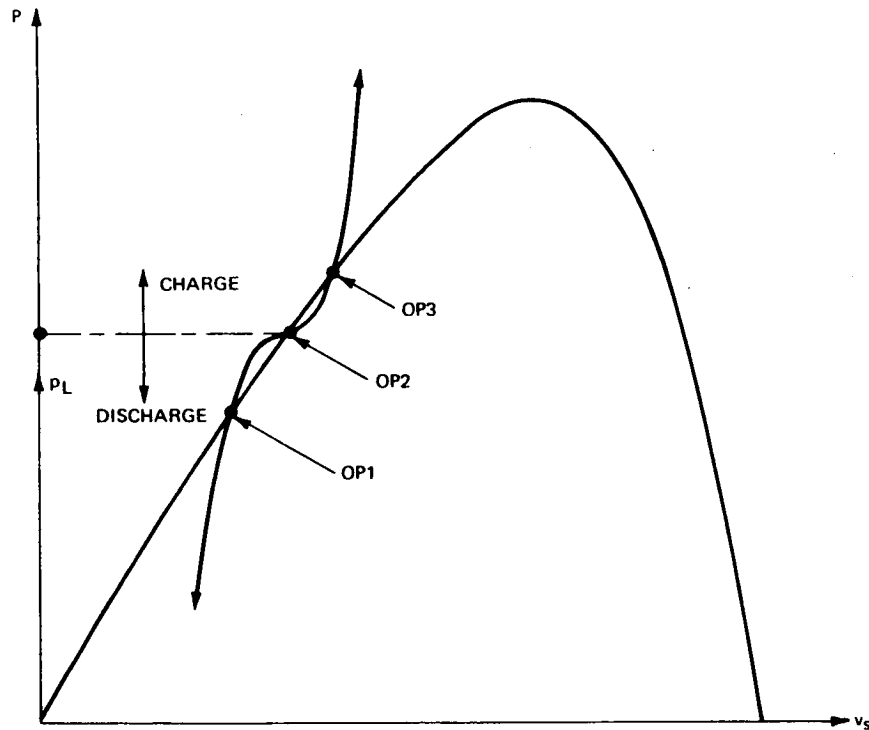


Figure II-9. Location of Operating Point for Small Values of α



Figures II-10. Multiple Operating Points for Large Values of α

Normal operation of the MPT would cause the battery characteristic to intersect the array at or about the p_{sm} point as shown on Figure II-11. In actuality, the v_b characteristic will oscillate about the p_{sm} point at the scan frequency as determined by the system dynamic properties.

3. Full-time System Mode

Thus far, the system characteristics have been considered from the standpoint that the available array power is in excess of load demand and batteries have been charging continuously. For the full-time systems, as

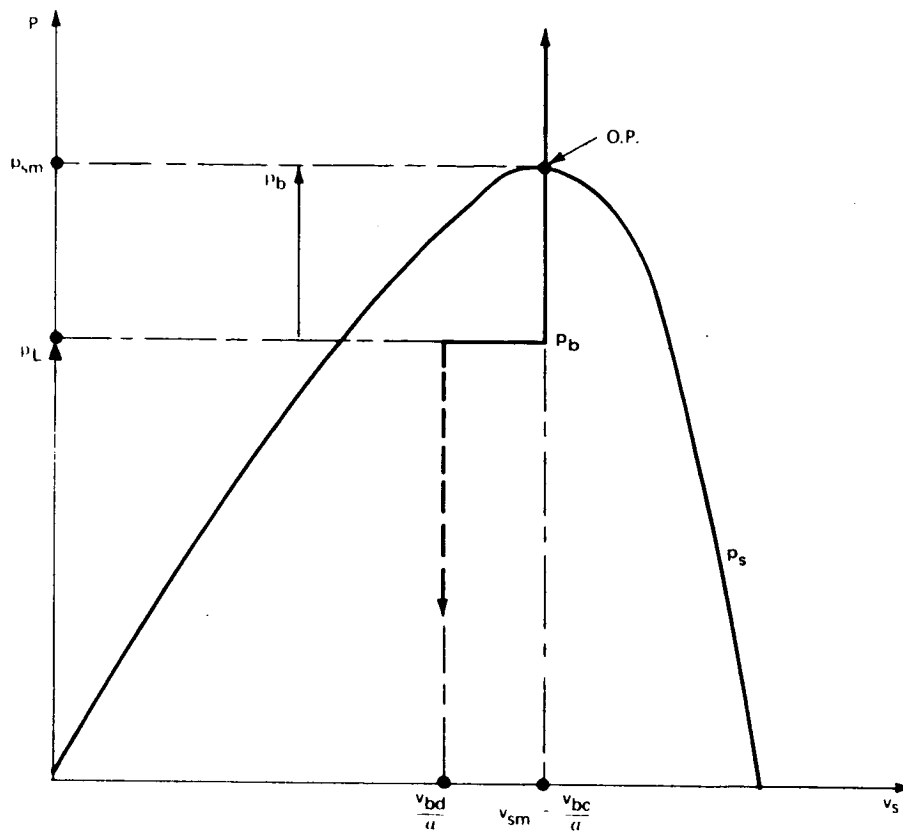


Figure II-11. Location of Operating Point for Normal MPT Operation

the name implies, maximum array power is delivered to the spacecraft regardless of load. For the condition where load demand exceeds the array capability, the difference between load and array is supplied by battery in the manner depicted in Figure II-12. In the part-time parallel tracker system, peak loading will result in an off-bias condition in which the array operating point voltage becomes equal to the battery discharge voltage. This is shown in Figure II-13.

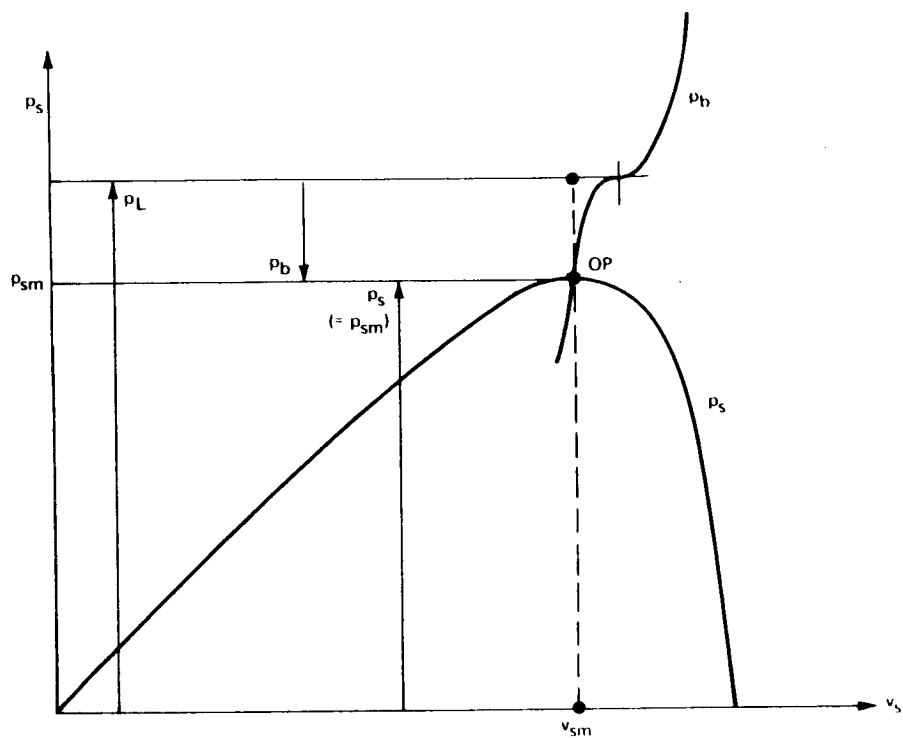


Figure II-12. Peak Load Handling for Full-Time Tracker Systems

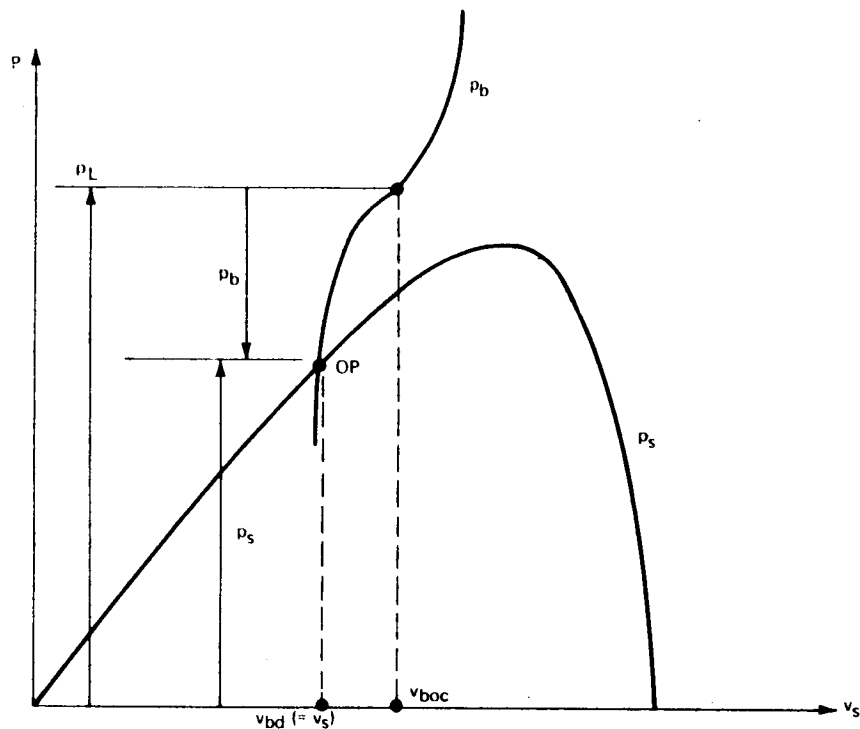


Figure II-13. Peak Load Handling for Part-Time Parallel Tracker Systems

An alternate representation of Figure II-13 is shown on Figure II-14. Here, the array and battery characteristics have been combined to form "available power vs. source voltage" characteristics. This is achieved by inverting the battery discharge characteristic and affixing its open circuit voltage point to the array power characteristic where $v_{boc} = v_s$. This is the effective characteristic presented to the PWM regulator input by the combined array-MPT-battery components of the system.

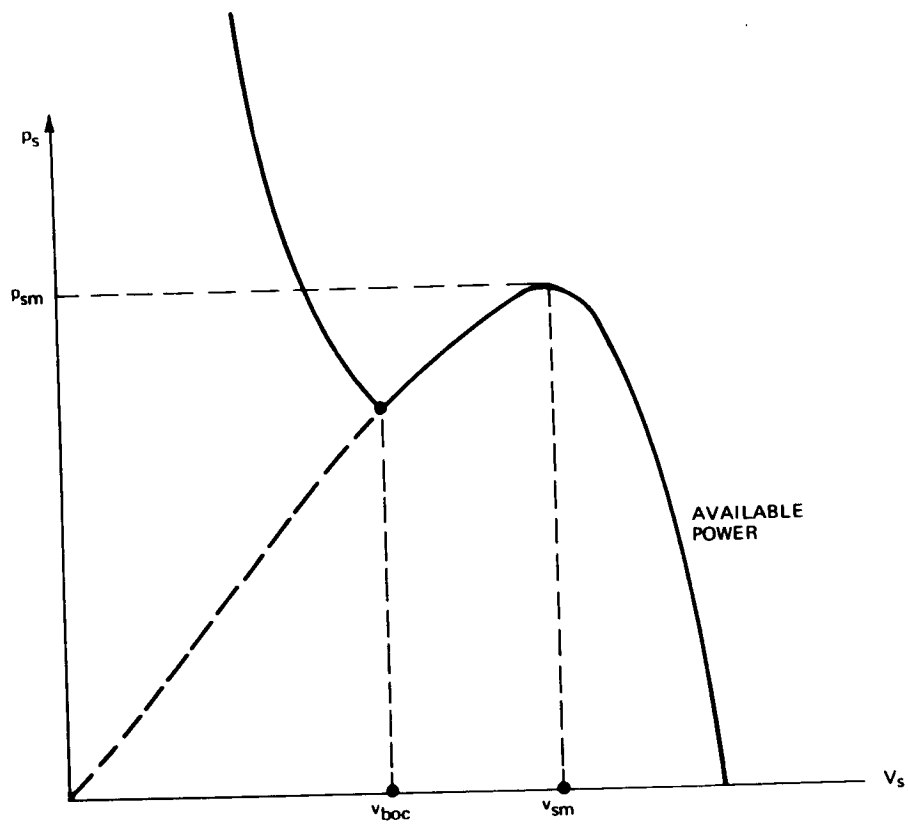


Figure II-14. Available Power vs. Source Voltage
for Part Time Tracker

APPENDIX III

DERIVATION OF AN EXPRESSION FOR SCAN FREQUENCY

The frequency at which the system oscillates about the maximum power point in a steady-state condition (scan frequency, f_s) may be evaluated in terms of the system parameters. A derivation follows:

The rate at which the power switch duty-cycle is changed $\left(\frac{d\alpha}{dt}\right)$ is, defined as r (%/second) and $R = r/100$. This number is a function of the system scan generator and PWM characteristics and may be quite easily evaluated or tailored to some desired value.

The array or source voltage is given as a function of the PWM output (or battery) voltage and duty-cycle as:

$$V_s = V_B/\alpha$$

and

$$\frac{dV_s}{dt} = \frac{-V_b}{2} \left(\frac{d\alpha}{dt}\right)$$

where the polarity relationship is:

$$\text{if } \frac{dV_s}{dt} > 0, \text{ then } \frac{d\alpha}{dt} = -R$$

$$\text{if } \frac{dV_s}{dt} < 0, \text{ then } \frac{d\alpha}{dt} = +R$$

The basic relation between time and source voltage is

$$dt = \frac{dV_s}{\left(\frac{dV_s}{dt}\right)} = \left(\frac{dt}{dV_s}\right) dV_s$$

if the source voltage limits are defined as

V_{su} = upper scan limit of source voltage

V_{sL} = lower scan limit of source voltage

and assume that the sweep is towards V_{sL} , then, from Figure III-1,

$$\int_{t_u}^{t_L} dt = \int_{V_{su}}^{V_{sL}} \left(\frac{dt}{dV_s}\right) dV_s$$

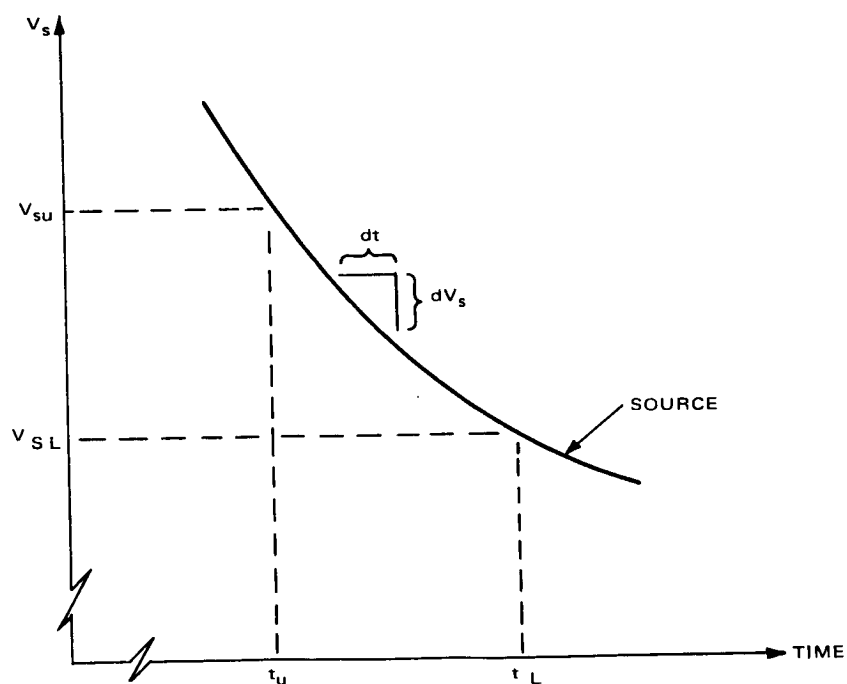


Figure III-1. Incremental Source Characteristic

integrating

$$t_1 - t_u = \Delta t = \int_{V_{su}}^{V_{sl}} \left(\frac{dt}{dV_s} \right) dV_s$$

evaluating the integr and

$$\frac{dt}{dV_s} = \frac{1}{\left(\frac{dV_s}{dt} \right)} = \frac{1}{\left(\frac{-V_b}{\alpha^2} \cdot \frac{d\alpha}{dt} \right)} = \frac{-\alpha^2}{V_b \frac{d\alpha}{dt}}$$

since source voltage is assumed to be decreasing,

then

$$\frac{d\alpha}{dt} = + R$$

and

$$\frac{dt}{dV_s} = \frac{-\alpha^2}{V_B R}$$

but, making the substitution

$$\alpha = \frac{V_B}{V_s}$$

becomes

$$\frac{dt}{dV_s} = \frac{-V_B^2}{V_B R V_s^2} = \frac{-V_B}{R V_s^2}$$

Substituting back into the integral,

$$\Delta t = \int_{V_{su}}^{V_{sL}} \left(\frac{-V_B}{R} \right) \frac{dV_s}{V_s^2} = \frac{V_B}{R} \int_{V_{su}}^{V_{sL}} \frac{dV_s}{V_s^2}$$

$$\Delta t = \frac{V_B}{R} \left(\frac{-1}{V_s} \right)_{V_{su}}^{V_{sL}}$$

$$\Delta t = \frac{V_B}{R} \left(\frac{1}{V_{sL}} - \frac{1}{V_{su}} \right)$$

and the full scan period is given by

$$T_s = 2 \Delta t = \frac{2V_B}{R} \left(\frac{1}{V_{sL}} - \frac{1}{V_{su}} \right)$$

therefore, the scan frequency is

$$f_s = \frac{1}{T_s} = \frac{R}{2V_B \left(\frac{1}{V_{sL}} - \frac{1}{V_{su}} \right)}$$

It now remains to fully characterize V_{sL} and V_{su} in terms of the array and other pertinent system parameters.

The system will shift the system operating point voltage above and below that of the array maximum power point (P_{sm}) in the manner described in Paragraph 2.3 in this report. The criterion for reversal of the scan direction is a reduction of the MPT output (or battery) current by some amount less than a previous

value. This represents the peak detector sensitivity, ΔI_B . Output power variation is then

$$\Delta P_o = \Delta I_B V_B$$

In terms of source power,

$$\Delta P_s = \frac{\Delta P_o}{\eta_T} = \frac{\Delta I_B V_B}{\eta_T}$$

where η_T is the MPT power transfer efficiency (variations of η_T with power level) should be accounted for in arriving at an accurate estimate of f_s .

Instantaneously,

$$\Delta p_s = \left(\frac{V_B}{\eta_T} \right) \Delta i_B.$$

The expression for the instantaneous power being delivered from the solar array, can now be written

$$p_s = p_{sm} - \Delta p_s$$

$$p_s = p_{sm} - \left(\frac{V_B}{\eta_T} \right) \Delta i_B.$$

A relationship which has been found to yield satisfactory approximations to solar array I-V characteristics in the first quadrant is

$$I_s = I_{sc} - B \left(e^{CV_s} - 1 \right)$$

(where I_{sc} is the short circuit current of the solar array) for a given solar array temperature.

The constants (B and C) may be determined via an appropriate algorithm. Temperature dependence was not included in this relationship because of the added complexity.

The instantaneous delivered array power is given as

$$p_s = V_s I_s = V_s I_{sc} - BV_s \left(e^{CV_s} - 1 \right)$$

At this point there are two methods of solution:

A. Analytical Solution

The power relationship is

$$V_s I_{sc} - BV_s \left(e^{CV_s} - 1 \right) = p_{sm} - \Delta p_s$$

which, at the limits V_{sL} and V_{su} , becomes

$$V_s I_{sc} - BV_s \left(e^{CV_s} - 1 \right) = p_{sm} - \frac{V_B \Delta i_B}{\eta_T}$$

This is a transcendental equation with at least two roots

$$V_{s1} = V_{sL}$$

$$V_{s2} = V_{su}$$

Several numerical techniques are available for solution and, in fact, solution will be considerably expedited through digital computer techniques. This method would necessarily require evaluation of the constants, B and C.

B. Graphical Solution

The basic power equation still governs

$$P_s = P_{sm} - \frac{V_B \Delta i_B}{\eta_T}$$

Here, P_s is described by a characteristic P-V curve for the desired solar array and a specific set of conditions. The solutions to the equation are the intersections of the P_s - V_s curve with a line representing a constant power

$$P_{sm} - \frac{V_B \Delta i_B}{\eta_T}$$

This is shown on Figure III-2.

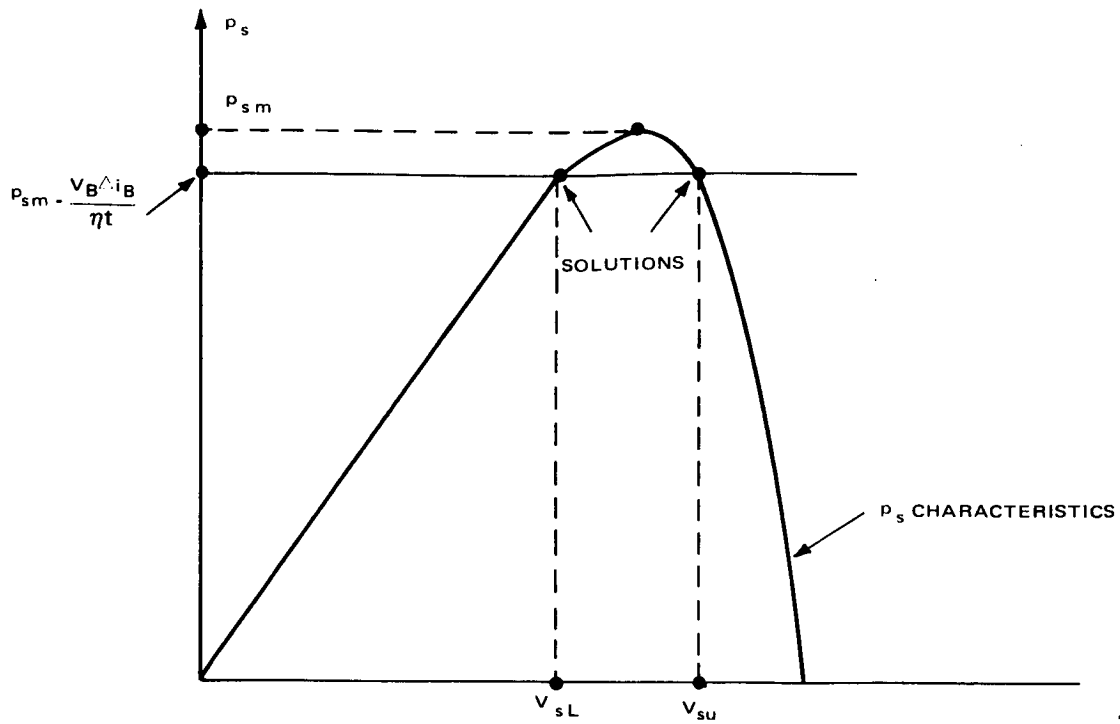


Figure III-2. Graphical Solution to Power Equation

Note that the tracking error may be easily derived by a small extension of the above derivation

$$\begin{aligned}
 p_s &= p_{sm} - \frac{V_B \Delta i_B}{T} \cdot \left(\frac{p_{sm}}{p_{sm}} \right) \\
 &= p_{sm} \left(1 - \frac{V_B \Delta i_B}{T p_{sm}} \right) = p_{sm} (1 - E_T)
 \end{aligned}$$

where

$$\frac{V_B \Delta i_B}{\eta_T P_{sm}} = E_T$$

gives the tracking error of the MPT system.

The tracking error may be considered as a quality factor or figure of merit for the MPT system, and is further defined as

$$E_T = \frac{\Delta P_s}{P_{su}}$$

which is in effect a measure of with which the MPT comes to actually operating at the maximum power point of the source.